Fully Coupled Dynamic Analysis of a
Floating Wind Turbine System

By

Jon E. Withee

M.S., Naval Architecture and Marine Engineering
and M.S., Nuclear Engineering
Massachusetts Institute of Technology, 2002

Submitted to the Department of Ocean Engineering
in Partial Fulfillment for the Degree of

Doctoral Degree in Naval Architecture and Marine Engineering

at the
Massachusetts Institute of Technology
June 2004
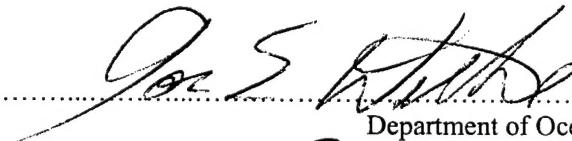
Signature of Author ....
Department of Ocean Engineering
March 15, 2004
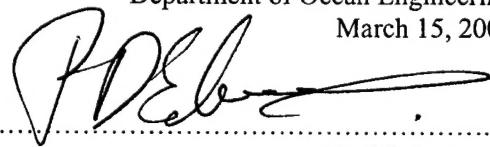
Certified by ....
Paul Sclavounos
Professor of Ocean Engineering
Thesis Advisor
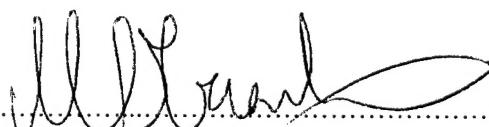
Accepted by...
Michael Triantafyllou
Professor of Ocean Engineering
Chairman, Department Committee on Graduate Studies

20040830 042

Fully Coupled Dynamic Analysis of a
Floating Wind Turbine System

by

Jon E. Withee

Abstract

The use of wind power is in a period of rapid growth worldwide and wind energy systems have emerged as a promising technology for utilizing offshore wind resources for the large scale generation of electricity. Drawing upon the maturity of wind turbine and floater technologies developed by the wind energy and oil and gas industries, respectively, large offshore wind energy systems have been developed and are being proposed for operation in offshore areas where environmental restrictions are less restrictive, large wind resources exist, and open sea areas are available for wind farm development.

A fully coupled dynamic analysis technique was developed to predict the response of a floating wind turbine system in a stochastic wind and wave environment. This technique incorporated both non-linear wave loading on the submerged floater and the aerodynamic loading on the wind turbine. A tension leg spar buoy was designed to support the wind turbine. This design was chosen due to its relatively small size and hence lower potential cost per wind turbine. The system's tethers were attached to the ends of spokes which radiated out from the spar cylinder. This arrangement of lines and spokes promised to be very stiff in the roll and pitch modes of motion.

The fully coupled analysis technique was used to evaluate the feasibility of the chosen floater design. Damping properties of the combined floater / wind turbine system were determined by conducting simulated free decay tests for the different modes of motion and wind turbine operating conditions. Numerical simulations for operational conditions were also carried out. The response of the floating wind turbine to three different sets of environmental conditions was determined and compared to a fixed base system. Additional simulations were conducted to determine extreme wind and wave event response. Stiffness of the floating system in roll and pitch was found to be a desirable attribute. The results of the analysis demonstrated that the tension leg spar buoy has the potential to support a wind turbine in an offshore environment without adversely affecting the loading on the system components.

Thesis Supervisor: Paul Sclavounos
Title: Professor of Ocean Engineering

Acknowledgements

I would first like to thank all of the people in industry who have helped me during this research. Special thanks to Sandy Butterfield and Jason Jonkman at the National Wind Technology Center for the assistance with the wind turbine design codes.

Secondly, I want to say how much I appreciate the help given to me by Professor Paul Sclavounos. As my thesis advisor, he provided a great source of advice and helped me to better understand how the hydrodynamics portion of my work should be integrated into the whole. I would also thank the members of my thesis committee: Professor Milgram, Professor Burke, Professor Drela, and Dr. Kern. Their input and assistance during this research has been very valuable and is greatly appreciated.

The United States Navy has been wonderful in allowing me to pursue my education here at the Massachusetts Institute of Technology. This has been the experience of a lifetime.

And finally, I want to express my deep love and appreciation for my wife Paun and children Lauren, Garet, and Logan. Their understanding and support during the time I have spent on my research has been invaluable.

Table of Contents

Table of Figures

7

List of Tables

8

Symbols

a: induction factor
A: wave amplitude (m)
A: added mass
B: viscous damping coefficient
B: number of blades
B: damping coefficient
c: cord length
C: restoring coefficient
C_d: drag coefficient
C_l: lift coefficient
C_m: pitching moment coefficient
C_p: power coefficient
CB: depth of center of buoyancy (m)
CG: height of center of gravity (m)
d: floater diameter (m)
d_{tether}: tether diameter (m)
D: water depth (m)
E: modulus of elasticity (MPa)
f: generator frequency (Hertz)
F: force (N)
g: gravitational constant (9.81 m/s^2)
H: tower height (m)
I: mass moment of inertia (kg·m^2)
J: polar mass moment of inertia
L_{arm}: length of moment arm (m)
L_{tether}: length of tether (m)
L_{spoke}: length of spoke (m)
m: mass (kg)
M: moment (N·m)
N: generator rotational speed (rpm)
N_{lines}: number of lines per spoke
P: power (kW)

P: number of generator poles
Q: torque (N·m)
r: radius (m)
t: time (s)
$S_\zeta(\omega)$: ambient spectral density
T: draft (m)
T_m period of oscillation (sec)
U: wind velocity (m/s)
U_{rel}: relative wind velocity (m/s)
w: spoke characteristic dimension (m)
z: vertical position (m)
α: angle of attack
α: power law exponent
β: angle between nacelle and waves
∇: displaced volume of the floater (m^3)
Φ: wave potential
Φ: floater excitation force
η: wave elevation (m)
λ: tip speed ratio
ω: frequency (rad/sec)
ω_{wind}: frequency (rad/sec)
ρ: density (kg/m^3)
Ω: rotor frequency (rad/sec)
σ: stress (Pa)
Ψ: angular position of blade (rotational)
θ_T: twist angle
θ_p: section pitch angle
θ_{wind}: wind incidence angle
θ_{yaw}: nacelle yaw angle
Ξ: complex response amplitude
φ: angle relative to wind
ξ: floater motion (six degrees of freedom)

1 Introduction

1.1 Motivation

Use of wind turbines for electrical power generation has become a major means of generating clean renewable energy around the world. Over the last five years the average annual growth rate for the wind energy sector has been 35% [12]. The main factors driving this growth have been a desire for some countries to reduce their dependence on fossil fuels and an improvement in wind power technology that has made it more economically feasible. The European Wind Energy Association (EWEA), a group representing European wind energy companies, has set a target of 75,000 MW installed wind power by 2010.

Wind energy systems have emerged as a promising technology for the utilization of offshore wind resources for the large scale generation of electricity. The relatively low surface roughness of the ocean results in higher wind speeds. Some of the problems associated with wind power, like taking up too much space on land, are lessened when the machines are moved offshore. Current projects for offshore wind power, like Horns Rev [11], are all situated in relatively shallow water using wind turbines fixed to the sea floor. The use of bottom mounted wind turbines may not be the best option for deeper offshore locations.

Ideally an offshore wind farm would be placed as close to the load it would be supplying and where the winds are of sufficient velocities. The water depths of these locations are sometimes too deep for bottom mounted wind turbines to be economically feasible (example: Hawaii). A wind farm should not interfere with coastal fishing, shipping, and recreational boating. Therefore, mounting wind turbines on floating supports may prove to be the best solution to utilize the wind resources in areas with water depths in excess of 50 meters.

The major goal of this research was to develop a fully coupled dynamic analysis technique which could be used for floating wind turbines. The analysis method had to incorporate wind loading on the rotor blades and wave loading on the floater. Also, a design for the floating support was developed to achieve the desired performance characteristics. The fully coupled analysis method was used to evaluate a wind turbine system mounted on a tension leg spar buoy operating in realistic wind and wave environments.

10

The fully coupled dynamic analysis was performed by combining wind turbine loading and control subroutines and a floater hydrodynamic loading subroutine using a commercially available mechanical dynamics program. A floating wind turbine system was analyzed in the time domain using a computer model. Damping properties of the system were evaluated by simulating free decay tests in the six modes of motion. Simulations included normal operations in various wind and wave conditions and extreme wind and wave event cases. The loading responses on the system components for test cases were evaluated to determine the feasibility of the chosen means of floating support.

1.2 Previous Studies

Floating wind turbine analysis and design research has been limited in the past. European institutions have been the leaders in this field of research. Most of the work has pertained to possible designs for the floating support system and economic analyses of various wind farms using these designs. The following list is a partial account of past research relating to floating wind turbines:

- In the United Kingdom, the FLOAT study [35] was conducted. This research looked at various designs for floating wind farms. Cost estimates were performed on the designs and found to be approximately twice that of bottom mounted wind turbines.

- Research at University College London investigated a design which mounted several turbines on a single structure with the potential advantage of reduced motion response and shared moorings [15], [16]. The results of this work were that the design was prohibitively expensive and might be subjected to excessive wave loading.

- The use of a toroidal shaped floater was evaluated by a group of Italian researchers [2]. This floater supported a single wind turbine in water depths between 30 and 100 meters. The support was held in place by mooring lines under tension. The shape of the floater was chosen to minimize wave interaction, but the design was deemed too expensive to build.

- Recently researchers at Delft University of Technology in the Netherlands performed a study on using a floating support for wind power applications in 50 meters of water. This research was presented at the Offshore Wind Energy in Mediterranean and Other European Seas Conference in April 2003 [6].

1.3 Chosen Floater Design

In the past many means for supporting a floating wind turbine have been proposed. Some of the possible designs are the pontoon, spar buoy (with catenary lines), and tension leg platform.   The requirements for a floating support are:

- Must support its weight and that of the wind turbine

- Must remain upright for all design wind and wave conditions

- Must prevent excessive loading on the wind turbine due to waves acting on floater

- Must be economically feasible

Every design has advantages and disadvantages. Mounting multiple wind turbines on a single pontoon reduces the amount of power line which must be run along the ocean floor. However, the disadvantages are high structural cost for the extremely large pontoon which would be required for adequate spacing, hence high cost, and large wave loads on the structure. The mounting of a single wind turbine on a spar buoy is the simplest and easiest design to build. However, with catenary mooring lines the system is not very stiff in the pitch and roll modes of motion and extremely large loads result on wind turbine components. The tension leg platform has very good performance characteristics (stiff in pitch and roll). However, the structure is relatively complex and hence the cost is likely to be higher.

A design used in this research combined the best features of both the spar buoy and the tension leg platform. It was theorized that a spar buoy which had been stiffened in the roll and pitch modes by using a combination of spokes and lines under tension could meet the requirements for a floating support. The proposed design was called the tension leg spar buoy (see Figure 1.1). The system would be set up such that operators could board the floating wind turbine via a walkway which circles the base of the tower. The inset in the figure shows the system attached to gravity anchors on the seafloor.

12
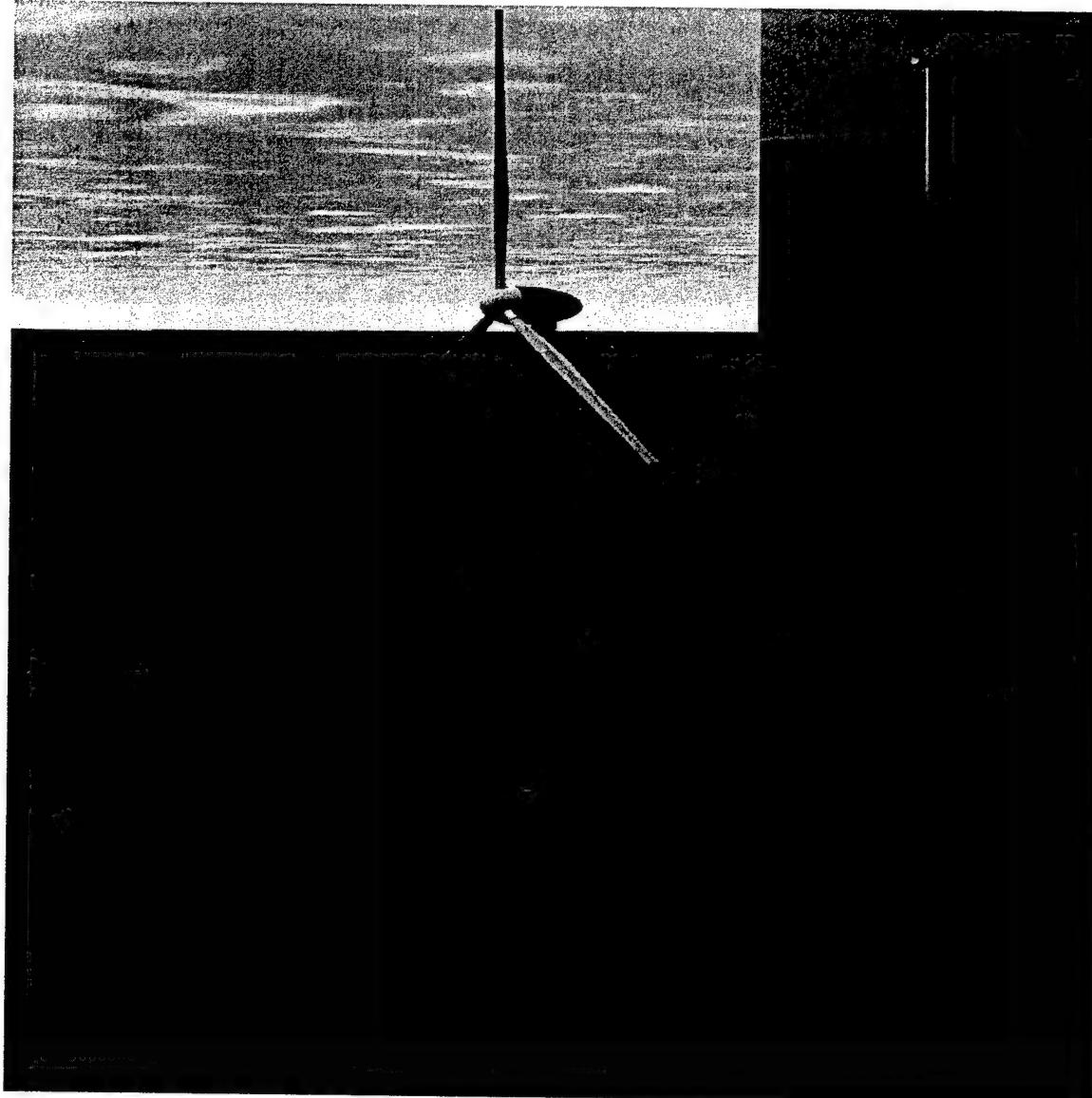
Figure 1.1 Floater design.

Figure 1.2 is a cross-sectional view of the floater structure. The design consists of a tower extension that connects the wind turbine tower to the spar cylinder. The orange portions represent the part of the structure that is normally under water. The relatively small diameter of this structure near the free surface reduces wave loading on the floater. A majority of the buoyancy comes from the spar cylinder. The figure shows the ballast chamber which has fill and drain pipes which run up the structure to the catwalk where they can be connected to pumps onboard a support ship. Installation of the system is accomplished by filling the ballast chamber and attaching the tethers. Then the ballast is pumped off and tension put on the lines.
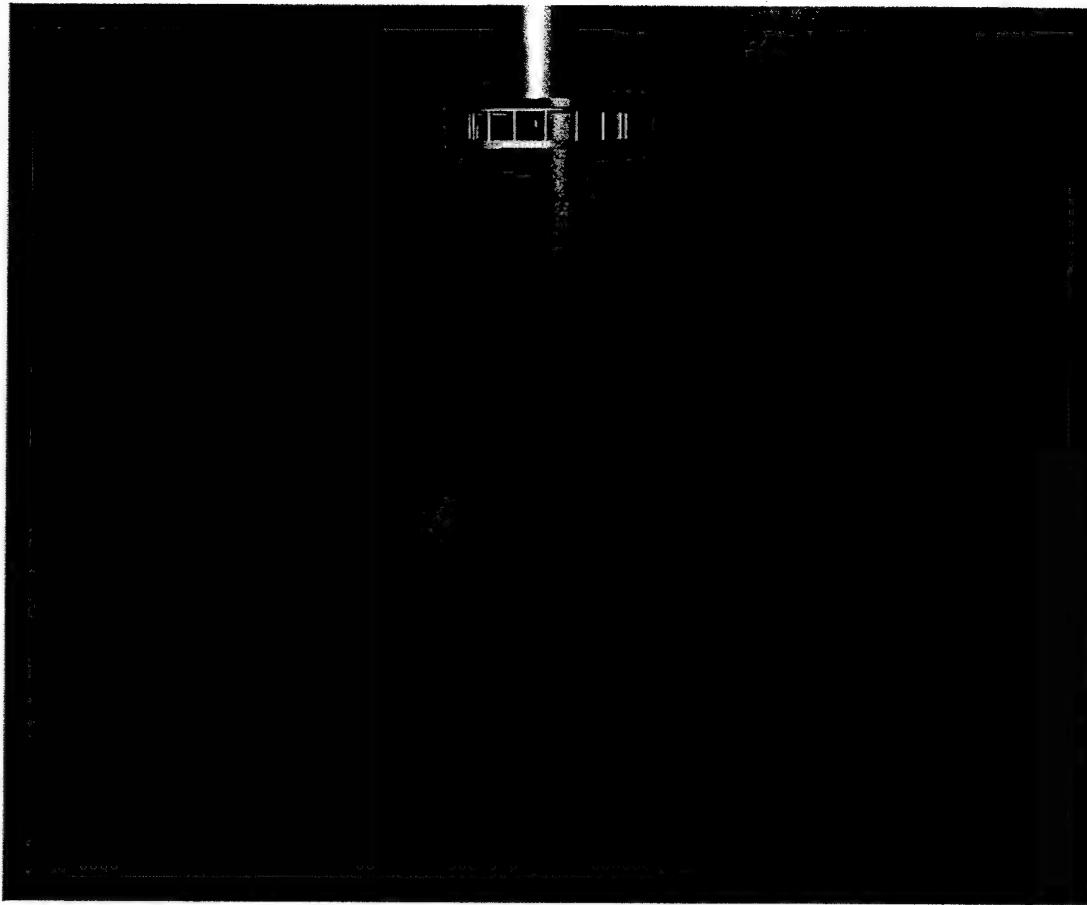
Figure 1.2 Cutaway of floater.

The wind turbine tower is attached to a vertical cylinder which provides a majority of the buoyancy for the system. The spokes are attached to tethers which connect the system to either anchors driven into the seafloor or gravity anchors. The design has relatively low restoring coefficients in the horizontal translational modes of motion.

The computer model used in this research models the spokes as rectangular members with square cross-sections. These spokes are reinforced to increase their stiffness in bending. The spokes could be made buoyant to reduce the required size of the spar cylinder. However, the use of a truss structure might be the most economical means to fulfill the function of the spokes which is to increase the stiffness of the system in all of the rotational modes of motion. One of the benefits of using a tension leg spar buoy is that the pitch and roll motions are lower than other types of floating support. As shown in Figure 1.3, the structure pitches very little when the tension leg spar buoy undergoes surge motion. The pitch motion is resisted by the tethers. Having pre-tension in the lines allows the system to absorb pitch / roll moments caused by the wind and waves. This rotational stiffness is determined by the spring coefficient provided by the lines and the length of the spokes.

14
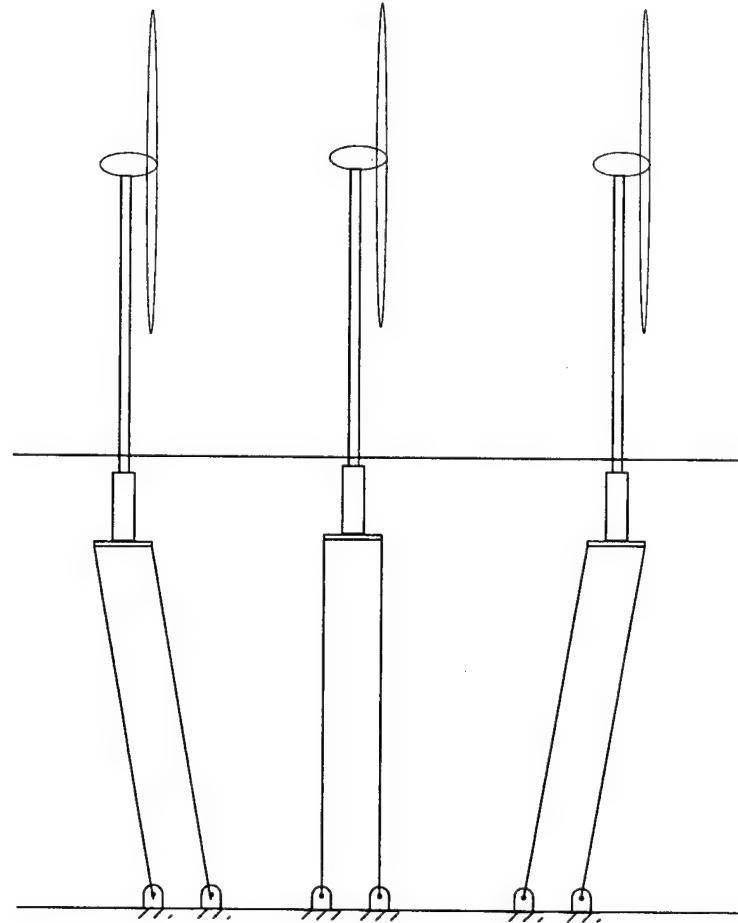
Figure 1.3 Diagram of system motion with horizontal excitation.

The floater is assumed to be a rigid body connected to the seafloor by flexible lines. The tethers only provide rotational stiffness so long as they maintain tension. Therefore, the amount of reserve buoyancy is a key design parameter which must be high enough to ensure that the lines remain under tension to prevent excessive amounts of pitch and roll which have a large effect on wind turbine loading.

1.4 Outline of Thesis

Many equations used in the modeling of the fully coupled analysis technique are described in this report. However, not all of the basic theory is covered in depth. Where necessary the applicable sources for this theory are given. The following is an outline of this thesis.

- Chapter 2 provides a basic description of the wind turbine. The primary components of the machine are described. This chapter also includes the wind turbine outputs and a general description of the wind environment.

- Chapter 3 describes the problem of modeling the fully coupled floating wind turbine system. The different forces and moments acting on the floater and turbine rotor are described. Finally, the different loading conditions used in evaluating the floater and analysis technique are presented.

- Chapter 4 is a brief description of the hydrostatic properties of the system. The effect of static loading on system deflection and the restoring coefficients are discussed.

- Chapter 5 details the hydrodynamic analysis of the system. The six modes of motion and their associated equations are detailed.

- Chapter 6 deals with hydrodynamic loading on the floater. Both the inertial and drag loading equations are described. The production of random wave records is discussed.

- Chapter 7 describes the means by which the floating wind turbine system model is generated and analyzed. The various computer codes which are used to conduct the fully coupled dynamic simulations are discussed. The wind turbine model is also detailed.

- Chapter 8 presents the results of the damping analysis of the system. Each of the individual modes of motion is discussed. The final portion of the chapter gives the results of the multiple mode damping tests.

- Chapter 9 details the results of the numerical simulations of the system model for normal and extreme operating environments. The loading responses of the wind turbine components and the lines are discussed.

2 Wind Turbine

A wind turbine is a device that coverts the kinetic energy in wind into useful work output. The output can be in the form of electrical power. In the last decade there has been an increased interest in using wind turbines to produce electrical power. This chapter is included to give the reader a basic understanding of wind turbines. A full description of how a wind turbine operates can be found in "Wind Energy Explained" by Manwell, McGowan, and Rodgers [24].

2.1 Components

The most common wind turbine design is the Horizontal Axis Wind Turbines (HAWT). The output shaft of the HAWT is parallel to the ground. A wind turbine consists of seven major subsystems. These subsystems are the: rotor, drive train, nacelle, generator, tower and foundation, control system, and electrical output system.

2.1.1 Rotor

The rotor consists of normally two or three blades attached to a hub. The system performance of the wind turbine is based on the selection of blade number, shape, and length. The rotor can be either upwind or downwind design. Most wind turbines currently in use are three bladed upwind designs. The blades can be designed with either constant pitch or controllable pitch. The power of the rotor is controlled via aerodynamic control (stall regulation) or variable pitch blades.

2.1.2 Drive Train

Wind passing across the rotor blades produces lift and drag. The lift force generates a torque about the rotational axis of the rotor. The output shaft of the wind turbine rotates at a relatively slow speed. For most electric generators, the rotor output must be stepped to a higher speed. A gearbox is used to step up the rotor output to spin the generator. The rest of the drive train consists of journal and thrust bearings which support the shafts and minimize movement of the drive drain in the radial and axial directions. The gearbox in wind turbines is one of the major sources of failure for the system. For this reason some wind turbines are designed to have generators that operate at the speed of the rotor.

2.1.3 Nacelle

The nacelle is the structure that houses the generator and drive train. This structure protects the wind turbine equipment from the elements. Offshore wind turbines are different from land based wind turbines in that the nacelle is sealed to prevent entry of sea air. A cooling system is installed to transfer the heat generated by the wind turbine machinery to the ocean air passing over the nacelle.

The alignment of the nacelle is controlled by the yaw system. This system connects the nacelle to the top of the tower. The yaw direction of all upwind wind turbines must be actively controlled so that the rotor faces into the wind. Some downwind turbines use free yaw systems, which align themselves with the wind automatically. Yaw of a wind turbine generates a gyroscopic moment proportional to the rate of yaw and the rotational inertia of the rotor. Therefore, rate of yaw of the nacelle must be limited. Active yaw control is usually accomplished using a pinion and bull gear arrangement.

2.1.4 Generator

The generator converts the mechanical work input of the wind turbine into useful electrical output. Most wind turbines use either induction or synchronous generators to accomplish this task. The majority of wind turbines use induction generators. The rotor of an induction generator spins slightly faster than the rotating magnetic field on the stator. The difference between the generator rotor frequency and the rotating magnetic field on the generator is called slip. The slip of an induction generator determines the amount of power produced by the machine.

2.1.5 Tower and Foundation

The wind turbine nacelle and rotor must be supported at their operational height. The height of the supporting tower can be over 100 meters high. The height of the tower is determined by the rotor diameter and the wind conditions at the site. The speed of wind increases with height above ground due to wind shear. Higher wind speeds result in increased power output. It is therefore desirable to raise the wind turbine nacelle up off the ground to take advantage of this effect.

The stiffness of the support tower must be chosen such that there is no dynamic coupling between the rotor and the tower. Coupled vibrations lead to reduced fatigue life of the machine. Downwind turbines also have to deal with vortices shed off of the tower, called tower shadow. As the rotor blades pass through the tower shadow noise and oscillations are produced. This results in increased noise and vibrations of the rotor blades.

18

2.1.6 Control System

The control system changes the blade pitch, nacelle yaw, and generator loading of a wind turbine. The yaw is changed to keep the nacelle aligned with the wind in order to maximize power output. If torque on the rotor becomes too high the control system can also change the yaw such that the rotor presents a smaller frontal area to the wind, and thereby reduces the amount of torque produced. The control system can also change the pitch of the blades to alter the amount of torque produced by the rotor. The purpose of the control system is to maximize power output and fatigue life. Manufactures use various means to accomplish this purpose.

2.1.7 Electrical Output System

Electrical output of the generator must be transferred to the electric grid or electric load. The output passes though other electrical components like: cables, transformers, power factor correction capacitors, solid state power converts, and switchgear. Some wind turbine designs use solid state power converts for increased flexibility. Normally the output voltage is stepped up to 34.5 kilovolts. Offshore wind turbines typically send power through cables buried on the seafloor.

2.2 Wind Turbine Output

Wind passing over the rotor blades generates torque and thrust. The torque is then converted into electrical power output. Rotor torque increases with wind speed. In order for the generator to produce useful power output the wind speed must exceed the cut-in speed of the generator. Wind speed increases to the rated power output of the wind turbine. Above the rated speed wind turbine power is controlled by changing the blade pitch or by stalling a portion of the blade. The speed above which the wind turbine can no longer operate is called the cutout speed. Figure 2.1 is a graph showing the power versus wind speed for a 500 kilowatt wind turbine. This graph was generated using a program called PROPID which is available on the National Wind Technology Center website.
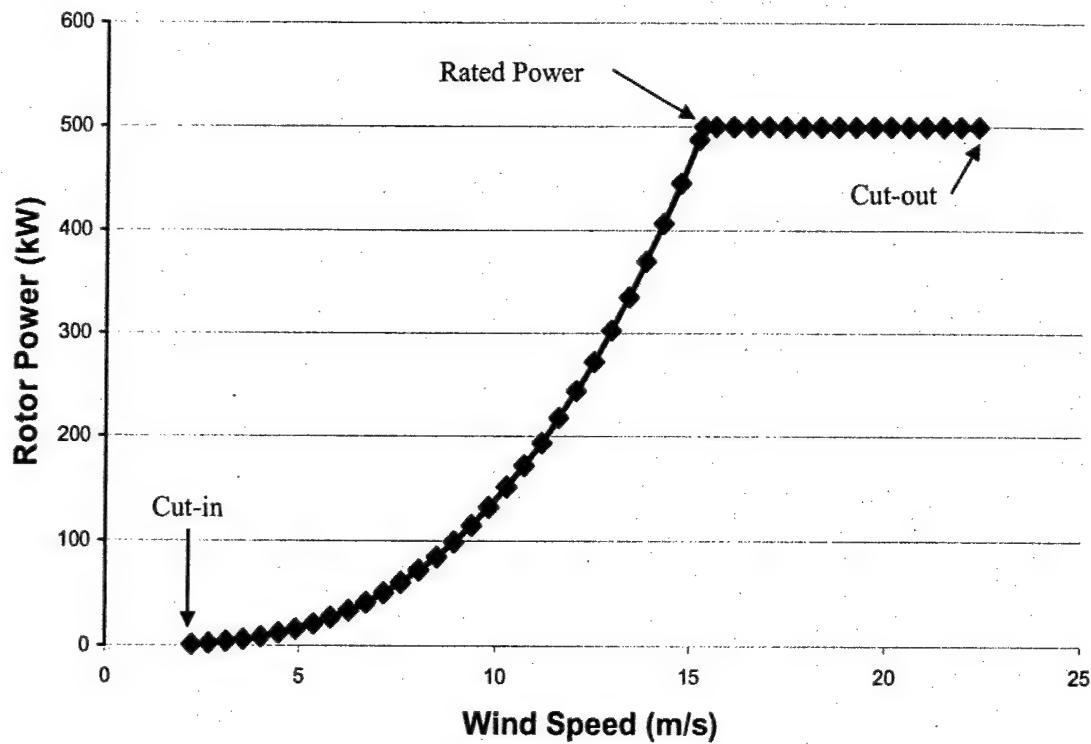
Figure 2.1 Rotor power versus wind speed.

2.3 Wind Environment

One of the benefits of building wind turbines offshore is the low surface roughness of the sea. Wind passing of obstacles such as trees, houses and hills acts to lower the wind speeds closer to the surface. Wind speeds increase with height above the surface. The wind profile is normally modeled using either the power law profile or the logarithmic profile [29].

$$\text{Power Law Profile: } V(z) = V(z_r) \cdot \left(\frac{z}{z_r} \right)^{\alpha}$$

$$\text{Logarithmic Profile: } V(z) = V(z_r) \cdot \frac{\ln(z/z_o)}{\ln(z_r/z_o)}$$

(2.1)

where:

$V(z)$ is the wind speed at height z
$V(z_r)$ is the reference wind speed
z is the height above ground
z_r is the reference height above ground used for fitting the profile
z_o is the roughness length
α is the power law exponent

20

A draft of IEC 61400-3 Safety Requirements for Offshore Wind Turbines [20] states that for offshore environments the power law exponent should be assumed to be 0.14. A value of 0.2 is typically used for normal wind environments on land. When the logarithmic profile is used for calm seas, the surface roughness length (z_o) is 0.50 millimeters (Table 2.2 of [24]). The wind profile out at sea is such that wind speeds are typically higher than on land for the same height above the surface. The difference in wind profiles improves the operation of the wind turbine. An offshore wind turbine rotor can be mounted on a shorter tower and still produce the same amount of power output as a land-based counterpart.

The wind speed increases with height above the surface of the water. As the rotor spins, the blades pass through the wind profile. This results in a changing inflow speed to each blade that varies with time in a periodic manner. Oscillating thrusts and moments are produced by the blades with a frequency corresponding to the number of blades (N) times the rotational speed of the rotor. Modeling the wind in a turbulent manner is important since actual winds are never constant. Figure 2.2 is a wind record for a mean wind speed of 20 meters / second.
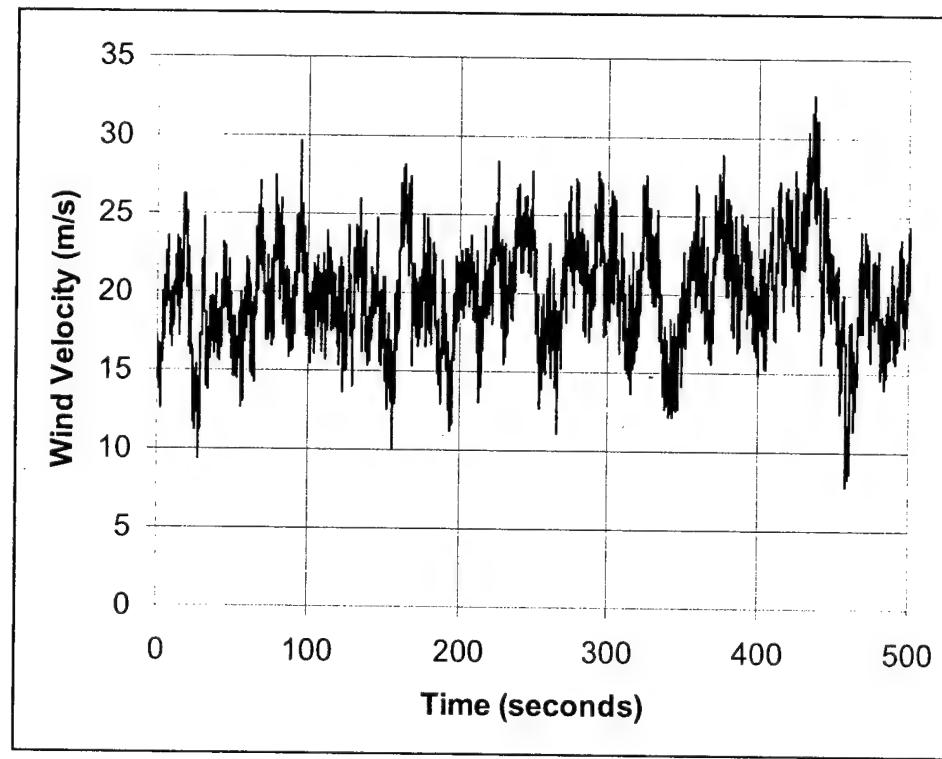
Figure 2.2 Turbulent wind record for 20 meter/second mean wind speed.

3 Problem Statement

Several problems must be solved in order to determine the feasibility of a tension leg spar buoy support for an offshore wind turbine. One part of the analysis is to determine the effect of floater motion on wind turbine performance and fatigue life. Another important part of the analysis is to determine the loading on the tethers that attach the floater to the ocean floor.

The wind turbine / floater system are acted upon by both waves and wind. The combination of the various components leads to the analysis of a coupled dynamic system. When wave loads cause the floater to move, the nacelle moves with it. The motion of the nacelle results in changes to the inflow wind to the turbine rotor. Changes in the inflow to the rotor can result in changes in rotor thrust loading. This change in thrust is felt by the floating support. Angular motion of the floater can also result in gyroscopic loads on the rotor.

The wind turbine itself is a very complex system to model accurately. Several wind turbine simulation codes can be used to accomplish this task. For this research the wind turbine is modeled using the FAST wind turbine code [4] in conjunction with ADAMS [1]. FAST (Fatigue, Aerodynamics, Structures, and Turbulence) code is produced by the National Renewable Energy Laboratory. ADAMS (Automatic Dynamic Analysis of Mechanical Systems) is commercially available software that is widely used to model mechanical systems. Codes modeling the floater loading and mechanical properties are coupled to the ADAMS wind turbine model to determine the effect placing it on a floating platform had on the wind turbine components. The system is modeled as a group of 71 rigid bodies (called parts) connected by springs and dampers. For example each rotor blade consists of 15 different parts, one for each blade element.

Loads due to wind and waves on the individual parts are calculated relative to each part's body based coordinate system. All of the forces and moments from the individual components of the system are incorporated into a complete dynamics analysis relative to the global coordinate system. The motion of every part is determined by evaluating of the combined dynamic equations for the system. These calculations are carried out in the time domain using the ADAMS Solver. The analysis tools and the system model are discussed in Chapter 7.

3.1 Modes of Floater Motion

The combined rigid body of the wind turbine and floating support undergoes oscillatory translation and rotation due to wind and wave loadings (see Figure 3.1). Surge and sway are horizontal motions along the x and y axes, respectively. The horizontal axes of the system are aligned with the four spokes to which the floaters tethers are connected. Heave is the vertical motion of the floater. The oscillatory angular motions are referred to as roll, pitch and yaw. Surge, sway, and yaw are the three rigid body motions. The tether lengths are assumed to remain constant during rigid body motion. Pitch, roll and heave occur when the tethers undergo elastic elongation / contraction. Heave also occurs when the structure undergoes surge or sway motion (like an inverted pendulum). The origins of the three axes are located at the center of the floater on the calm waterline. The reference for the global coordinate system is a point at the center of the tower where it connects to the floater (on the free surface). The orange portions of the structure are submerged when the system is at rest.
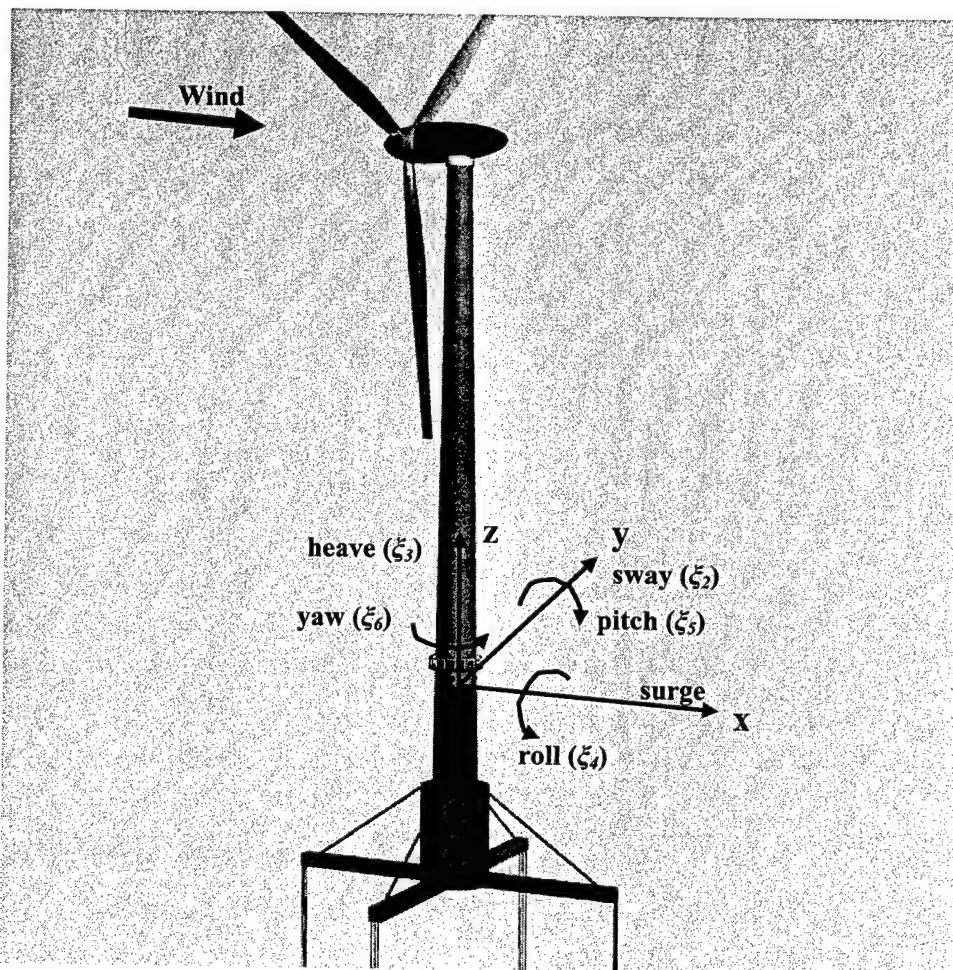
Figure 3.1 Floater modes of motion.

3.2 Forces and Moments

Forces and moments due to gravity, wind, and waves are exerted on both the wind turbine assembly and the floater. Wind forces and moments are primarily exerted on the rotor of the wind turbine, while wave forces act only on the floater. The forces and moments produced on the wind turbine blades are transferred to the floater. The following is a discussion on the forces and moments acting on the combined system.

3.2.1 Wind Turbine

Wind passing across the rotor blades produces lift and drag forces. The two forces result in a torque on the rotor, a thrust along the rotor axis, and a pitching moment. The thrust on the blades is also felt by the tower and the floater. Figure 3.2 is a diagram of forces and moment on a stationary airfoil in a wind stream. For ideal non-separated flow, these forces and moment act along the cord at a distance of approximately $c/4$ from the leading edge [24], where c is the cord length.
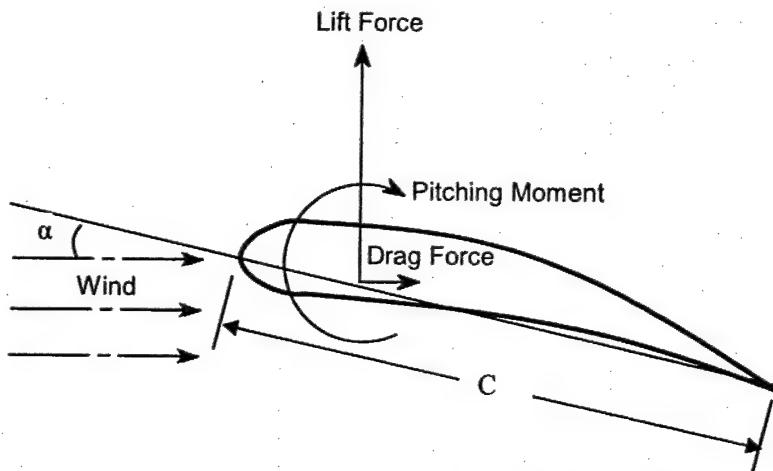
Figure 3.2 Forces and moments on a stationary airfoil.

The lift force is defined as the force component that is perpendicular to the incoming air flow. The drag force is defined to be parallel to the direction of the incoming airflow. Drag arises from vortex shedding, viscous friction, and separated wakes. The pitching moment is the summation of the moments created by the individual forces acting on the airfoil. This moment acts about an axis that is perpendicular to the cross-section of the airfoil. On a wind turbine the rotation of the rotor increases the inflow into the airfoil, while at the same time changing the effective angle of attack.

24

The thrust on individual blades causes a moment at the blade root which is perpendicular to the pitching moment. When the nacelle is aligned as in Figure 3.1 these moments act about the y and z axes (rotor torque acts around the x-axis.) The orientations of the blades change as they rotate. Therefore, cyclic moments are produced with frequencies equal to the blade frequency. These moments are excitation for the floater in both yaw and pitch. It should be noted that the effects of these moments will be small relative to the rotor torque and moment due to rotor thrust at the base of the tower. The reasons for this will be shown in the analysis section.

Wind speed increases with elevation. Oscillating forces and moments are produced as the rotor blades pass through this varying wind field. These cyclic loads can affect the fatigue life of large diameter wind turbines. The magnitudes of these oscillating loads on the floater are small compared to the forces and moments generated by the rotor torque and the rotor thrust acting with the moment arm of the tower. The oscillating forces may excite resonant motion of the floater and wind turbine and must therefore be considered.

Gyroscopic motion of a wind turbine is a factor in turbine fatigue. In land based turbines this results primarily from yawing of the wind turbine. When the wind turbine is mounted on a floating structure, both yaw and pitch of the floater cause gyroscopic moments. When the plane of rotation of the wind turbine rotor is changed, a precession torque is developed. This precession torque acts about an axis perpendicular to both the rotor axis and the axis about which the plane of rotation is being changed. Pitch motion will generate a gyroscopic moment while roll motion will not produce a gyroscopic moment since the plane of rotor rotation does not change during roll when the wind turbine is aligned as in Figure 3.1. The gyroscopic moment (M_{gyro}) produced is the cross product of the angular momentum vector ($J\vec{\Omega}$) and the angular velocity vector ($\dot{\vec{\xi}}$). Where the angular velocity is the first derivative of the pitch, roll, or yaw motions [24, p.148]:

$$\vec{M}_{gyro} = \dot{\vec{\xi}} \times J\vec{\Omega} \qquad (3.1)$$

where J is the polar moment of inertia of the rotor and $\vec{\Omega}$ is the angular velocity vector of the rotor.

3.2.2 Floater Wave Loading

As shown in Figure 3.1, the tethered spar buoy consists of a vertical cylinder that provides buoyancy and four spokes to which the tethers are attached. The floater is symmetrical about the z-axis. Therefore, only heave, surge, and pitch are considered in the hydrodynamic analysis. There is very

little wave excitation in the yaw mode, since the major portions of the floater are vertical cylinders. However, forces and moments generated on the wind turbine may excite the other modes of floater motion. The following discussion deals with surge, pitch, and heave excitation. Sway and roll are similar to surge and pitch since all these modes are caused by horizontal forces on the submerged structure. Therefore, the discussion for surge and pitch are applicable to sway and roll.

For a typical spar buoy, the pitch and surge motion equations are coupled. The system is not very stiff in the surge direction. The stiffness of the system in both heave and pitch will result in very small motions of the floater in these two modes. Since the system acts like an inverted pendulum, some of the motion in the heave mode is due to the set-down caused by surge. As the floater moves away from the rest position its draft increases. This coupling between surge / sway and heave is non-linear and determined by the length of the tethers. Shorter tethers have more coupling, since set-down is large for the same amount of horizontal motion.

The motions of the floater may have an effect on the wind turbine. Wave loading is assumed to be produced by regular sinusoidal waves. The motion of a floating structure in irregular waves can be determined by linearly superimposing the results from multiple regular waves to produce realistic seastates. This method will discussed later in this thesis and is fully described in Faltinsen, 1990 [13] and Sclavounos, 2003 [31].

The analysis of the tethered spar buoy uses the long wavelength assumption that applies when the wavelength is much longer than the spar diameter ($\lambda > 5$ d). This assumption results in no significant wave disturbance being generated by the spar buoy. The excitation forces are caused by both incoming wave and diffraction potential flow effects. The excitation forces and moments are obtained from the incoming wave potential and using analytical expressions for the added mass terms. The force caused by the incoming wave is approximated using the long-wavelength GI Taylor equations [31]. The equations of motion for the spar buoy are presented in the analysis section.

The behavior of a floating wind turbine is complex. Modes of motion interact to produce complex behaviors. For example, normal operation of a floating wind turbine will produce a yaw moment on the floater two ways. The first yaw moment is due to the oscillating yaw produced by the normal operation of the rotor blades spinning which results in the yaw moment changing with time. The second yaw moment is produced due to the fact that a floating wind turbine tilts slightly while under load. With both wind and waves aligned with the x-axis, a roll moment is exerted on the floater by the generator torque. The tethers which lie on the y-axis (lines 2 and 4) resist this motion. The

moment causes a small roll deflection of the floater due to the elongation of one tether and the contraction of another tether on the opposite side of the floater. This roll deflection is small due to the relatively high modulus of elasticity of the tethers. Roll of the floater results in the nacelle moving off axis. This movement produces a moment arm along the y-axis that is acted on by the rotor thrust. A yaw moment is produced. It should be stressed that in most cases this moment is small, since the stiffness of the system in roll is high. Figure 3.3 shows how roll is generated by torque on the generator (amount of roll is exaggerated). With wind into the rotor, you can see how a moment is produced about the z-axis.
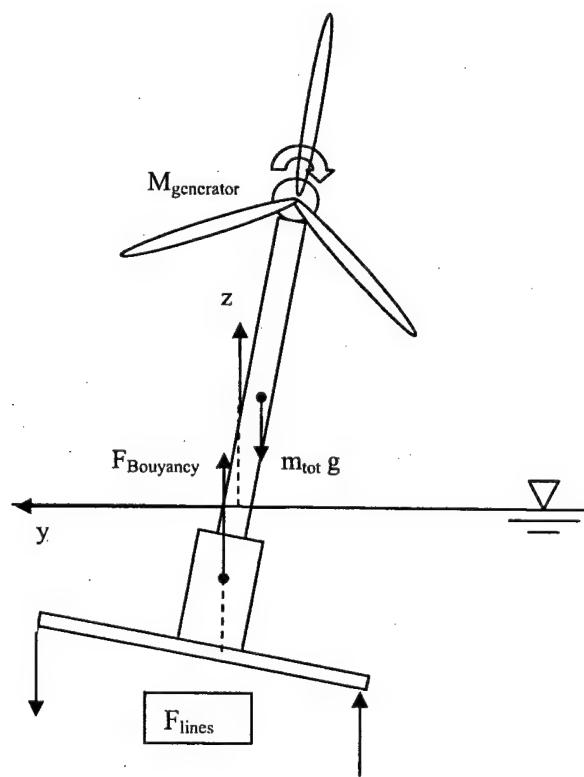
Figure 3.3 Roll Diagram

3.3 Loading Conditions used for Analysis

For most of the following discussion wind is assumed to blow in the positive x-direction and the rotor is aligned along the x-axis. This assumption is only for the purposes of this discussion. The actual calculations take into account variations in the wind and wave directions. However, any angular difference between wind and waves can be accounted for using the wave incidence angle, β. Five different loading conditions are applicable to the analysis presented in this thesis.

27

- Static loading with no wind or waves
- Static loading with constant wind.
- Static and dynamic loading with waves acting on the floater and no wind.
- Static and dynamic loading for random wind and/or waves on the system.
- Extreme wind or wave loading events.

The static loading condition accounts for forces and moments which arise from gravity and buoyancy. The floater supports the combined weight of the system. The floater has excess buoyancy (buoyant force > system weight), which puts tension on the four tethers. The buoyancy is dependent on the submerged volume of the floater. For a simple spar buoy, the total volume of seawater displaced by the floater (∇) is a function of the floater diameter (d) and floater draft (T):

$$\nabla = \frac{\pi}{4} d^2 T \qquad (3.2)$$

This displacement results in an associated buoyant force that is greater than the total weight being supported. The excess buoyancy produces tension in the four tethers. The following equation presents how to calculate the static tether force:

$$F_{tethers} = \left(\nabla \cdot \rho_{sw} - m_{total} \right) g \qquad (3.3)$$

where m_{total} is the total mass of the system.

The second loading condition is steady state winds with no waves. This loading condition is very useful for the damping coefficients for the system. Steady state winds result in nearly constant thrust and torque being exerted on the rotor. Movement of the floater results in changes to the wind inflow to the rotor. This change in wind inflow alters the thrust and torque loading on the rotor results. The wind turbine acts as a damper for some modes of system motion.

The third loading condition is applicable when the turbine is not operating and waves are acting on the floater. Waves acting on the floater produce excitation forces and moments in the surge, sway, roll, pitch and heave modes of motion. Since the floater is a right circular cylinder, yaw excitation is generated only by waves acting on the spokes. This condition is used to model shutdown operations.

The next loading condition has both random wind and waves acting on the system. This condition is useful for determining expected system response during normal operations for different reference wind speeds and sea states.

The response of the system to extreme wind and wave events is a key design feature which has to be understood if a particular system is being analyzed for suitability. Wind and wave inputs modeling extreme events are used in to the numerical simulation. The fully coupled dynamic response is evaluated and the resulting component loading values are determined.

4 Static Analysis of Floater

The physical characteristics and loading conditions of the combined floater / wind turbine system must be understood in order to develop a computer model that accurately predicts the physical response. The purpose of this chapter is to describe the analytical methods used to solve the problems presented in the previous chapter. First, the static analysis of the system is presented. The means by which static deflection can be obtained by calculating the floater restoring coefficients are described.

An important design parameter is tether line stress. If line stress exceeds the ultimate stress for the tethers catastrophic failure of the system could result. Excess buoyancy of the spar is used to put tension on the tethers. The tension present in the tethers while the system is at rest is referred to as the pre-tension. Excitation forces and moments by waves and wind on the system cause the line stress to vary about this tether pre-tension. The following equation is used to calculate the pre-tension stress of tethers with diameter (d_{tether}) for a given number of tethers per spoke ($N_{tethers}$):

$$\sigma_{line} = \frac{\left(\nabla \cdot \rho_{sw} - m_{total}\right)g}{4 \cdot N_{tethers} \cdot \frac{\pi}{4} d_{tether}^2} = \frac{F_{tethers}}{N_{tethers} \cdot \pi \cdot d_{tether}^2} \tag{4.1}$$

External forces on the system cause increases and decreases in the tether line stresses. As described above a moment will cause lines to increase and decrease in tension. Changes in vertical forces are shared by the four tethers. As the floater moves line stresses change. It is important to know how the line stress in each of the four tethers will change during operations.

In steady state operation, static loading of the wind turbine produces a horizontal force along the x-axis called thrust. This force causes a horizontal displacement of the floater in the x-direction (see Figure 1.3). This thrust is resisted by a horizontal restoring force produced by the tethers as their fairlead position is moved from the rest position which is directly above the anchor point for each tether. As the floater surges away from the rest position its draft increases, due to the fact that the tethers act as rods in tension. This increase in draft would cause an increase in the line tension. However, for small surge displacements ($\xi_1 \ll$ water depth, D) a linearization assumption can be made that the line tension remains constant. This assumption is based on the fact that the tethers will have a very large tension stress while at rest. The draft of the buoy is also assumed not to increase for small surge motions. To the leading order, the surge and sway restoring coefficients are identical due

to symmetry. This restoring coefficient can also be obtained by setting the moment about the tethers anchors on the sea bottom to zero and solving for the force which produces an opposite moment to the moment due to excess buoyancy for a given displacement. For small displacements (small angle approximation), the surge and sway restoring coefficients are given by the following equation:

$$C_{11} = C_{22} = \frac{F_{tethers}}{L_{tether}}$$
(4.2)

where L_{tether} is the water depth minus the depth at which the lines connect to the buoy. Horizontal displacement for a given loading can then be found by dividing the force applied to the floater by the restoration coefficient as described by expression (4.3). These restoration coefficients are also used when estimating the natural periods in surge and sway.

$$\xi_1 = \frac{F_1}{C_{11}}$$
$$\xi_2 = \frac{F_2}{C_{22}}$$
(4.3)

Heave restoring forces results from both tether and hydrostatic effects. If the structure moves only in the heave direction the tethers extend and contract. For a system using stiff lines for tethers, this restoring mechanism is much greater than the hydrostatic restoring mechanism. The heave restoring coefficient is given by the following equation:

$$C_{33} = \frac{4 \cdot E_{tethers} A_{tethers}}{L_{tethers}} + \rho_{sw} g A_{wp}$$
(4.4)

where $A_{tethers}$ is the total cross sectional area of the tethers attached to a spoke. The vertical displacement from a vertical load can be found by:

$$\xi_3 = \frac{F_3}{C_{33}}$$
(4.5)

Wave loading on the submerged structure creates pitch and roll moments on the system. Thrust on the rotor acting along with the moment arm of the tower creates a moment about the y-axis, which also results in pitch of the floater. Pitch and roll restoring coefficients are similar due to symmetry. Pitch and roll restoring coefficients are calculated by taking into account the moments produced by the lines due to extension and contraction, the moment due to line tension ($F_{tethers}$), the moment due to

system mass, and the moment due to system buoyancy (see Figure 4.1). For stiff lines the largest restoring moment comes for the extension and contraction of the lines on the opposite sides of the axis about which the moment is being applied. The restoring coefficients can be obtained by assuming a small rotation ($\xi_{4 \text{ or } 5}$) at any point along the center of the tower / spar and summing the moments produced. The following is a derivation of the roll restoring coefficient.

$$\sum M_{Base} = M_{Extend} + M_{Contract} + M_{buoyancy} + M_{gravity} + M_{tethers}$$

$$F_{tethers} = F_{buoyancy} - m_{total} g$$

$$M_{Extend} = -\underbrace{\frac{(E_{tether} \cdot A_{tethers})}{L_{tether}} \left(L_{spoke} + \frac{d}{2}\right) \sin(\xi_4)}_{\text{change in line tension due to elongation of one set of lines}} \underbrace{\left(L_{spoke} + \frac{d}{2}\right)}_{\text{moment arm}}$$

$$M_{Contract} = \underbrace{\frac{(E_{tether} \cdot A_{tethers})}{L_{tether}} \left(L_{spoke} + \frac{d}{2}\right) \sin(\xi_4)}_{\text{change in line tension due to contraction of one set of lines}} \underbrace{\left(-L_{spoke} - \frac{d}{2}\right)}_{\text{moment arm}}$$

$$M_{Extend} + M_{Contract} = -2\frac{(E_{tether} \cdot A_{tethers})}{L_{tether}} \left(L_{spoke} + \frac{d}{2}\right)^2 \sin(\xi_4)$$

where d is the spar diameter and T is the draft of the spar. The center of buoyancy is at $z = -T/2$. The center of gravity for the system at rest is $z = z_g$. The length of the spokes extending beyond the spar is L_{spoke}.

$$\sum M_{Base} = \left[-2\frac{(E_{tether} \cdot A_{tethers})}{L_{tether}} \left(L_{spoke} + \frac{d}{2}\right)^2 + F_{bouyancy} \cdot \frac{T}{2} + m_{total} g \cdot (z_g) - (F_{buoyancy} - m_{total}g)T \right] \sin(\xi_4)$$

small angle approximation: $\sin(\xi_4) = \xi_4$

$$\sum M_{Base} = -\xi_4 \left(2\frac{(E_{tether} \cdot A_{tethers})}{L_{tether}} \left(L_{spoke} + \frac{d}{2}\right)^2 - F_{bouyancy} \cdot \frac{T}{2} - m_{total} g \cdot (z_g) + (F_{buoyancy} - m_{total}g)T \right)$$

$$-F_{bouyancy} \cdot \frac{T}{2} - m_{total} g \cdot (z_g) + (F_{buoyancy} - m_{total}g)T = F_{buoyancy} \frac{T}{2} - m_{total}g(z_g + T)$$

$$\sum M_{Base} = -\xi_4 \left(2\frac{(E_{tether} \cdot A_{tethers})}{L_{tether}} \left(L_{spoke} + \frac{d}{2}\right)^2 + F_{buoyancy} \frac{T}{2} - m_{total}g(z_g + T) \right)$$

Therefore, the roll and pitch restoring coefficients are found to be:

$$C_{44} = C_{55} = 2\frac{(E_{tether} \cdot A_{tether})}{L_{tether}} \left(L_{spoke} + \frac{d}{2}\right)^2 + F_{buoy} \frac{T}{2} - m_{total}g(z_g + T) \qquad (4.6)$$
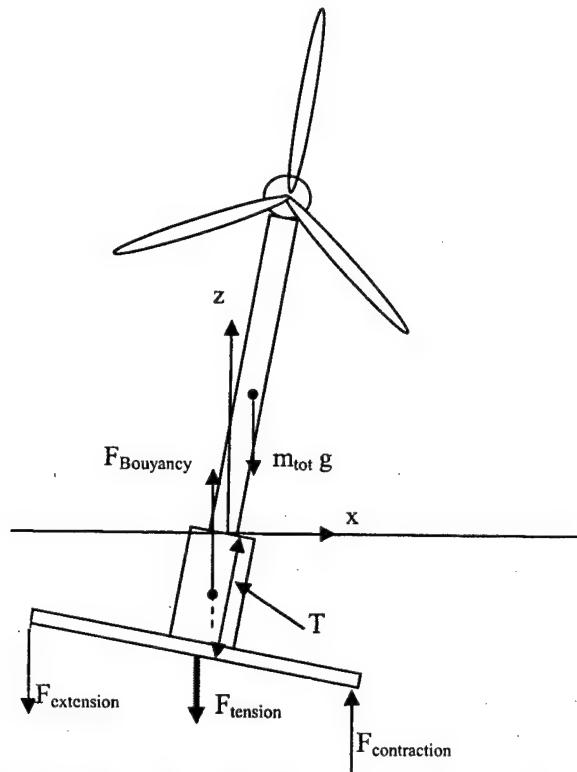
Figure 4.1 Diagram used to calculate pitch restoring coefficient.

The restoring moments due to the change in water plane during pitch and roll are small for this system and are therefore ignored. It is important to understand that this restoring coefficient is only an approximation. The actual model used in the fully-coupled simulation has each of the individual forces (lines, buoyancy, gravity, etc.) that produce the restoring effect. The approximation of this restoring coefficient is useful in a linear analysis of the system.

For any applied moment, the amount of pitch or roll motion can be found by the following equation:

$$\xi_4 = \frac{M_4}{C_{44}}$$

$$\xi_5 = \frac{M_5}{C_{55}}$$

(4.7)

Although wave forces will not generate significant yaw motion of the floater, wind turbine loading can cause yaw motion. The restoring coefficient for yaw is similar to the surge restoring coefficient. Movement of the tether fairleads produces horizontal force components which act along the spokes and buoy diameter to generate moments that counteract the yaw motion. The yaw restoring coefficient and yaw displacement is found using the following equations:

33

$$C_{66} = \frac{\left(\dfrac{d}{2} + L_{spoke}\right)^2}{L_{tethers}} \cdot F_{tethers}$$

$$\xi_6 = \frac{F_6}{C_{66}}$$

(4.8)

The preceding equations defined the response of the floating wind turbine system to external loads. The restoring coefficients are estimates of the system behavior. The fully-coupled floating wind turbine model does not use these coefficients. Instead, the various physical properties (lines, masses, and buoyancy) are modeled individually and their combined behavior determined by the mechanical dynamics solver. This will be discussed more fully in Chapter 7. The estimates of the restoring coefficients are useful in predicting the natural periods of the system and verification of the time domain hydrodynamic analyses using linear theory.

5 Dynamic Analysis of Floater

The linear frequency domain method can be used to obtain an initial understanding of the importance of the various modes of motion of the floater. This method allows the response of a system to be determined analytically instead of empirically. This method allows for fast calculations that predict motion in a hydrodynamic environment. Linear analysis is a useful tool for determining the motion of the floater for small wave amplitudes. However, the combined wind turbine / floater system has non-linear excitation and quadratic damping properties that are better handled in the time domain. Large amplitude waves result in large horizontal displacements. Many of the restoring coefficients for the system are non-linear for large displacements. Also, the non-linear cross-coupling between surge/sway and heave (due to set-down) becomes more pronounced as the horizontal motions increase. The non-linear cross-couplings are not accounted for in a frequency domain analysis.

The frequency domain analysis is primarily used to verify the proper operation of hydrodynamic computer code coupled with the ADAMS/Solver system model and estimate natural periods for the system. Frequency domain analysis is fully described in the following references: Newman [28], Faltinsen [13], and Sclavounos [31]. Excitation forces for hydrodynamic motion arise due to waves interacting with the submerged structure. For infinite water depth, the following equations give the velocity potential (Φ) and elevation (η) for a wave of amplitude A and direction β:

$$\phi(x,y,z,t) = \mathrm{Re}\left\{\frac{igA}{\omega} e^{kz - ikx\cos\beta - iky\sin\beta + i\omega t}\right\}$$
$$\eta(x,y,t) = \mathrm{Re}\left\{A e^{-ik(x\cos\beta + y\sin\beta)} e^{i\omega t}\right\}$$

(5.1)

where k is the wave number and ω is frequency. In deep water $k = \omega^2/g$.

As stated earlier the long wave length assumption applies to the linear hydrodynamic analysis. Also, the damping is assumed to be linear. This assumption allows the motion equations for surge, heave, pitch, and yaw to be solved in the frequency domain. Sway and roll are identical to surge and pitch and will therefore not be discussed further. The wind turbine could excite the structure in yaw. It is assumed that no waves are generated by the floater, due to the fact that the wavelengths of the ambient waves are assumed to be much greater that the floater diameter. The wave-floater interaction problem can therefore be solved in a simplified manner. The excitation forces are obtained from the

incoming wave potential and analytical expressions for the buoy and spokes added mass. For a spar buoy the pitch and surge motions are coupled. The coupled surge/pitch motion equations are:

$$\begin{pmatrix} M_{11} + A_{11} & A_{15} \\ A_{51} & M_{55} + A_{55} \end{pmatrix} \begin{pmatrix} \ddot{\xi}_1 \\ \ddot{\xi}_5 \end{pmatrix} + \begin{pmatrix} B_{11} & B_{15} \\ B_{51} & B_{55} \end{pmatrix} \begin{pmatrix} \dot{\xi}_1 \\ \dot{\xi}_5 \end{pmatrix} + \begin{pmatrix} C_{11} & C_{15} \\ C_{51} & C_{55} \end{pmatrix} \begin{pmatrix} \xi_1 \\ \xi_5 \end{pmatrix} = \begin{bmatrix} F_1(t) \\ F_5(t) \end{bmatrix} \qquad (5.2)$$

and the uncoupled heave and yaw equations of motion are:

$$(M_{33} + A_{33})\ddot{\xi}_3 + (B_{33})\dot{\xi}_3 + C_{33}\xi_3 = F_3(t)$$
$$(M_{66} + A_{66})\ddot{\xi}_6 + (B_{66})\dot{\xi}_6 + C_{66}\xi_6 = F_6(t) \qquad (5.3)$$

M_{ij}:   Inertia coefficient
A_{ij}:   Added mass coefficient
B_{ij}:   Damping coefficients which include damping due to viscous drag and the wind turbine.
C_{ij}:   Restoring coefficient
F_i: Excitation force or moment

In order to solve the equations of motion all of the above coefficients must be solved.

The following analysis is taken from a paper by Kim and Sclavounos [21]. In order for the system to be analyzed using linear frequency domain analysis all of the linear quantities must be analyzed relative to the wave elevation:

$$\eta(t) = \text{Re}\left\{ A e^{-ik(x\cos\beta + y\sin\beta)} e^{i\omega t} \right\} \qquad (5.4)$$

where A is the wave amplitude. The linear wave excitation forces f_i acting on the platform are defined relative to the local coordinate system (x, y, z) and by virtue of linearity adopt the complex representation:

$$f_i = \text{Re}(A \cdot X_i e^{i\omega t}), \qquad i = 1,\ldots,6 \qquad (5.5)$$

where X_i is the complex amplitude of the exciting force or moment in the i-direction. The platform motions ξ_i in the six degrees of freedom also adopt the complex representation:

$$\xi_i = \text{Re}(A \cdot \Xi_i e^{i\omega t}), \qquad i = 1,\ldots,6 \qquad (5.6)$$

36

where Ξ_i is the complex response amplitude for the platform in the j-direction. They are called the Response Amplitude Operators (RAO's). The classical forms of the matrix equations for the RAO's are:

$$\left[-\omega^2(M_{ij}+A_{ij})+i\omega\left(b_{wtij}+b_{ij}+b_{sij}\right)+\left(C_{ij}+c_{ij}\right)\right]\Xi_i=X_i \tag{5.7}$$

Where the damping has three main contributors: damping due to the wind turbine (b_{wt}), damping due to viscous drag on the vertical cylinders (b), and the viscous drag on the spokes (b_s). These damping terms are combined into the total damping term (B). Linear analysis is used to verify the output of the hydrodynamics loading subroutine in this research. Therefore, the wind turbine is assumed to be secure during linear analysis of the floater. When the wind turbine is secured all of the damping terms associated with it are zero. The other assumption made during the linear analysis is that the lines provide negligible damping. This is a valid assumption since the floaters will require relatively short lines for the water depths being considered. By making these assumptions the frequency domain equations of motion are obtained when the equations (5.2) and (5.7) are combined:

$$\left[-\omega^2\begin{pmatrix} M_{11}+A_{11} & A_{15} \\ A_{51} & M_{55}+A_{55} \end{pmatrix}-i\omega\begin{pmatrix} B_{11} & B_{15} \\ B_{51} & B_{55} \end{pmatrix}+\begin{pmatrix} C_{11} & C_{15} \\ C_{51} & C_{55} \end{pmatrix}\right]\begin{pmatrix} \Xi_1 \\ \Xi_5 \end{pmatrix}=\begin{bmatrix} X_1 \\ X_5 \end{bmatrix} \tag{5.8}$$

$$\left[-\omega^2(M_{33}+A_{33})+i\omega(B_{33})+\left(C_{33}+c_{33}\right)\right]\Xi_3=X_3$$
$$\left[-\omega^2(M_{66}+A_{66})+i\omega(B_{66})+C_{66}\right]\Xi_6=X_6 \tag{5.9}$$

Knowledge of the platform resonant frequencies for the various floater modes of motion is essential for the design of the platform. Resonant vibrations in the floater can excite similar motion in the tower and wind turbine if natural frequencies are not taken into account. The resonant frequencies are found from the solution of the eigenvalue problem:

$$\left[-\omega^2(M_{ij}+A_{ij})+\left(C_{ij}+c_{ij}\right)\right]\Xi_i=0, \qquad i=1,\ldots,6 \tag{5.10}$$

The eigenvalues of this equation give the natural frequencies for the modes of motion that are applicable to the floater.

5.1 Coupled Surge and Pitch Analysis

The purpose of this section is to detail how the various coefficients necessary for the linear analysis are derived. Horizontal forces acting on the floater and wind turbine excite motion in the surge direction. These forces produce moments about the y-axis of the system. These moments cause pitching motion of the floater. The combined surge and pitch motion of the floater results in the movement of the nacelle. This motion can result in changes in thrust and moment loading on the floater from the wind turbine. Equations (5.2) and (5.8) are used in the analysis of surge and pitch motion.

5.1.1 Surge and Pitch Added Mass

The inertia portion of the surge equation deals with the calculation of the force that is necessary to accelerate the mass associated with the structure in the surge direction. This inertia consists of mass and added mass. The mass M_{11} is the combined mass of the wind turbine, floater, and lines. The inertia term M_{55} in pitch is the mass moment of inertia of the structure about the point where rotation is being assumed.

The added mass coefficients for the coupled surge/pitch equations are determined by evaluating the forced oscillations of the floater in surge and pitch. Strip method is used in this evaluation. The spokes at the bottom of the structure must be treated separate from the cylindrical spar (see Figure 5.1). Each strip along the spar has the acceleration:

$$a_{strip} = \ddot{\xi}_1 + z_{strip} \cdot \ddot{\xi}_5 \qquad (5.11)$$

where z_{strip} is the distance of the strip being evaluated from the rotation point at the base of the spar. The added mass creates an inertia force on the surface of the floater due to the accelerations. Two of the spokes contribute to the added mass of the structure in surge since they lie perpendicular to the x-axis. The added mass of the other two spokes has a negligible effect on the structure in pitch. The added mass of the structure is determined by assuming that the structure surges and pitches about the point where the added mass coefficients are being evaluated about.

The reaction forces due to forced oscillations are obtained by integrating the reaction force on each strip. The added masses of the cylinder are found using the definition of added mass:

$$F_{reaction} = -A_{kj}\ddot{\xi}_j \qquad (5.12)$$

38

$$F_{1,reaction} = \int_{-T}^{0} A_{11}^{2D} \cdot a_{strip} dz = -\ddot{\xi}_1 \underbrace{\left(\frac{d^2}{4} \rho_{sw} \pi T \right)}_{A_{11}} - \ddot{\xi}_5 \underbrace{\left(\frac{d^2}{8} \rho_{sw} \pi T \right)}_{A_{15}}$$

$$F_{5,reaction} = \int_{-T}^{0} A_{11}^{2D} \cdot a_{strip} \cdot z_{strip} dz = -\ddot{\xi}_1 \underbrace{\left(\frac{d^2}{8} \rho_{sw} \pi T^2 \right)}_{A_{51}} - \ddot{\xi}_5 \underbrace{\left(\frac{d^2}{12} \rho_{sw} \pi T^3 \right)}_{A_{55}}$$

(5.13)
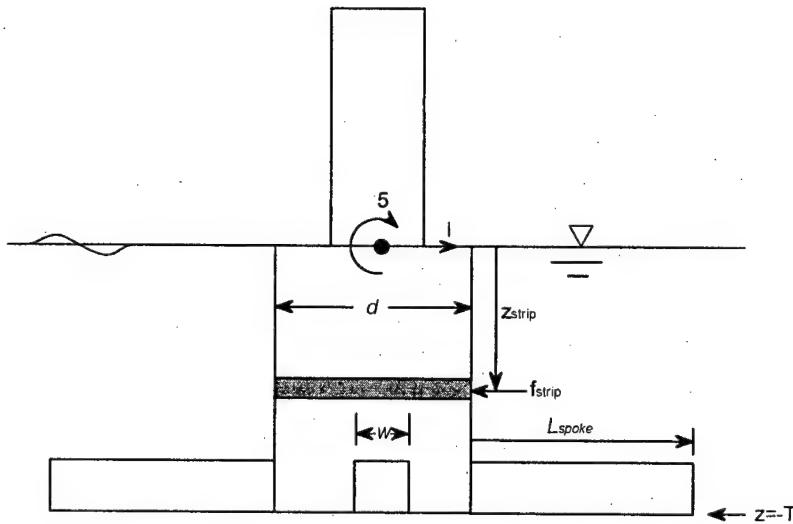
Figure 5.1 Derivation of surge and pitch added mass.

where a_{strip} is the acceleration of the strip being analyzed due to both translation and rotation at the point around which the added mass is being determined. The two dimensional added mass term for a cylindrical strip is equal to the volume displaced. Next the contribution of the spokes is added to the surge added mass.

$$A_{11} = \underbrace{\frac{d^2}{4} \rho_{sw} \pi T}_{spar} + \underbrace{\frac{w^2}{2} L_{spoke} \rho_{sw} \pi}_{spokes}$$

(5.14)

5.1.2 Surge and Pitch Restoring Coefficients

The restoring coefficients for pitch and surge are derived in the previous chapter. The spar buoy which consists mainly of vertical cylinders is strongly coupled in the surge and pitch modes of motion. The restoring coefficients for a tethered spar cylinder are:

39

$$C_{11} = \frac{F_{tethers}}{L_{tether}}$$

$$C_{55} = 2\frac{(E_{line} \cdot A_{tethers})}{L_{tether}}\left(L_{spoke} + \frac{d}{2}\right)^2 + F_{buoy}\frac{T}{2} - m_{total}g(z_g + T)$$

(5.15)

5.2 Heave Analysis

Heave of the floater is motion in the vertical direction. Motion in the heave mode is minimized due to the configuration of the lines on the tension leg support system. However, as the system moves in surge and sway modes it settles lower in the water since the legs remain nearly constant in length. This results in a coupling that is non-linear. This coupling is readily handled using a fully coupled ADAMS model, which will be discussed later. Linear analysis can be used to evaluate small amplitude heave oscillations and determination of the heave natural frequency.

5.2.1 Heave Inertia and Added Mass Coefficients

The inertia term for heave motion is the total mass of the combined structure. Added mass in heave is due to the mass of water under the spar that is accelerated when the structure moves in the vertical direction. This added mass can be approximated by the displacement of a half sphere of water with a radius equal to that of the base of the spar cylinder [31], [15]. The spokes also contribute to the heave added mass. Heave added mass is given by:

$$A_{33} = \underbrace{\frac{2}{3} \cdot \rho\pi r^3}_{spar} + \underbrace{4 \cdot \left(4.754 \cdot L_{spoke}\rho\left(\frac{w}{2}\right)^2\right)}_{spokes}$$

(5.16)

where r is the radius of the bottom of the spar

5.2.2 Heave Restoring Coefficient

The heave restoring force is generated by two mechanisms. First, as the buoy heaves, the line tension changes and very large forces are generated due to the relatively high modulus of elasticity for the tethers. The other part of the restoring force is the change in buoyancy of the floater as it moves in the vertical direction. This second factor is roughly two orders of magnitude smaller than the line restoring force for water depths in the range of 100 to 300 meters for relatively stiff lines. The heave restoring coefficient is given by equation (5.17).

40

$$C_{33} = \frac{4 \cdot E_{tethers} A_{tethers}}{L_{tethers}} + \rho g A_{wp} \tag{5.17}$$

where A_{wp} is the area of the spar buoy waterplane.

5.3 Yaw Motion

Yaw motion in the support system is exited by yaw moments generated on the wind turbine rotor and wave loading of the submerged spokes. These excitations are counteracted by the restoring force of the tethers which act over the moment arm of the spokes. As the floater rotates the fairlead position is moved away from the rest position and a horizontal force component is produced. The force results in a counter moment which opposes the yaw displacement.

5.3.1 Yaw Inertia and Added Mass Coefficients

The yaw moment of inertia and added mass are found by combining the contributions of the individual components. Cylindrical components centered on the yaw axis do not contribute to the yaw added mass. Therefore only the spokes make a contribution to the yaw added mass. The spokes are modeled as rigid box structures that have a square cross section.

The yaw moment of inertia is the moment of inertia about the z-axis. The yaw added mass of the spokes is found using the strip method along the spokes. The total yaw added mass for all four spokes with length (L_{spoke}) and width (w) is given by [28]:

$$A_{66} = 4 \left(4.754 \cdot \left(\frac{w}{2} \right)^2 \rho \left(\left(L_{spar} + \frac{d}{2} \right)^3 - \left(\frac{d}{2} \right)^3 \right) \right) \tag{5.18}$$

5.3.2 Yaw Restoring Coefficient

For small yaw motions, a linear restoring coefficient can be assumed. This coefficient is similar to the linear heave restoring coefficient, since both coefficients are generated by movement of the fairlead position. As the system yaws the tension in all of the tethers produces a moment in the opposite direction of the displacement. The linear yaw restoring coefficient is given by:

$$C_{66} = \frac{F_{tethers}}{L_{tethers}} \cdot \left(L_{spoke} + \frac{d}{2} \right)^2 \tag{5.19}$$

41

6 Hydrodynamic Loading

Waves act on the submerged portion of the floater and cause motion of the system. This chapter deals with the determination of wave excitation on the submerged portion of the tower, the spar buoy, and the spokes. The forces and moments due to the waves are found using potential theory. The velocity potential of a planar progressive wave with frequency (ω), wavenumber (k), and direction (β) is given by the following equation:

$$\phi(x, y, z, t) = \Re e \left\{ \frac{igA}{\omega} e^{kz - ikx \cos \beta - iky \sin \beta + i\omega t} \right\} \tag{6.1}$$

where k is the wavenumber (ω^2/g).

6.1 Interface of Hydrodynamic Loading Module with ADAMS

Prior to beginning the discussion of the derivation of hydrodynamic loading it is important to understand how the calculations are used in the fully coupled dynamic analysis. Every time step the ADAMS solver sends the hydrodynamic loading subroutine the position, velocity, and acceleration of a point on the part for which loads are being determined. The rotational components are relative to that parts body based coordinates (roll, pitch, and yaw), not the rotations about the global coordinate system. The local rotations change the loading on the system. Loads are then calculated relative to the body based Coordinate system and sent back to the solver. Every part in an ADAMS model has its own body based coordinate system, which moves with the part. Roll, pitch, and yaw are the angular differences between the body coordinate system axes and the global coordinate axes. The solver combines the loads on the six different floater components and combines them with the aerodynamic loads from the 45 blades elements in the rotor while performing the total system dynamic analysis.

6.2 GI Taylor's Loading Approximation

The diameter of the floater is small compared to the wavelength of most of the waves of interest. The diameter of the spar will fall into a range of 6 m to 30 m. A wave with period (T) of 10 seconds will have a wavelength of approximately (wave period rule of thumb): $\lambda \simeq T^2 + T^2/2 = 150$ m. Therefore the wavelength is much greater than the diameter of the spar. The long wavelength approximation can therefore be used when determining the excitation forces and moments on the structure by the

42

incoming waves. This approximation allows calculations to be made at the center of the body and assume that the wave potential is constant across the body. GI Taylor's equation for wave excitation is given by equation (6.2).

$$F_i = \left(\rho\forall + A_{ii}\right)\left(\frac{\partial u_i}{\partial t} + u_i\frac{\partial u_i}{\partial i}\right) - A_{ii}\frac{d^2 x_i(t)}{dt^2} \tag{6.2}$$

Where A_{ii} is the added mass of the structure in the direction of the force being calculated and x_i is the displacement of the structure in the direction of interest. The velocity of the undisturbed wave field in the direction of the force at the center of the structure is denoted by u_i. The above equation is called GI Taylor formula. It is applicable to structures whose principal dimension is much less than the wavelength of the incident waves.

6.2.1 Excitation Loads on Submerged Cylinders

The GI Taylor formula is used in a strip-wise integration to evaluate the total hydrodynamic force on the wind turbine floater. The motion of the floater is accounted for in these integrations. The horizontal and vertical forces on the floater are phase shifted by 90°. The following is a derivation of the forces exerted on a vertical cylinder. For the following discussion, refer to Figure 5.1. The strip method for excitation forces are

$$F_i = \left(\rho\forall + A_{ii}\right)\left(\frac{\partial u_i}{\partial t} + u_i\frac{\partial u_i}{\partial x_i}\right) - A_{ii}\frac{d^2 x_i(t)}{dt^2}$$

$$\phi = \Re\left\{\frac{igA}{\omega}e^{kz - ikx\cos\beta - iky\sin\beta + i\omega t}\right\}, A : \text{wave amplitude}$$

where $u_i\dfrac{\partial u_i}{\partial i} \approx 0$ to the leading order. Which results in the above excitation equation becoming:

$$F_i = \left(\rho\forall + A_{ii}\right)\left(\frac{\partial u_i}{\partial t}\right) - A_{ii}\ddot{x}_i$$

$$\frac{\partial}{\partial t} \sim i\omega \quad ; \qquad \frac{\partial}{\partial x} \sim -ik\cos\beta \tag{6.3}$$

The velocity components of the undisturbed water at position are found by taking the x, y, and z derivatives of the wave potential equation.

$$u_1 = \frac{\partial \phi_i}{\partial x} = A\omega \cos \beta \cdot \Re\left\{e^{kz - ikx\cos\beta - iky\sin\beta + i\omega t}\right\}$$

$$u_2 = \frac{\partial \phi_i}{\partial y} = A\omega \sin \beta \cdot \Re\left\{e^{kz - ikx\cos\beta - iky\sin\beta + i\omega t}\right\}$$

$$u_3 = \frac{\partial \phi_i}{\partial z} = A\omega \cdot \Re\left\{ie^{kz - ikx\cos\beta - iky\sin\beta + i\omega t}\right\}$$

The added mass terms in surge / sway for a strip of thickness dz and the heave added mass due to the bottom of the spar cylinder are given by the following equations:

$$a_{11} = a_{22} = Area_{cyl} \cdot \rho_{sw} \cdot dz = \pi r_{cyl}^2 \cdot \rho_{sw} \cdot dz$$

$$A_{33} = \frac{2 \cdot \pi}{3} \cdot r_{cyl}^3 \cdot \rho_{sw}$$

where A_{33} is the added mass of a half sphere of water with a radius equal to that of the spar cylinder. The final part of the equation that is need is the acceleration terms:

$$\frac{\partial u_1}{\partial t} = \Re\left\{iA\omega^2 \cos \beta e^{kz - ikx\cos\beta - iky\sin\beta + i\omega t}\right\}$$

$$\frac{\partial u_2}{\partial t} = \Re\left\{iA\omega^2 \sin \beta e^{kz - ikx\cos\beta - iky\sin\beta + i\omega t}\right\}$$

$$\frac{\partial u_3}{\partial t} = \Re\left\{-A\omega^2 e^{kz - ikx\cos\beta - iky\sin\beta + i\omega t}\right\}$$

Now, by using these terms in (6.2), the forces can be found. The strip method is used to sum up the contributing horizontal forces along the length of the vertical cylinder. For heave the excitation force is assumed to the vertical force acting on a displaced volume of water at the depth of the floater bottom. This volume is assumed to be that of a half sphere with a radius equal to the bottom of the cylinder. The forces on the individual strips are given by the following equations.

$$dF_{x-strip} = \left(\rho Area \cdot dz + A_{11-strip}\right)\left(\Re\left\{iA\omega^2 \cos \beta e^{kz - ikx\cos\beta - iky\sin\beta + i\omega t}\right\}\right) - A_{11-strip}\ddot{x}_1$$

$$dF_{y-strip} = \left(\rho Area \cdot dz + A_{22-strip}\right)\left(\Re\left\{iA\omega^2 \sin \beta e^{kz - ikx\cos\beta - iky\sin\beta + i\omega t}\right\}\right) - A_{22-strip}\ddot{x}_2 \quad (6.4)$$

$$dF_{z-bottom} = \left(\frac{4\rho\pi R_{spar}^3}{6} + A_{33}\right)\left(\Re\left\{-A\omega^2 e^{kd_2 - ikx\cos\beta - iky\sin\beta + i\omega t}\right\}\right) - A_{33}\ddot{x}_3$$

where *Area* is the cross-sectional area of the strip being analyzed ($Area = \pi \cdot r_{cylinder}^2$). The first two equations in (6.4) apply for both the spar and the submerged portion of the tower. The forces on the bottom of the spar in the z-direction are treated separately since only the bottom of the structure has vertical wave excitation forces acting on it. The derivation of the pitch and roll moments are similar to those of the forces in the x and y directions. Forces acting on the cylindrical strips are multiplied by the moment arm to the bottom of the cylinder (the point at which forces and moments are summed). The line configuration of the tension leg platform results in very small motion in the pitch and roll directions so long as the all the lines remain in tension and stiff lines are used. Since the spar cylinder may not extend all the way to the surface, the top of the cylinder is assumed to be at depth – d_1 and the bottom is at $-d_2$.

$$dM_5 = 2 \cdot \rho\, Area \cdot A\omega^2 \cos\beta \cdot \Re\left\{ie^{-ikx\cos\beta - iky\sin\beta + i\omega t}\right\}(d_2 + z) \cdot e^{kz}dz - A_{55-strip}\ddot{x}_5$$

$$dM_4 = 2 \cdot \rho\, Area \cdot A\omega^2 \sin\beta \cdot \Re\left\{ie^{-ikx\cos\beta - iky\sin\beta + i\omega t}\right\} \cdot (d_2 + z) \cdot e^{kz}dz - A_{44-strip}\ddot{x}_4$$

(6.5)

6.2.2 Spoke Excitation Forces

The spokes of the floater are used to give the lines longer moment arms to act over. Longer spokes result in lower changes in stress when pitch and roll moments are applied to the system. The actual shape of the spokes is not known. They could be open trusses or closed box structures with buoyancy. For modeling purposes the spokes are treated as boxes with a characteristic dimension equal to the length of one side (*w*). The wave excitation on the spokes can be changed by varying the characteristic dimension. It should be noted that the forces and moments on the spokes are low compared to that of the other portions of the floater. The hydrodynamic forces on the spokes are calculated at their center of mass. Assuming the spokes are attached to the bottom of the spar ($z = -d_2$), the loading equations for the spokes are:

$$F_x = (\rho Vol_{spoke} + A_{11})A\omega^2 \cos\beta \cdot \Re\left\{ie^{-kd_2 - ikx\cos\beta - iky\sin\beta + i\omega t}\right\} - A_{11}\ddot{x}_1$$

$$F_y = (\rho Vol_{spoke} + A_{22})A\omega^2 \sin\beta \cdot \Re\left\{ie^{-kd_2 - ikx\cos\beta - iky\sin\beta + i\omega t}\right\} - A_{22}\ddot{x}_2$$

$$F_z = (\rho Vol_{spoke} + A_{33})A\omega^2 \cdot \Re\left\{e^{-kd_2 - ikx\cos\beta - iky\sin\beta + i\omega t}\right\} - A_{33}\ddot{x}_3$$

(6.6)

where $\ddot{x}_1$, $\ddot{x}_2$, and $\ddot{x}_3$ are the x, y, and z accelerations of the center of mass of the spoke. The contribution of spokes to the floater loading is small compared to the vertical cylinders that make up the submerged portion of the tower and the spar. This is due to the fact that the spokes have a relatively small volume and are mounted near the bottom of the floater. These two characteristics

45

reduce their influence on excitation forces. Moments due to spoke excitation forces are generated by applying these forces at the center of the spokes.

6.3 Viscous Drag

Most of the underwater structure of the floater / wind turbine system consists of a buoyant cylinder and the extension of the tower into the water. Viscous drag on a vertical cylinder can be calculated using Morison's equation. The horizontal differential force in the x-direction (dF) on a strip of length dz of a cylinder using Morison's equation is:

$$dF = \rho \frac{\pi D^2}{4} dz C_M a_1 + \frac{\rho}{2} C_D D dz |u - \dot{x}_1|(u - \dot{x}_1) \qquad (6.7)$$

Where the first term in this equation is the inertial forces and has been handled using the GI Taylor equation. The second term is the viscous damping term. It is used to calculate the viscous drag on the submerged portions of the floater. There are three non-dimensional factors that influence the viscous flow around a submerged body:

$$\text{Keulegan-Carpenter number} \quad KC = 2\pi \frac{a}{D}$$

$$\text{Reynolds number} \qquad Rn = UD/v \qquad (6.8)$$

$$Rn/KC \qquad \beta = \frac{D^2}{vT}$$

where a is the amplitude of oscillation, D is the characteristic length of the body, T is the period of oscillation, and v is the kinematic viscosity (15° C salt water: 1.19E-6 m²/s). As described in the notes by Molin [26], the determination of viscous effects on submerged structures is very problematic. For this reason simplifying assumptions are made to handle the drag forces on the cylinders and spokes. Drag coefficients are assumed to be constant values. Testing has shown that drag coefficients for oscillating bodies change with amplitude and frequency along with floater geometry.

6.3.1 Drag on Submerged Cylinders

For the floating wind turbine system, the spar cylinders used in the floaters have diameters of fall in the range of 7 to 12 meters. The amplitude of motion in most sea states is in the range of 1 to 12 meters for surge and sway. For cylinders with this range of diameters and amplitudes of motion the

46

range for KC is 0.5 to 10. According to Faltinsen (p. 239,[13]), for KC<10 the drag coefficient (C_D) for a cylinder can be estimated using the KC: $C_D \simeq 0.2KC$. A large range of drag coefficients are therefore present on the structure (0.1 to 2.0).

A constant drag coefficient of 0.7 is used in equation (6.7) for determining drag on the cylinders. The relative velocity is the difference between the horizontal velocity (u) of the water at the depth z and the velocity of the structure in the surge direction ($\dot{x}_1$). By substituting the fluid velocity terms from potential flow theory the second term in Morison's equation in monochromatic waves becomes:

$$dF_{drag} = \frac{\rho}{2} C_D D dz \left| A\omega \cos\beta \cdot \Re e\left\{ e^{kz-ikx\cos\beta-iky\sin\beta+i\omega t} \right\} - \dot{x}_1 \right| \left(A\omega \cos\beta \cdot \Re e\left\{ e^{kz-ikx\cos\beta-iky\sin\beta+i\omega t} \right\} - \dot{x}_1 \right) (6.9)$$

where D is the diameter. This equation cannot be directly integrated, therefore the total drag force on the cylinder at each time step is found by dividing the submerged cylinders into strips and summing the forces for these strips. The contribution this force has on the pitch and roll moments is found by multiplying each dF_{drag} by the moment arm of that strip (distance from the strip to the point about which the moments are being calculated). The differential moment (about the base of the cylinder, $z = d_2$) produced by the drag force on a cylindrical strip is given by the following equation:

$$dM_{drag} = \frac{\rho}{2} C_D D \cdot (d_2 + z) dz \left| A\omega \cos\beta \cdot \Re e\left\{ e^{kz-ikx\cos\beta-iky\sin\beta+i\omega t} \right\} - \dot{x}_1 \right| \cdot$$
$$\left(A\omega \cos\beta \cdot \Re e\left\{ e^{kz-ikx\cos\beta-iky\sin\beta+i\omega t} \right\} - \dot{x} \right) \qquad (6.10)$$

6.3.2 Drag on Spokes

Morison's equation is also used to determine the viscous drag on the four spokes of the structure. The drag force in the surge, sway, and heave modes is found by using the drag equation for a single strip with the area term being the frontal area the spoke presents to the wave. The spokes have a square cross-section so a drag coefficient of 1.0 is used. The drag forces are given by the equation:

$$F_1 = \frac{\rho}{2} C_D (w \cdot L \cos(\xi_6 - \beta)) \left| A\omega \cos\beta \cdot \Re e\left\{ e^{kz-ikx\cos\beta-iky\sin\beta+i\omega t} \right\} - \dot{x}_1 \right| \cdot$$
$$\left(A\omega \cos\beta \cdot \Re e\left\{ e^{kz-ikx\cos\beta-iky\sin\beta+i\omega t} \right\} - \dot{x}_1 \right) \qquad (6.11)$$

where $w \cdot L \cos(\xi_6 - \beta)$ is the effective frontal area of the spoke to the wave, w is the spoke width, and L is the spoke length. The x, y, and z positions and velocity of the spoke correspond to the point

47

at the center of mass for the spoke. ξ_6 is the yaw angle of the spoke. The equation is evaluated at a depth z equal to the depth of the center of the spoke. Damping in the yaw mode of motion is due to viscous drag on the spokes.

6.4 Representation of Random Waves

Hydrodynamic analysis of a floating structure in a realistic sea environment requires that statistical estimates be made to represent different sea states. Irregular seas are generated by linear superposition of waves of different frequencies. Since the individual waves are independent of each other they can be treated separately when calculating the excitation forces on the floater. In depth discussions on this procedure can be found in Sclavounos, 2003[31] and Faltinsen, 1990 [13].

A sea state can be represented by the ambient wave spectral density $S(\omega)$. The spectrum is a statistical representation of an ocean environment. As the sea state of the ocean environment increases its spectral density increases. Figure 6.1 is a graph of the spectral density versus frequency. The spectrum is broken up into frequency bands of width $\Delta\omega$.
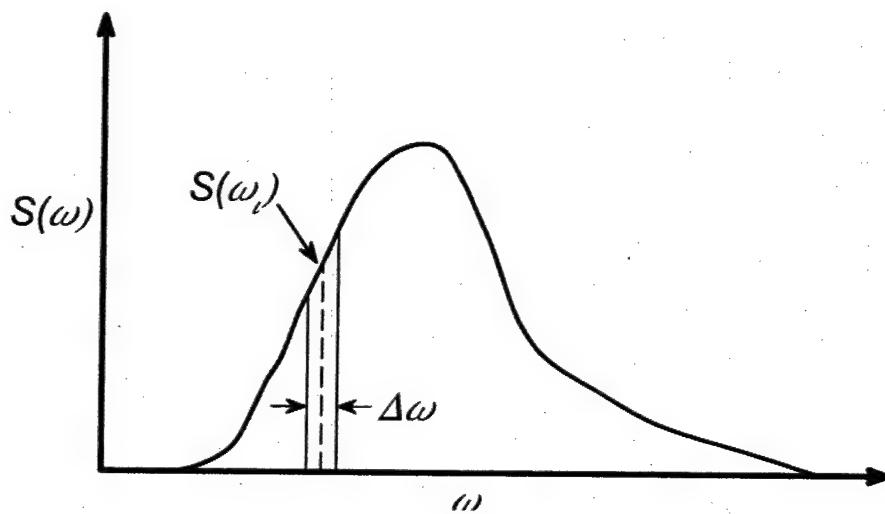
Figure 6.1 Ambient Wave Spectral Density

The spectral density is used to determine the amplitude for a frequency band of width $\Delta\omega$ by using the equation (6.12). This equation allows a group of waves of amplitudes A_i to be generated for use in the excitation analysis of the floater. As the spectral density of a band increases so does its amplitude.

48

$$\frac{1}{2} \cdot A_i^2 = S(\omega_i) \cdot \Delta\omega \tag{6.12}$$

$$S(\omega) = H_{1/3}^2 \cdot T_1 \cdot \frac{0.11}{2\pi} \cdot \left(\frac{\omega T_1}{2\pi}\right)^{-5} \cdot e^{-0.44\left(\frac{\omega T_1}{2\pi}\right)^{-4}} \tag{6.13}$$

Where $H_{1/3}$ is the significant wave height which is defined as the mean of the highest 1/3 of waves. T_1 is the mean wave period for the wave spectrum being represented and is calculated using (6.14).

$$T_1 = 2\pi \frac{m_0}{m_1} \tag{6.14}$$

The moments m_k are defined as:

$$m_k = \int_0^\infty \left[\omega^k \cdot S(\omega)\right] d\omega \tag{6.15}$$

The standard deviation (σ) of the spectrum is calculated by setting k equal to zero.

$$m_0 = \int_0^\infty S(\omega) d\omega = \sigma^2 \tag{6.16}$$

The standard deviation can be used to calculate the significant wave height (Sclavounos, 2003):

$$H_{1/3} \cong 4\sqrt{m_0} = 4\sigma \tag{6.17}$$

Another spectrum that was used during this research was the Joint North Sea Wave Project (JONSWAP) type spectrum which is given in Faltinsen, 1990 [13].

$$S(\omega) = 155 \frac{H_{1/3}^2}{\omega^5 T_1^4} \cdot 3.3^\gamma \cdot e^{\left(\frac{-944}{\omega^4 T_1^4}\right)^{-4}} \tag{6.18}$$

where

$$Y = e^{-\left(\frac{.191\omega T_1 - 1}{2^{1/2}\mu}\right)^2}$$

and

$$\sigma = 0.07 \text{ for } \omega \le \frac{5.24}{T_1}$$

$$\sigma = 0.09 \text{ for } \omega > \frac{5.24}{T_1}$$

The frequencies of the individual wave components determine if the combined wave output will appear to be random or periodic. If the frequency bands are equally spaced along the frequency axis and the center of the bands are used for the associated wave frequency, the output will be periodic. Therefore, it is important that the bands frequencies not be multiples of each other. Another important consideration is computational time. The processing time for a simulation is directly proportional to the number of bands being used in the analysis. It is desirable to only use frequency components which have an spectral energy associated with them to describe a given sea state.

The technique used in this thesis involved a two step process. First, the wave spectrum was generated using 1000 bands as described previously. Then the desired number of bands was generated by choosing the band widths such that the area under the wave spectrum curve was approximately equal for each of the frequency ranges. The area of the new frequency bands was found using the following equation:

$$Area_{band} = \frac{\sum_{i=1}^{1000} S(\omega_i)\Delta\omega}{N_{bands}} \tag{6.19}$$

The spectrum was broken up into bands which had equal areas (see . This resulted in the bands being more closely spaced near the peak and wider spaced at the tails of the spectrum. If the bands were of equal width, the tails (high frequency and low frequency) would consist of wave components with very low (sometimes zero) amplitudes. Processor time would be wasted analyzing these extraneous bands. Instead, by using bands with equal spectral energy, every wave component contributed significantly to the floater loading and processor usage was optimized. The frequency of each band was found by taking the moment of area for the band and dividing by the area instead of the center of the band.

50
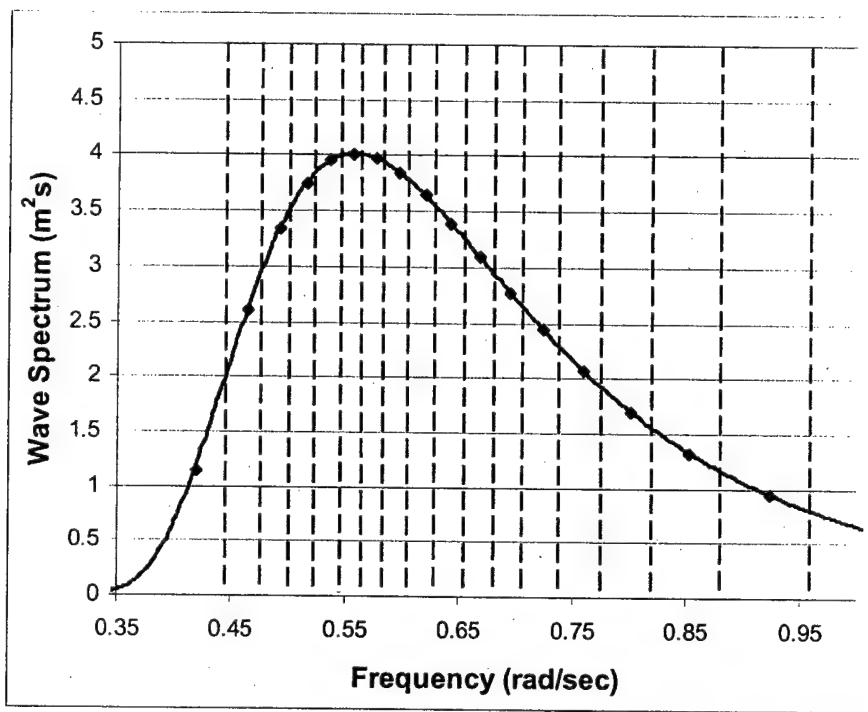
Figure 6.2 Example of sea state 6 wave spectrum divided into bands with equal spectral energy.

The two wave spectra given by (6.13) and (6.18) are used to generate random sea states for use in the hydrodynamics analysis of the floater portion of the floating wind turbine system. The amplitudes associated with each frequency band is then calculated using a (6.12) with the area contained by the band substituted for $S(\omega_i)\Delta\omega$ term. The superposition of the different waves results in an irregular sea elevation. The wave elevation (η) for long crested seas is given by:

$$\eta(t) = \sum_{N=1}^{j} A_j \sin(-k_j x + \omega_j t + \varepsilon_j) \qquad (6.20)$$

where ε_j is the random phase angle for the ith frequency band drawn from a uniform distribution.

The time varying wave elevation is very important in the floater load analyses. Nonlinear drift forces result due to the fact that more of the structure is in the wave field when a crest is passing than when the trough is passing. These forces will be discussed in the following section.

6.5 Nonlinear Hydrodynamic Forces

The time varying wave elevation generates second order drift forces. These forces cause the floater to be displaced from the rest position and oscillate about a mean drift position. Second order forces are not reflected in linear analysis. This is due to the fact that linear theory assumes that all analysis can

51

be carried out using a constant z equal to zero for the upper portions of the floater. The potential flow equations give identical magnitudes for forces acting in both the direction of wave propagation and the reverse direction. This results in linear theory producing oscillating forcing function with a mean of zero. The mean horizontal drift force due to wave diffraction and radiation effects is assumed to be negligible because of the small cylinder diameter relative to the ambient wavelength.

In this research, nonlinear hydrodynamic forces are modeled using the approximation method described in Faltinsen, 1990 [13]. This method involves accounting for changes in wave elevation by performing strip theory calculations over the actual volumes instead of using the mean free surface as one endpoint in the computations. Wave elevations above the mean free surface are a problem due to the e^{kz} term in potential equations, which would result in very large fluid velocities and accelerations in steep waves. The approximation method involves setting z equal to zero in the ambient wave kinematics equations above the mean free surface and using the wave elevation for z in troughs. Figure 6.3 shows the distributions of acceleration and velocity under the waves as they change with depth.

This method of modeling nonlinear forces is useful in a time domain analysis of the floater. The hydrodynamic loads are determined by summing the inertial and viscous loads for the strips. These forces are calculated using the equation of GI Taylor and Morison.
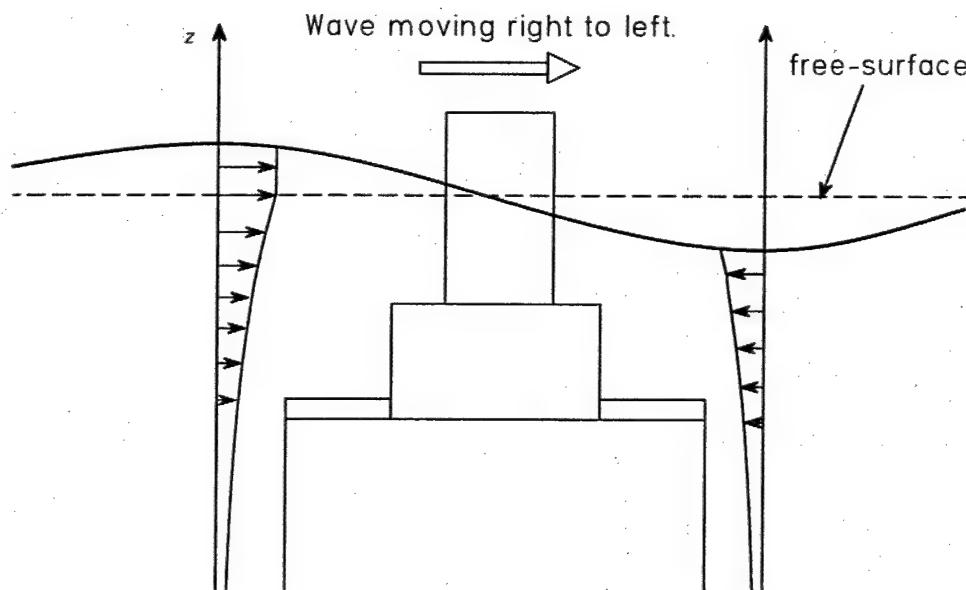
Figure 6.3 Distribution of horizontal velocities and accelerations.

52

7 Computer Model

The wind turbine / floater system was best modeled in the time domain. This was due to the fact that accurate representations of the various components and loading conditions involve many non-linear terms. Several different wind turbine computer models are used in industry to simulate various loading conditions and predict machine response. However, none of these codes simulate a wind turbine mounted on a floating base. Modifications to existing codes and new subroutines were written to model the fully coupled response of the combined floater wind turbine system.

Several different computer codes were used in this research. The majority of the work involved a hydrodynamics program that modeled the excitation forces on the floater, a modeling subroutine that generated a computer model of the floater, ADAMS and FAST. FAST was used to generate the ADAMS model of the wind turbine and to perform additional wind turbine calculations. The ADAMS input file was modified to include the floating base. ADAMS was used to perform the time domain simulation of the system model. The following chapter discusses the computer codes used in the analysis. Also, a description of the analysis model is given.

7.1 FAST

The FAST (Fatigue, Aerodynamics, Structures, and Turbulence) code is a wind turbine simulation code produced by the National Renewable Energy Laboratory (NREL). It is a combination of three different codes: FAST2 (2-bladed horizontal axis wind turbines (HAWTs), FAST3 (3-bladed HAWTs), and AeroDyn (aerodynamics subroutines for wind turbines). A full description of FAST can be found in the FAST User's Guide [4].

The Fast2Adams subroutine in FAST was used to generate the portion of the ADAMS model that represents the wind turbine. This subroutine was modified so that it calls the *fltr_prop* subroutine, which adds the floater representation to the ADAMS model file. The Fast2Adams subroutine also generates the ADAMS control file which governs the operation of the solver analysis.

7.2 ADAMS

The simulation of the total system is carried out in the time domain using MSC.ADAMS. ADAMS (Automatic Dynamic Analysis of Mechanical Systems) is a commercially available software package that is used for dynamic analysis. It is produced by Mechanical Dynamics, Inc. ADAMS is a

program that consists of many subprograms that can be used to accomplish various engineering analysis tasks. ADAMS/Solver was used to combine the loading on the floater with the loading on the wind turbine to create a dynamically coupled system .

ADAMS/Solver^{TM} is a numerical analysis application that automatically solves the equations of motion for kinematic, static, quasi-static, and dynamic simulations. It is useful for analyzing systems that have complex loading and flexural properties. The combined floater and wind turbine system requires this kind of analysis tool in order to achieve the proper coupling. The following section describes how the ADAMS/Solver works and how it is used in this research. The ADAMS/Solver subprogram will henceforth be referred to as ADAMS. The description of ADAMS operation is taken from the ADAMS Users Manual [1].

7.2.1 Description of an ADAMS Model

The inputs to ADAMS are a model file and a control file. The model file describes the system being analyzed. Mechanical systems are represented with interconnected parts. Flexible components are modeled by splitting the component up into smaller parts which are then connected to adjacent parts with springs and dampers that represent the flexural and damping properties of the component being modeled. For example each blade consists of 15 parts which range from the blade root out to the blade tip. A system like the wind turbine and floater combination consists of approximately 60 parts.

Each part is modeled as a lump mass with a position and inertial properties which reflect the region being modeled. Field statements are used to connect a part to adjacent parts. These statements describe the translational and rotational restoring and damping properties of the component in the region of the part. The springs and dampers represented by the field statements are attached to points on the parts called markers. Figure 7.1 is an example of how individual parts are interconnected with these field statements. When the number of parts used to describe a component is chosen correctly an accurate prediction can be made of the dynamic response for the component.
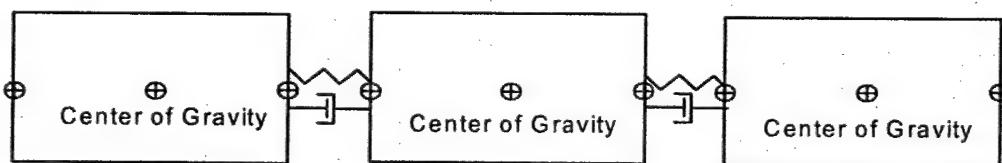
Figure 7.1 Example of ADAMS model.

Once the parts physical properties and interconnections are described the next step in modeling is application of external forces. Parts can also be connected using various kinds of joints. Forces are applied to markers on parts. The force of gravity is applied to the center of gravity marker. External forces can be applied to any marker on a body.

Forces are calculated using functions or external subroutines. The forces exerted on the wind turbine blade elements are computed by the AeroDyn subroutine. The hydrodynamic forces on the submerged portions of the systems are computed by the *fltr_loads* subroutine. These two subroutines are described further in other sections.

7.2.2 ADAMS Control File

The operation of the ADAMS solver is governed by the control file. The commands in this file initiate motion, unlock or lock joints, and dictate the type of numerical integration used during the simulation. The combined wind turbine / floaters system is relatively stiff; this fact leads to the choice of a stiff numerical integration technique for the simulation.

The dynamic analysis of a mechanical system consists essentially of numerically integrating the nonlinear differential equations of motion. The type of system (soft or stiff) governs the choice of numerical integration used by the ADAMS/Solver. For this research the best integrator was found to be the GSTIFF routine. This routine is good for high speed and accurate analysis of a wide range of systems. A thorough description can be found in the ADAMS/Solver Users Guide.

7.3 Floater Model Description

The input model for the ADAMS analysis is generated to model the wind turbine and floater as a combined system. The wind turbine portion of the model is generated by the FAST pre-processor. The floater portion is then added to the model file. The floater consists of several different parts: submerged tower, spar cylinder, spokes, and tethers. All of these parts, their associated properties, and loading conditions had to be determined by new subroutines that interfaced with ADAMS.

This program uses the data in the floater characteristic input file and generates the ADAMS input file. Figure 7.2 is an example of a floater input file. The *fltr_prop* subroutine serves two purposes. This subroutine calculates the physical parameters for the floater, and then writes the description statements to the model file. The second purpose is to perform additional calculations which are used to verify the output of the time domain analysis against linear analysis. Figure 7.3 is an example of the parameters calculated in the *fltr_prop* subroutine.

```
10.0              ! Floater Diameter ALL UNITS SI
10.0              ! Tower Diameter
15.0              ! Depth of tower
0.0               ! Length of cylinder (Height)
0.0               ! Height of spokes on cylinder (0 = bottom)
12.0              ! Length of spokes
2.0               ! Characteristic width of spokes (square cross-section)
0.0253            ! Thickness of spar
0.104             ! Line Diameter (m)
1                 ! Number of lines
743.0             ! Breaking Load in tonnes
0.045             ! Maximum line Extension
200.0             ! Water depth
0.0               ! Wave Direction (degrees)
0.0               ! Wave Direction Range (+/- this value)
30                ! Number of Bands (integer value)
.false.           ! Buoyant spokes
2                 ! (1) PierceMoskowitz or (2) JONSWAP
5.0               ! Significant wave height (H1/3)
8.686             ! Mean wave period, T1
```

Figure 7.2 Example of floater input file

```
=====================Calculated Floater Properties ==================
    46675.9    Spar Mass
        0.0    Mass Cylinder
    15558.6    Mass Spar Plate
    93351.9    Submerged Tower Mass
    79239.6    Mass of Spokes
   219267.4    Total Floater Mass
   201059.2    Mass of Wind Turbine
   420326.6    System Mass
  1212261.1    Buoyant Mass
   791934.5    Reserve Buoyancy
      188.41   Percent Reserve Buoyancy
        0.0340 Total Area of Lines
      885.5    Spring Constant
    23306.29   Intial Line Stress
        2.19   Intial Line Stretch
=============== System Properties =================
    52.5060    CG of Wind Turbine
   -11.8069    CG of Floater
    18.9565    CG of System
  1225191.9    A11 and A22
   574157.8    A33
106552323.0    A44 and A55
 31229673.8    A66
721810181.6    Ixx
721810181.6    Iyy
 60009264.4    Izz
   -41993.9    C11 and C22
 -4334783.3    C33
-460989441.0   C44 and C55
   -713896.9   C66
======== Natural Frequencies of Floater System =============
    0.1598     Surge and Sway Natural Frequencies (rad/sec)
    2.0878     Heave Natural Frequency(rad/sec)
    0.7460     Roll and Pitch Natural Frequencies (rad/sec)
    0.0885     Yaw Natural Frequency (rad/sec)
```

Figure 7.3 Output of *fltr_prop* subroutine.

56

The floater model describes the physical characteristics of the floater so that it realistically represents the floater in the time domain analysis. The floater is modeled4 as a single rigid body which is attached to the tower base with a spring and damper. Figure 7.4 shows the locations for the loading applied to the floater. The following loading characteristics are incorporated into the ADAMS model:

- Force due to gravity.
- Buoyancy force for the spar portion.
- Buoyancy force for the submerged tower.
- Buoyancy forces for the spokes (if buoyant).
- Forces due to tethers.
- Hydrodynamic forces (calculated in *fltr_loads* subroutine)
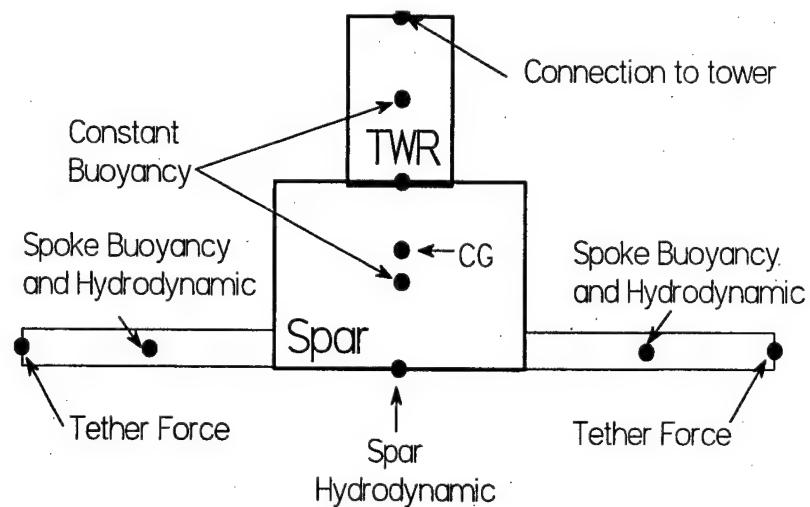
Figure 7.4 Loading for floater model.

The hydrodynamic forces and moments are applied at different points in the structure. As previously discussed "markers" are used in the model as application points for forces and moments. The loading markers for the submerged portion of the tower and the spar are located at their bases. The application points for hydrodynamic forces on the spokes are located at their geometric centers. The solver can then use these loads and their application points to determine the effect on the rest of the system. The hydrodynamic loads are calculated by an external subroutine which is discussed in the next section.

7.4 Hydrodynamic Loading Module

Every time step the ADAMS solver calculates the loading at every point in the system several times in order to achieve the proper prediction of system response. The forces on the blade elements and floater sections require external modules to be called to calculate the loads associated with them. The floater consists of 6 components: spar, submerged portion of tower, and four spokes. Each of these components hydrodynamic forces are calculated in *fltr_loads* subroutine. The following is a description of the calculations performed in the *fltr_loads* subroutine.

7.4.1 Initial Calculations

The first time the *fltr_loads* subroutine is called the floater input file is read. The input file consists of parameters that describe the sea state being analyzed: number of bands, type of spectrum (Pierson-Moskowitz or JONSWAP), $H_{1/3}$, and T_1. The number of bands dictates how many different frequencies will be used to generate the sea state.

The type of spectrum is chosen based on the geographic location where the floater is being analyzed. The JONSWAP spectrum is useful for modeling waves in the north Atlantic. It is the spectrum used for most of the analyses in this research. As shown in Figure 7.5, the JONSWAP spectrum has a higher peak value but is narrower than the Pierson-Moskowitz spectrum for a given sea state. The JONSWAP spectrum has higher peak values of wave elevation due to this difference in spectrum.
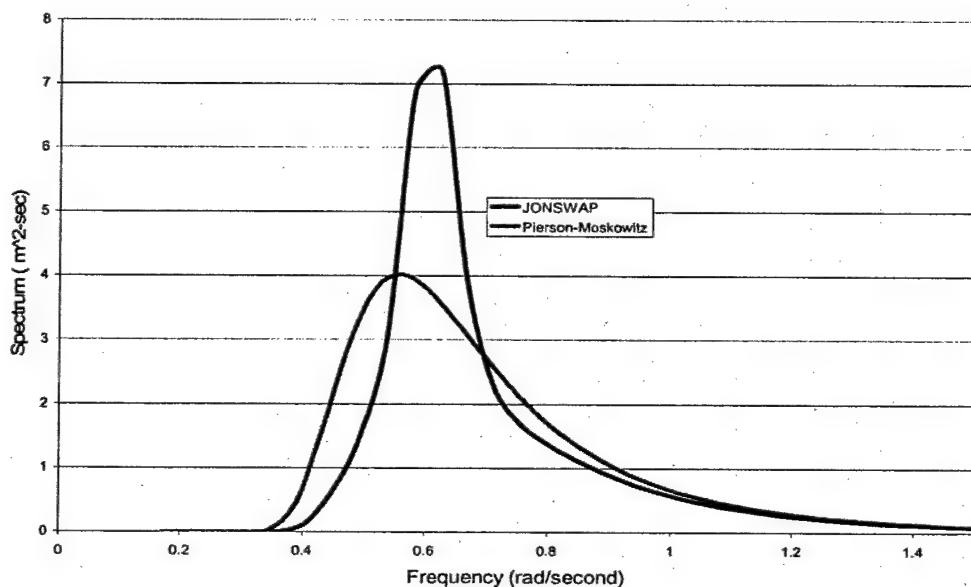
Figure 7.5 Graphs of Pierson-Moskowitz and JONSWAP spectrums sea state 5.

The frequency bands are described by a wave number, amplitude, and phase. The phase of each wave is chosen randomly from a continuous distribution of -180° to +180°. The random seed used for this process is set at a constant value. This ensures that identical frequency bands are generated every time a run is conducted with the same number of bands. Changing the random seed changes the phases associated with these bands. The spectrum data is written to an output file. A time history of the wave elevation at the origin is also written to an output file. Figure 7.6 is an example of a wave elevation record for a sea state 5 Pierson-Moskowitz spectrum.
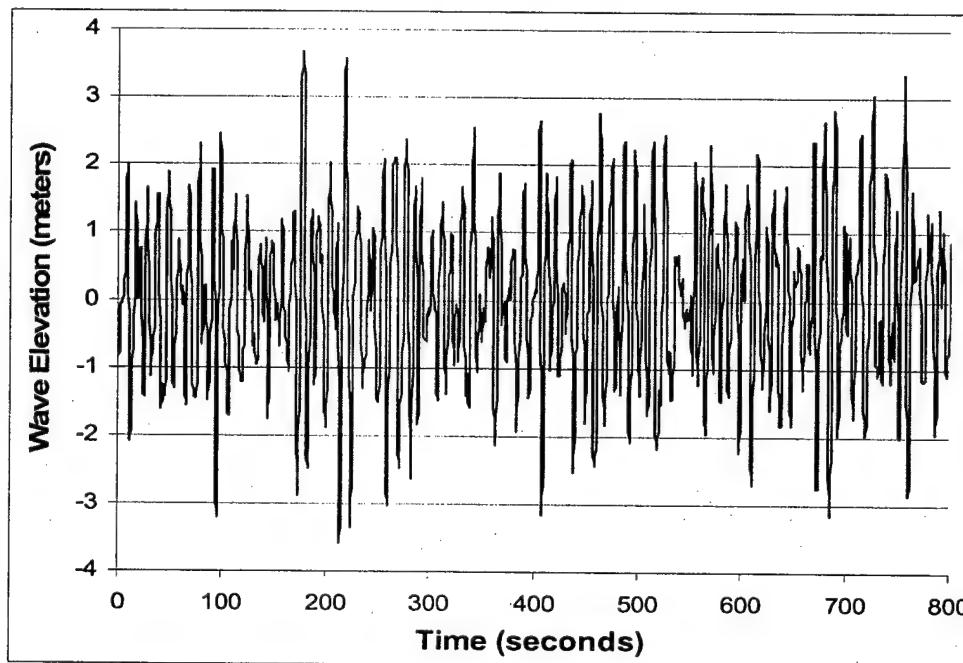
Figure 7.6 Record of wave elevation for sea state 5 with 30 bands.

7.4.2 Hydrodynamic Loads

Every time step the solver requests the forces and moments on the six components of the floater. The hydrodynamic forces consist of inertial and viscous drag. Horizontal forces on the submerged portion of the tower and the spar create moments about their bases. The description of the excitation forces are given in Chapter 6. The long wavelength approximation is assumed to be true since the diameter of the spar is much less than the expected wavelengths. The structure is assumed to produce negligible amounts of waves due to its relatively small diameter.

The spar and submerged tower calculations are very similar. There are two differences. The first difference is the heave added mass. The heave added mass is produced related to the surface area of the bottom of the spar. Since the tower is connected to the spar, it has no added mass in heave.

59

Therefore, a heave single added mass is used for the tower and spar combination. The second difference is how the viscous drag is calculated. Drag in the z-direction is assumed to be zero for the submerged portion of the tower. The vertical component of viscous drag is produced by the bottom of the spar.

The solver sends the following data to the *fltr_loads* subroutine: time, component identification, component positions, component velocities, and component accelerations. The strip method is used for both the submerged tower and the spar. The position of each is used to calculate the horizontal and vertical velocity and acceleration of the water displaced by the floater strip. These velocities and accelerations are then used to calculate the initial and drag forces and moments using GI Taylor (6.4) and Morison (6.9). Summing the strips contributions results in the total force (3 components) and moments (2 components). No yaw moment is produced by hydrodynamic loads on the cylinders.

The spokes have a very small contribution to the overall loads on the system. The actual configuration of the spokes is unknown. The spokes could be open trusses or closed boxes or cylinders. For ease of modeling the spokes are represented by closed rectangular boxes with a characteristic dimension (*w*).
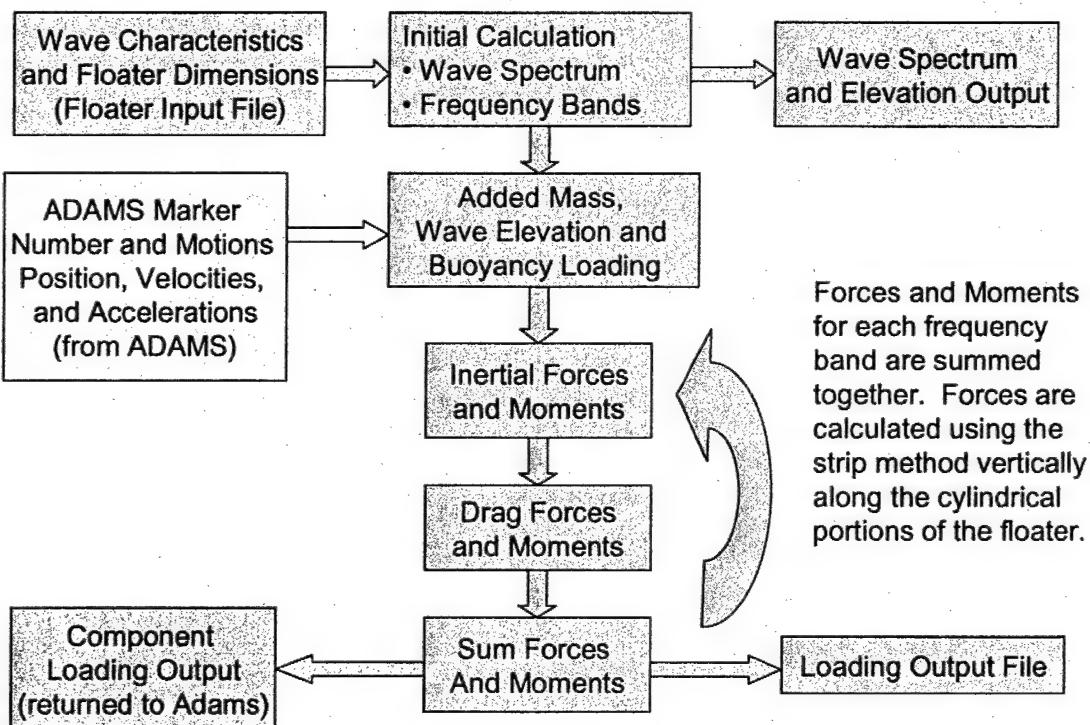
Figure 7.7 Flowchart for *fltr_loads* subroutine.

60

7.5 Complete System Model Description

The floating wind turbine system is modeled by coupling the dynamic models of a wind turbine and floater using the ADAMS mechanics dynamic analysis program. The wind turbine model is made up of elements that are connected by springs and dampers. The physical values for the restoring and damping coefficients are chosen to represent the mechanical properties of the wind turbine blades, drive train, and tower. Figure 7.8 shows how the model and control files are generated. The ADAMS preprocessor in FAST (*Fast2Adams* subroutine) and the floater preprocessor (*fltr_prop* subroutine) act together to write the files necessary to run the fully coupled analysis.
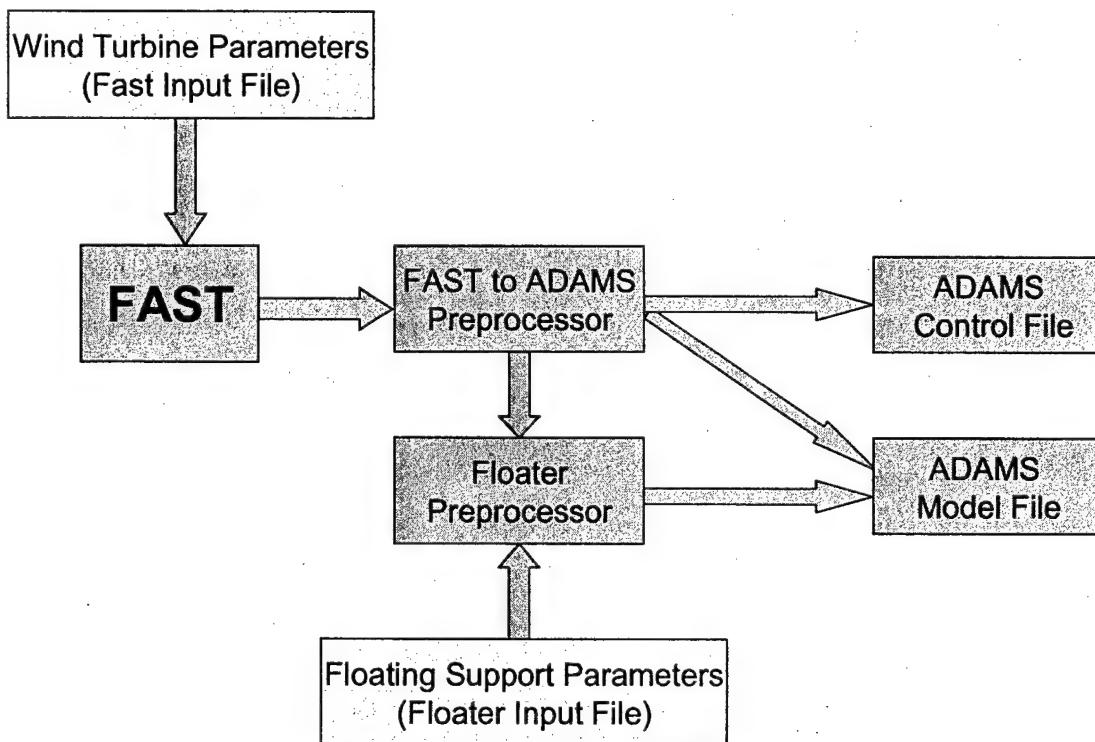
Figure 7.8 Flowchart for writing model and control files.

The control file governs the operation of the solver. The solver determines the motion and total loading of the elements that make of the system. The aerodynamic forces acting on the individual blade elements are calculated in the AeroDyn subroutine. AeroDyn is an element-level wind-turbine aerodynamics analysis routine. It requires information on the status of a wind turbine from the dynamics analysis routine and returns the aerodynamic loads for each blade element to the ADAMS Solver [22].

The input wind field to the rotor of the wind turbine is a data file that contains either a time marching set of hub height wind velocities or a time marching three dimensional turbulent wind velocity profile. A program produced by the NWTC called SNWind is used to generate the wind input files. AeroDyn uses the position of the blade element to determine the local wind flow and then calculates velocity vectors for that element.

As discussed in Section 7.4 the solver also uses an external subroutine to calculate the hydrodynamic forces on the floater components. The overall operation of the solver and how it interacts with the external subroutines and data files is shown in Figure 7.9. The pitch of the wind turbine blades are regulated by a pitch control subroutine. Blade pitch is changed to control speed of the rotor or power of the turbine.
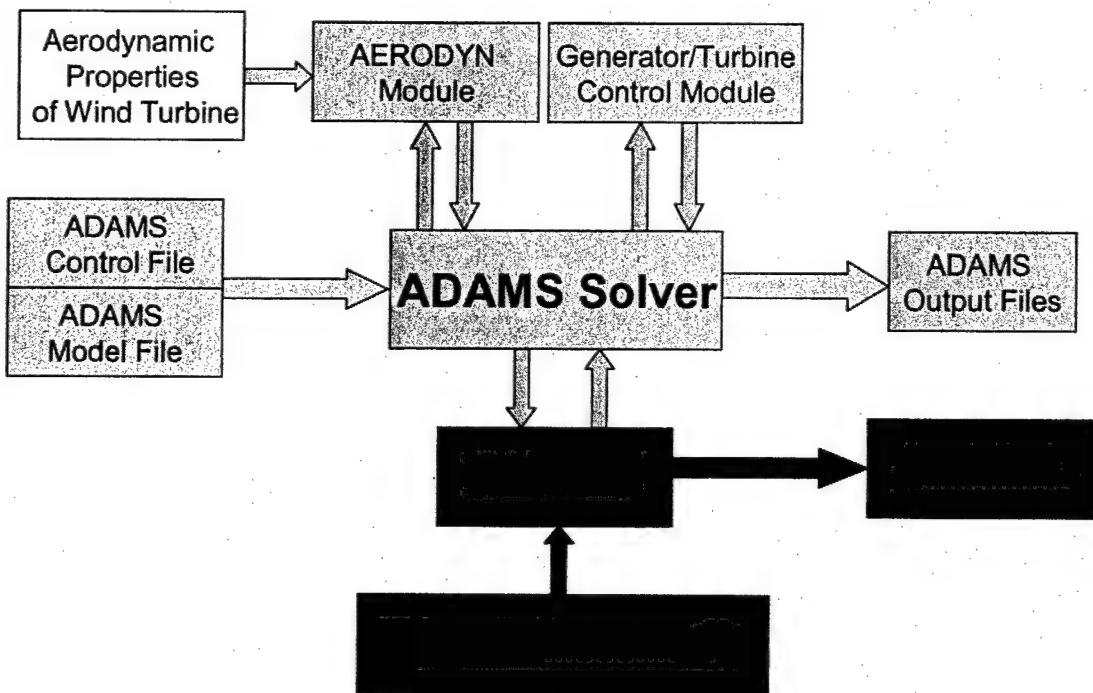
Figure 7.9 Analysis of model flowchart.

The output of the solver consists of two files. The first is a graphics file that contains the motion of every element that makes up the system. This file can be viewed in the postprocessor. The second output file that is generated is the request file. The request file stores all additional data requested by the operator, such as loads, displacements, velocities, and accelerations.

7.6 Model Verification

An important step in the analysis of the combined wind turbine / floater system is to ensure that the systems are being modeled correctly. The verification of the system as a whole against a physical models response in a simulated ocean environment would be ideal. Unfortunately, for this research, that method was cost prohibitive. Instead, the individual tools used in the analyses are verified independently of each other.

The hydrodynamic modeling of the floater is performed by calculating the excitation forces on the six floater elements in the *fltr_loads* subroutine and integrating them into the system dynamic model in the solver. The verification of the floater modeling is accomplished by comparing the predicted floater motion of a simulation with the analytical solution obtained from linear theory.

The operation of the floater model and associated hydrodynamic loading subroutine was tested by analyzing a tension leg spar buoy without a wind turbine attached. This allowed for the operation of the floater loading model to be evaluated without interference from the wind turbine. The verification tests were conducted for two different wave frequencies. Both of these test cases used the same floater design which is shown below in Figure 7.10. The floater input file is included in Appendix A. This file contains a detailed description of the structures physical properties.

With the wind turbine removed from the system the linear dynamic analysis becomes easier. The system shown in has a center of gravity which is below the center of buoyancy. The distance between the center of gravity and the center of buoyancy greatly affects the cross-coupling between surge and pitch. Table 7-1 lists the important physical characteristics of the floater used in the verification tests. A time domain simulation was conducted for the modified system response in 1 meter waves with frequencies: 0.75 and 0.9 rads/sec.
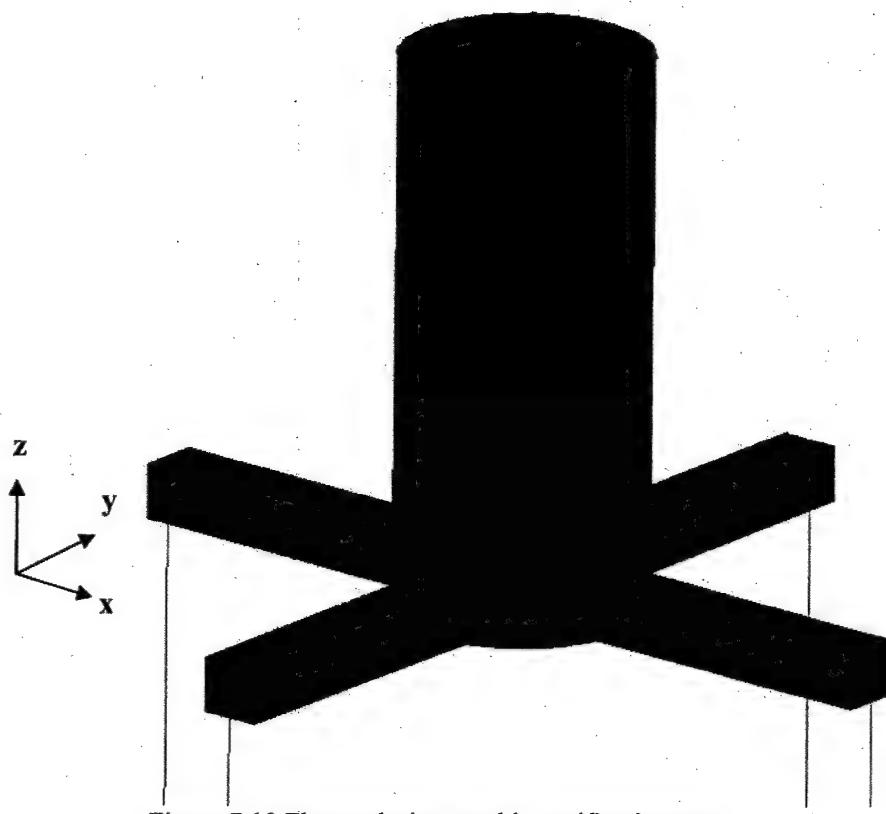
Figure 7.10 Floater design used in verification test.

Table 7-1 Properties of floater used in verification tests.

Spar Diameter	4 m	Water Depth	200 m
Spar Draft	10 m	System Mass	49002.3 kg
Spoke Depth	10 m	Buoyant Mass	149887.8 kg
Structure Thickness	2.53 cm	Reserve Buoyancy	205.9 %
Spoke Length	5 m	Center of Gravity	-6.698 m
Spoke Width	1 m	Center of Buoyancy	-5.687 m
Buoyant Spokes	Yes	BG	-1.011 m
Line Diameter	50 mm	Moments of Inertia	$kg\text{-}m^2$
Number of Lines	1 / spoke		
Line Minimum Break Load	200 tonnes	Ixx	1140080.9
Maximum Line Extension	4.5 %	Iyy	1140080.9
Line Length	188.9 m	Izz	451478.0

The results of the surge verification tests are shown in Figure 7.11. The surge response of the floater generated by the time domain simulation using the hydrodynamics loading module and ADAMS

solver is plotted for a 100 second period of time for the two test frequencies. The analytical predictions for the system motion are also plotted. The results of the time domain simulation match the expected response for both frequencies. The equation of motion that governs the surge behavior is given by (7.1). Surge is strongly coupled with pitch.

$$\begin{pmatrix} M_{11} + A_{11} & A_{15} \\ A_{51} & M_{55} + A_{55} \end{pmatrix} \begin{pmatrix} \ddot{\xi}_1 \\ \ddot{\xi}_5 \end{pmatrix} + \begin{pmatrix} B_{11} & B_{15} \\ B_{51} & B_{55} \end{pmatrix} \begin{pmatrix} \dot{\xi}_1 \\ \dot{\xi}_5 \end{pmatrix} + \begin{pmatrix} C_{11} & C_{15} \\ C_{51} & C_{55} \end{pmatrix} \begin{pmatrix} \xi_1 \\ \xi_5 \end{pmatrix} = \begin{bmatrix} F_1(t) \\ F_5(t) \end{bmatrix} \qquad (7.1)$$

The motion of the structure in pitch is also given by equation (7.1). The cross-coupling between surge and pitch was very evident. When the A_{51} and A_{15} terms were set to zero in the linear analysis the difference between the predicted results and simulations became very large. The plots of the predicted and simulated values of pitch are shown in Figure 7.12. The predicted and simulated pitch values are the same.

The agreement between the simulated and predicted response of both modes of motion verifies the accuracy of the method by which the floater is modeled. Therefore, the motion of the complete system can be determined using the time domain analysis method with the coupling between the floater and wind turbine being handled in the mechanical dynamics solver.

The wind turbine model and its loading and control subroutines are obtained from the National Wind Technology Center. The prediction of aerodynamic lift and drag forces is a difficult problem. Computer code results are sometimes very different from wind tunnel data. However, AeroDyn is seen as an acceptable method for determining the loads on blade elements. Therefore, this method of modeling wind loading on the rotor blades is used for the analysis of the floating wind turbine system.

The ADAMS/Solver has been widely used by industry and educational organizations. Its operation has been fully verified for several different mechanical systems. The information related to the verification process of the Solver can be found in the ADAMS Verification Guide in the ADAMS User's Manual [1].
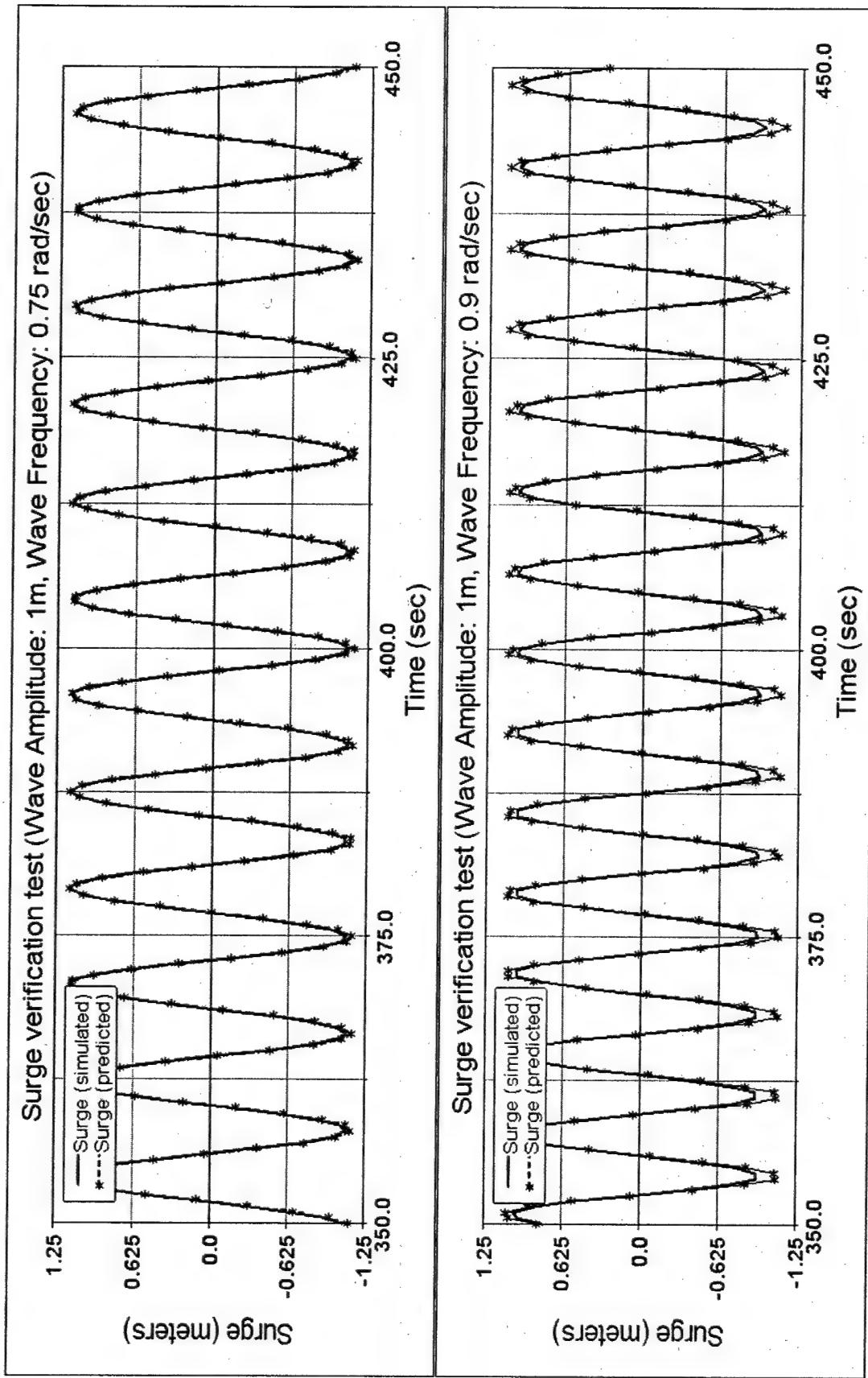
Figure 7.11 Results of surge verification test.

66
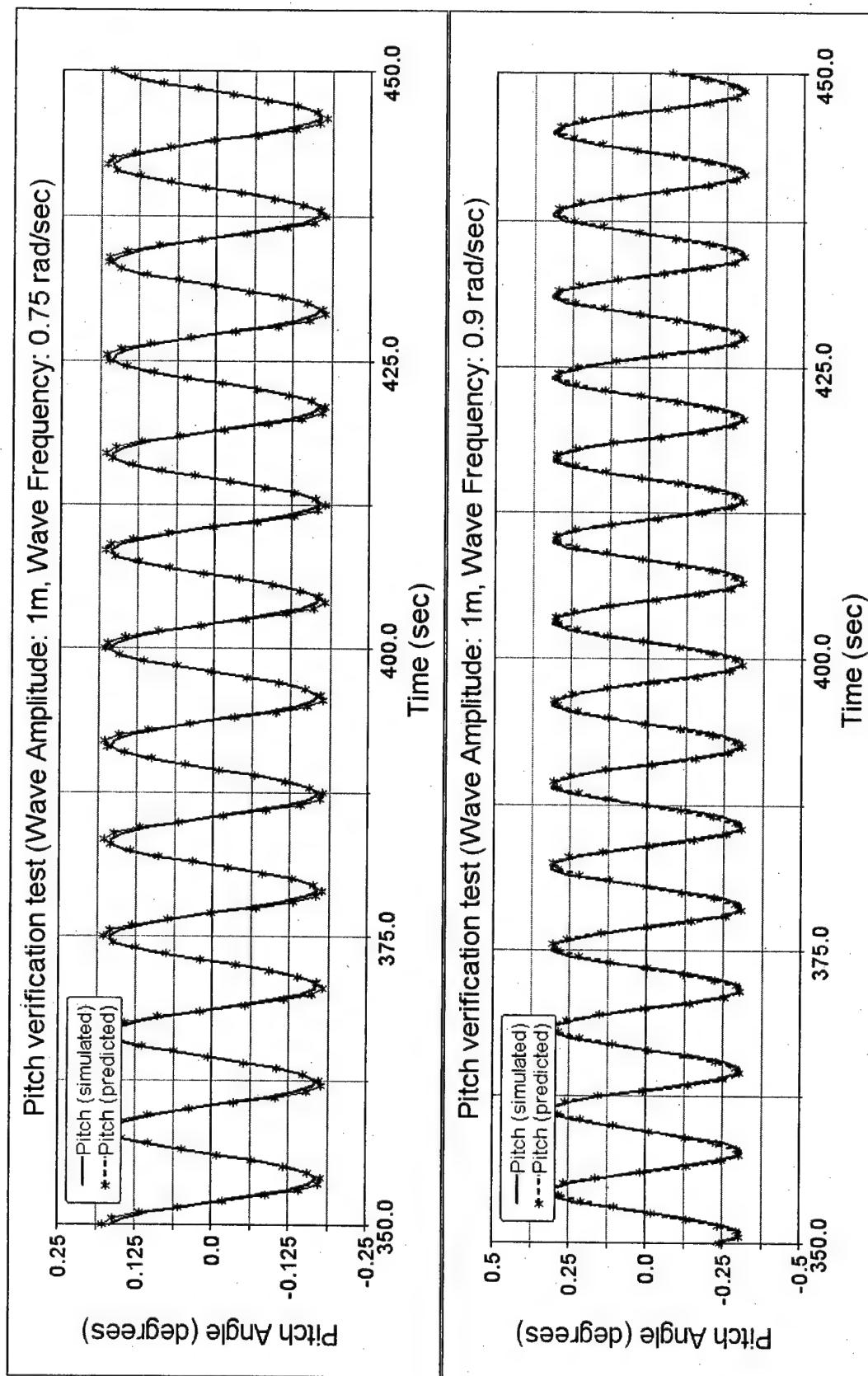
Figure 7.12 Results of pitch verification test

67

7.7 Description of Wind Turbine

The wind turbine used in this analysis was a 1.5 MW Horizontal Axis Wind Turbine (HAWT). It was a three bladed upwind design. The model for this machine was obtained from the NWTC Design Codes website. It is referred to as the 1.5 MW Baseline wind turbine. This turbine was chosen for two reasons. First, it had been used by the NWTC in the past for evaluating the FAST analysis code. The second reason for the selection of the 1.5 MW Baseline wind turbine was it was the only model available which was of sufficient size to warrant mounting it on a floating platform. Most currently installed offshore wind turbines are of this size and rating or larger. The principal characteristics of the 1.5 MW Baseline turbine are given in Table 7-2.

The wind turbine model consists of a description of the systems mechanical, aerodynamic, electrical characteristics. An ADAMS model is generated by the FAST preprocessor based on the input files that describe the wind turbine system. A FAST input file for the 1.5 MW Baseline wind turbine can be found in APPENDIX B. The other information required to describe the turbine are the blade, tower, and AeroDyn input files. The blade input file details the aerodynamic properties of the different airfoils that make up the entire turbine blade. The tower input file lists the physical characteristics of the tower section masses, elasticity, and positions. The AeroDyn input file controls how the subroutine calculates aerodynamic forces.

Table 7-2 Characteristics of the 1.5 MW Baseline wind turbine.

Power Output	1.5 MW	Nacelle Mass	51200 kg
Hub Height	84.29 m	Hub Mass	15100 kg
Rotor Diameter	70 m	Tower Mass	123003 kg
Number of Blades	3	Number of Tower Segments in Model	10
Rotational Speed	20 rpm	Number of Blade Elements in Model	15 / blade
Cut-in Wind Speed	5 m/s	Active Pitch Control	yes
Cutout Wind Speed	25 m/s	Type of Regulation	Speed Regulate

The 1.5 MW Baseline wind turbine model can be modified to simulate different operating conditions. User written controls subroutines can be substituted for the default controls algorithms. This model is a useful tool in analyzing the effect of placing a wind turbine on a floating base and subjecting the system to offshore loads. Figure 7.13 is the graphical representation of the wind turbine.
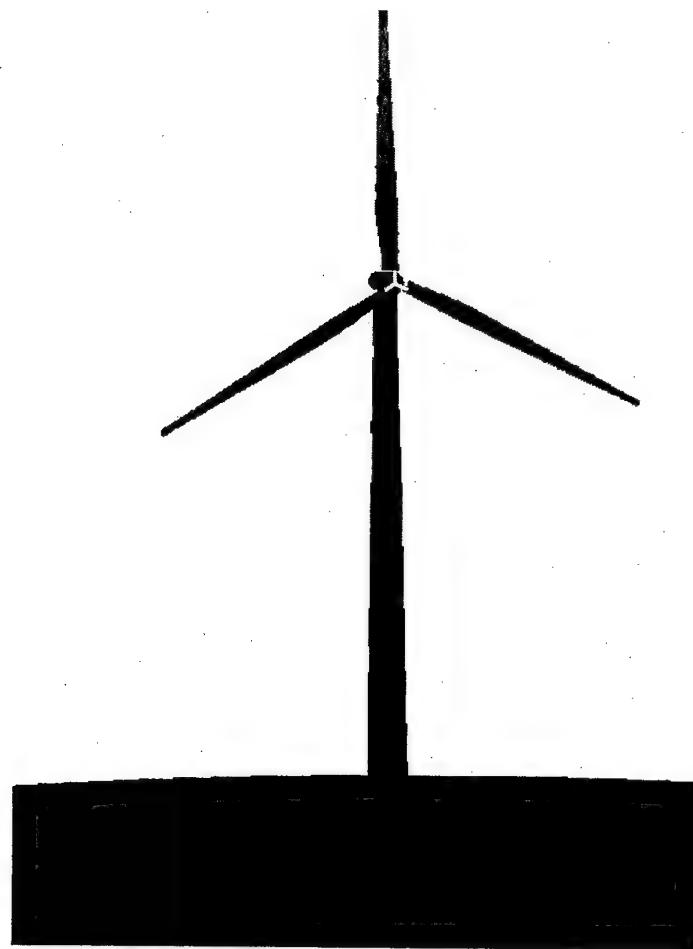
Figure 7.13 Graphic model of 1.5 MW Baseline wind turbine model.

8 Damping

Damping is one of the primary characteristics which must be understood for a moored offshore structure. The floater wind turbine system has three means of damping motions: viscous drag, changes in aerodynamic forces, and structural damping. The effects of these damping mechanisms are analyzed and comparisons made between them.

The damping of vertical cylinders in an ocean environment has been a topic of concern for the offshore industry for many years. The translational motion of the system is of the same order of magnitude as the diameter of the floater. The viscous drag forces on the floater are discussed in section 6.3. Viscous drag is a quadratic damping term.

The damping effects on the wind turbine arise due to changes in inflow of air to the wind turbine when the system moves. Changes in airflow across the blades result in changes in thrust and torque on the rotor. For example; the relative velocity of the wind into the turbine increases when the system surges into the wind. The thrust on the rotor then increases. This increased thrust resists the motion of the system and thereby acts as a damping mechanism. This damping mechanism will be shown to be a linear damping mechanism.

Structural damping occurs when a material is deformed under stress. Some of the energy exerted in the deformation is absorbed by the material. The motion of the structure is therefore attenuated. The effect of structural damping is relatively small for the floating wind turbine. In order to determine the damping from the structure all of the other damping mechanism must be secured. A single surge free decay test was conducted with all other damping mechanisms secured. The results showed that over a 4000 second data run the amplitude of the oscillation changed by less than 1 percent. No further efforts were made to understand the structural damping.

The damping of the system for various modes of motion is found by conducting free decay tests on the model. These tests are initiated by applying a loading to the floater to cause a displacement. Then the load is removed and the response of the system evaluated. Thirty two damping runs where conducted with and without the wind turbine operating. In some tests viscous drag was set to zero so that the wind turbine could be evaluated separately from the floater. The results of the damping tests are detailed in the following sections.

Faltinsen described a method for evaluating the results of free decays to extract the linear and quadratic damping coefficients (p. 252, [13]). This method is normally used to physical tests. It can be applied to the simulations that involve more than one damping mechanisms. Using this technique can enable single free decay data runs to be used to exact both damping coefficients for the system. The equation of motion for a body undergoing free decay is:

$$\ddot{x} + p_1 \dot{x} + p_2 |\dot{x}| \dot{x} + p_3 x = 0 \tag{8.1}$$

where p_1 is the linear damping coefficient and p_2 is the quadratic coefficient. If the damping is constant with the amplitude of oscillation the damping coefficients can be found using the following relationship:

$$\frac{2}{T_m} \log\left(\frac{X_{n-1}}{X_{n+1}}\right) = p_1 + \frac{16}{3} \frac{X_n}{T_m} p_2 \tag{8.2}$$

where X_n is the amplitude of the *nth* oscillation. The oscillations are separated by a time equal to half the period. The left side of equations (8.2) is plotted as the dependant quantity of term $16 X_n / 3 T_m$. The points are then fitted with a straight line using the least squares method. The y-intercept and slope of the fitted line correspond to p_1 and p_2 coefficient.

This method allows for the non-dimensional coefficients p_1 and p_2 to be determined for a time record of a motion that damps out with time. These coefficients are useful when discussing the relative importance of a damping mechanism (viscous drag or wind turbine) for a given mode of motion. In some modes of motion viscous drag is found to dominate and in others the linear damping of the wind turbine. These coefficients are also useful when trying to extract the effect individual parameter changes (such as blade pitch) have on system damping.

8.1 Description of Floating Wind Turbine used in Damping Tests

A single floater design was used for all of the damping tests. It consisted of both a spar cylinder and an extension of the tower below the surface. The floater supported the 1.5 MW wind turbine. Table 8-1 gives the dimensions and characteristics of the floating support.

Table 8-1 Dimensions and properties of floater used in damping tests.

Spar Diameter	10 m	Line Diameter	112 mm
Spar Height	12 m	Number of Lines	2 / spoke
Tower Diameter	8 m	Line Minimum Break Load	371 tonnes
Tower Draft	5 m	Maximum Line Extension	14 %
Spoke Length	20 m	Line Length (un-stretched)	176.2 m
Spoke Width	1 m	Water Depth	200 m
Buoyant Spokes	No	Structure Thickness	2.53 cm

The lines used in the damping test were chosen for their flexibility. Having flexible lines allowed for larger amplitudes of oscillation during the free decay tests. Polyester lines have elongation properties similar to those of the damping floater model. The calculated properties of the system are given in Table 8-2. The natural periods are included for the sole purpose of comparing them to the simulation results. A rendering of the floating wind turbine model is shown in Figure 8.1. No wave excitation is used during the damping tests.

Table 8-2 Calculated attributes of the floating wind turbine used in the damping tests.

Mass of Floater	210435.4 kg	Center of Gravity (system)	19.608 m
Buoyant Mass	1228424.6 kg	Center of Buoyancy	-9.211 m
Total Mass of System	411494.5 kg	BG	28.819 m
Reserve Buoyancy	198.5 %	Surge / Sway Natural Period	39.02 sec
Initial Line Stress	101.7 MPa	Heave Natural Period	4.45 sec
Breaking Line Stress	369.3 MPa	Pitch and Roll Natural Period	10.82 sec
Center of Gravity (floater)	-11.82 m	Yaw Natural Period	10.52 sec
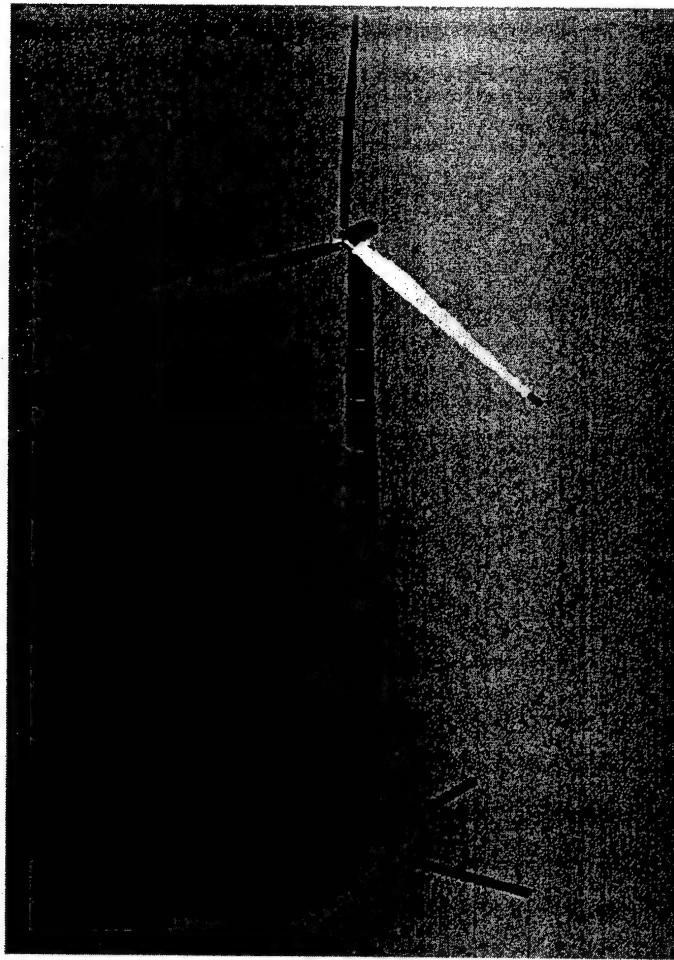
Figure 8.1 Floating wind turbine system used in damping tests.

8.2 Surge Damping

The major contributor to ocean wave generation is wind acting on the surface of the water. Wind generated waves tend to propagate in the direction of the winds. In a steady wind environment, with winds blowing in the positive x-direction, the wave motion of the floating wind turbine will be in the surge direction. Therefore, surge damping is one of the most important properties to understand.

The free decay test for the surge damping is conducted by applying a load in the x-direction. This load causes a deflection in the floater away from its rest position. Damping is determined with no waves acting on the structure. Five tests were run for the surge damping analysis. When the wind turbine is operating wind is assumed to be steady at 20 m/s. For the first test the wind turbine was secured so that the damping of the viscous drag could be evaluated. The next three tests were run with the viscous drag set to zero for the floater. These three tests evaluated the effect of blade pitch on the

system damping. The blade pitch of the wind turbine was set at three different values: 18 degrees, 22 degrees, and 26 degrees. The final test consisted of the wind turbine operating with viscous drag on the structure.

8.2.1 Floater Damping

The damping properties of the floater were analyzed by performing a surge free decay simulation with the wind turbine secured. The results of this damping test are shown in Figure 8.2. There are two graphs of the response to the surge impulse. The viscous drag attenuates the amplitude over 1250 seconds. The bottom graph is the absolute value of the surge amplitude on a logarithmic scale. This graph shows that viscous drag is a quadratic damping mechanism, since the decay is greater than linear.

The quadratic damping coefficient for the system is 0.7. It should be noted the frequency of the surge response during the free decay test is 39.4 seconds. Which corresponds to the natural frequency predicted using linear theory. The output of this test was evaluated using the method described by at the end of the previous section. Viscous damping results in a rapid attenuation of the oscillations early on. This damping force becomes very small once the motion of the floater slows, since viscous damping is proportional to the square of the floater velocity.
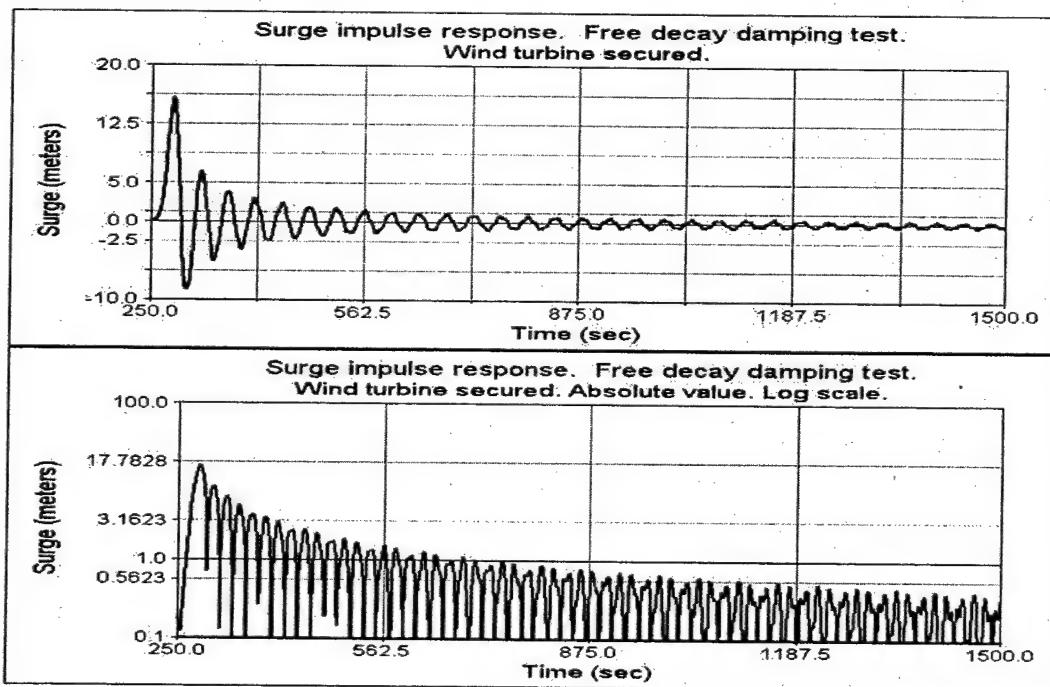
Figure 8.2 Viscous damping response in surge. Wind turbine secured.

The values for the surge damping of the system with the wind turbine secured were found by fitting a curve through the data points in Figure 8.3. The value for p_1 was found to be very small negative number. This indicates that linear damping was negligible during the damping test. When the wind turbine was secured the system experienced small oscillations in modes other that surge and pitch during this simulation. These vibrations resulted in data scatter which is responsible for the negative value for p_1. Ideally, this value would be zero. The p_2 coefficient was determined to be 0.0392.
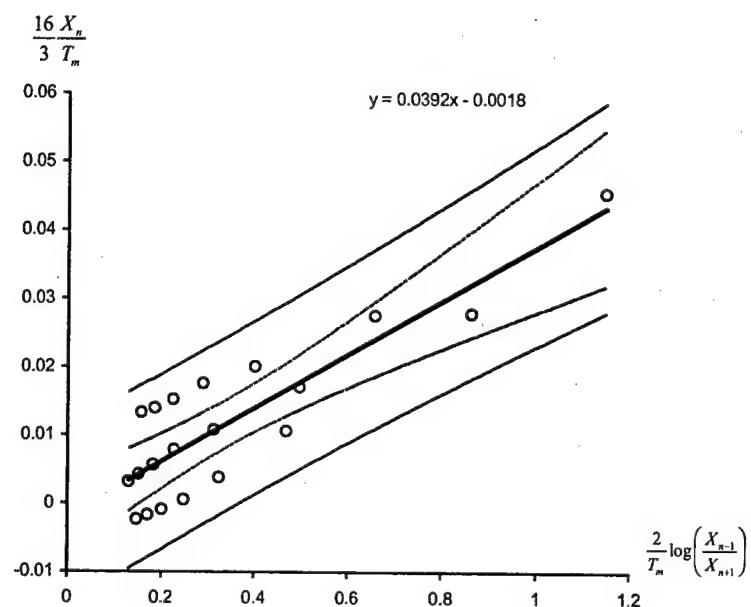
Figure 8.3 Plot used to determine p_1 and p_2 for the surge damping test. Wind turbine secured.

8.2.2 Damping due to Wind Turbine

The damping properties of the wind turbine were evaluated by setting the viscous drag of the floater to zero. The damping of the wind turbine was found to be linear as expected. The pitch of the blades was found to affect pitch damping of the wind turbine. Free decay simulations were conducted for three settings of blade pitch: 18 degrees, 22 degrees, and 26 degrees. The results of the free decay tests are shown in Figure 8.4. It should be noted that when in operation the wind turbine causes a mean displacement of the floater due to the thrust on the rotor.

The wind turbine was shown to have a stabilizing effect on the system due to its linear damping characteristics. Small oscillations which were present for the surge free decay test with the wind turbine secured were not seen when the wind turbine was operating.
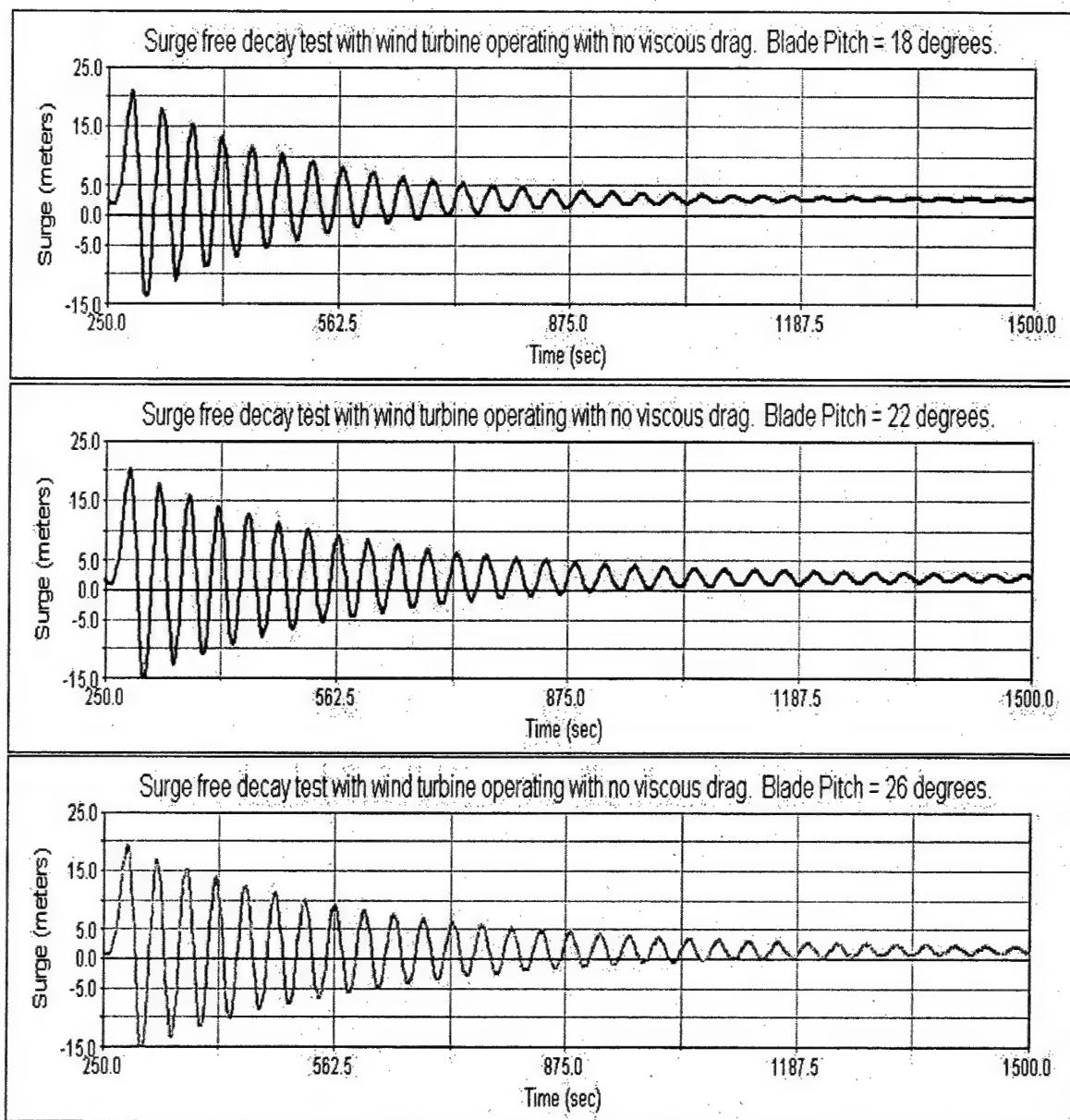
Figure 8.4 Surge damping results for wind turbine with blade pitch equal set at 18, 22, and 26 degrees. 20 m/s constant winds. No viscous drag.

Changing the blade pitch changes the angle of attack of the airfoil. Lift and drag of an airfoil is dependant on angle of attack. Therefore, the amount of thrust for a given change in inflow to the rotor changes with blade pitch. This is the reason that the damping characteristics of the three tests differ. In order to extract the linear damping coefficients of the mean offsets are removed and the absolute values of the surge oscillations plotted on a logarithmic scale.

76
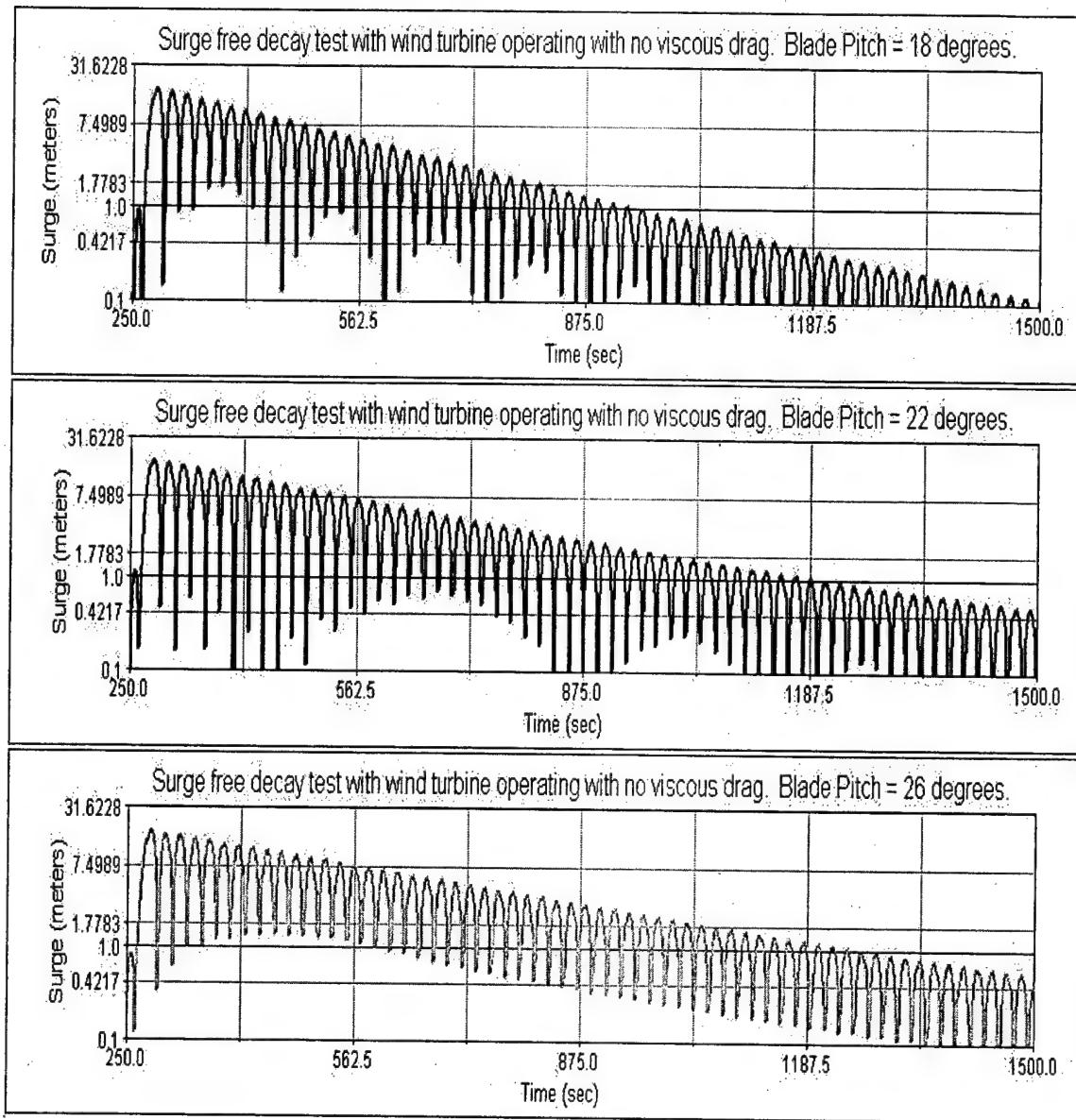
Figure 8.5 Absolute value of surge response for free decay tests with 18, 22, and 26 degree blade pitch. 20 m/s constant winds. No viscous drag.

Evaluation of Figure 8.5 yields the linear damping coefficients for the three tests. When there is no quadratic damping the p_2 in the equation that governs a linear damping response is:

$$p_1 = \frac{2}{T_m} \log\left(\frac{X_{n-1}}{X_{n+1}}\right)$$ (8.3)

Where $X(t)$ is the amplitude of oscillation at time t and X_O is the initial displacement. A more useful form of this equation allows for multiple cycles to be used in a single calculation:

77

$$p_1 = \frac{2}{N \cdot T_m} \log\left(\frac{X_0}{X_{2N}}\right) \qquad (8.4)$$

where N is the number of half cycles. The linear damping coefficients for the three different blade pitches are given in Table 8-3. The damping coefficient decreases with increasing blade pitch. Changing the blade pitch also affected the power output of the wind turbine. This is due to the fact that thrust and torque on the rotor are both governed by inflow speed of the wind and the blade pitch.

Table 8-3 Damping coefficients for the wind turbine with three different blade pitch angles: 18 degrees, 22 degrees, and 26 degrees. 20 m/s constant winds. No viscous drag.

Blade Pitch	Damping Coefficient (p_1)
18°	8.37 E-3
22°	6.90 E-3
26°	5.1 E-3

8.2.3 Surge Response with both Linear and Quadratic Effects.

The final free decay test involved testing the floating wind turbine system as a whole. The test simulated the damping response of the system operating near the cutout wind speed for the turbine. The wind turbine was operating with 20 m/s constant winds into the rotor. The pitch of the rotor blades was fixed at 22 degrees. The second test simulated the damping response of the system operating in 12 m/s winds. In normal operation the pitch of the rotor blades are actively controlled to either maintain rotor speed or maximize generator power. For this second test the wind turbine was operating in speed regulate, with the control system maintaining the rotor at 20 rpm. Viscous drag effects of the floater were also included. These tests model the response of the system undergoing an impulse load in the direction of the positive x-direction.

Figure 8.6 is a set of graphs of the surge response to the free decay test for the wind turbine operating in 20 m/s. By comparing these graphs to Figure 8.2 and Figure 8.4 is can be seen that the combined effect of the two modes of damping greatly decrease the time it takes the system motion to damp out. The results graphed on a log scale in the following figure shows how the damping is greater than linear at the beginning of the test when quadratic effects dominate. At the end of the test the linear damping from the wind turbine dominates.
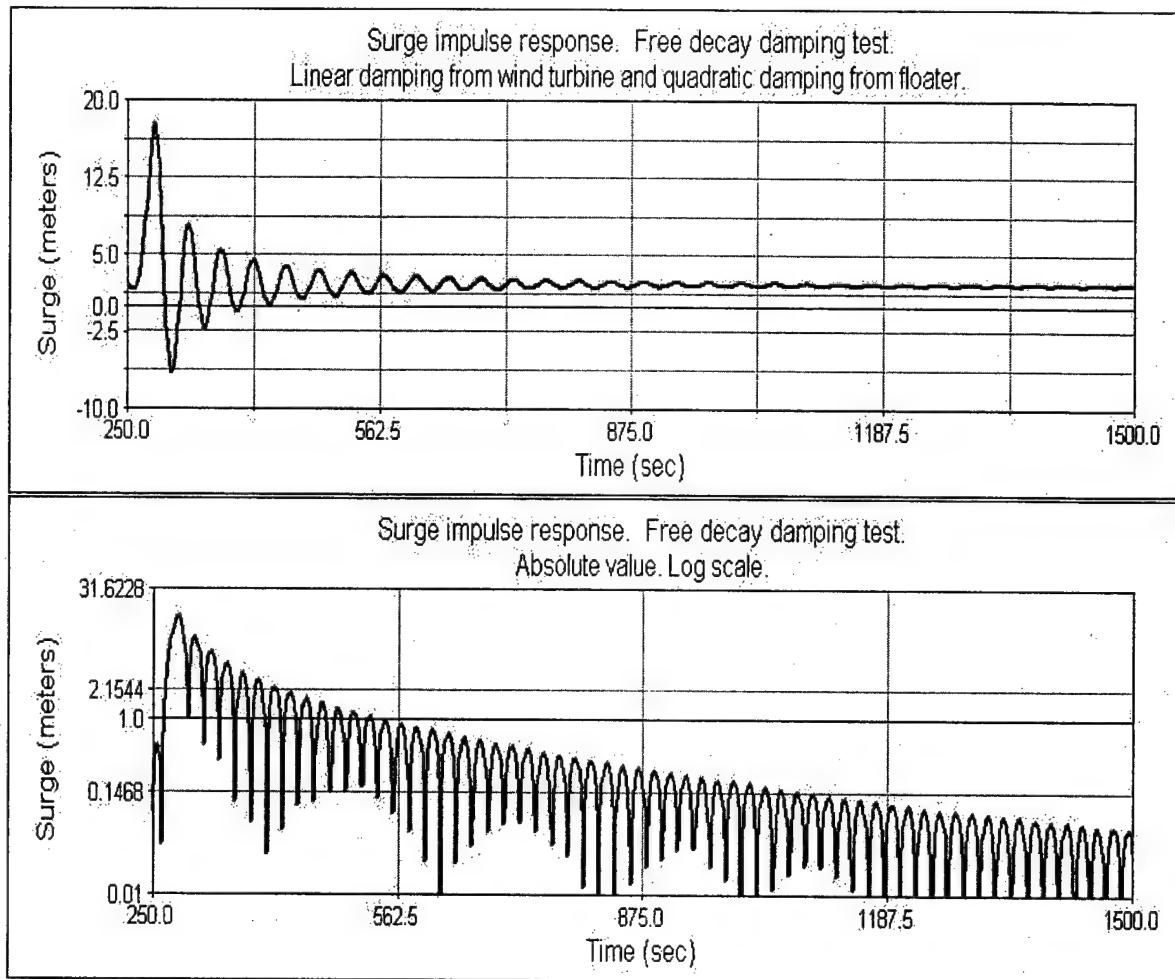
Figure 8.6 Surge free decay test with both linear and quadratic damping effects. Wind turbine operating in 20 m/s constant winds.

The coefficients p_1 and p_2 are found by evaluating the second graph using the method previously described. The terms on the left and right side of equation (8.2) are plotted against each other and a linear regression performed on the data points. Figure 8.7 is the plot used to determine the damping coefficients. The linear damping coefficient (p_1) is found to be 0.0052 and the quadratic damping coefficient (p_2) is found to be 0.0486.

79

$$\frac{2}{T_m} \log\left(\frac{X_{n-1}}{X_{n+1}}\right)$$

$$y = 0.0486x + 0.0052$$

$$\frac{16}{3}\frac{X_n}{T_m}$$
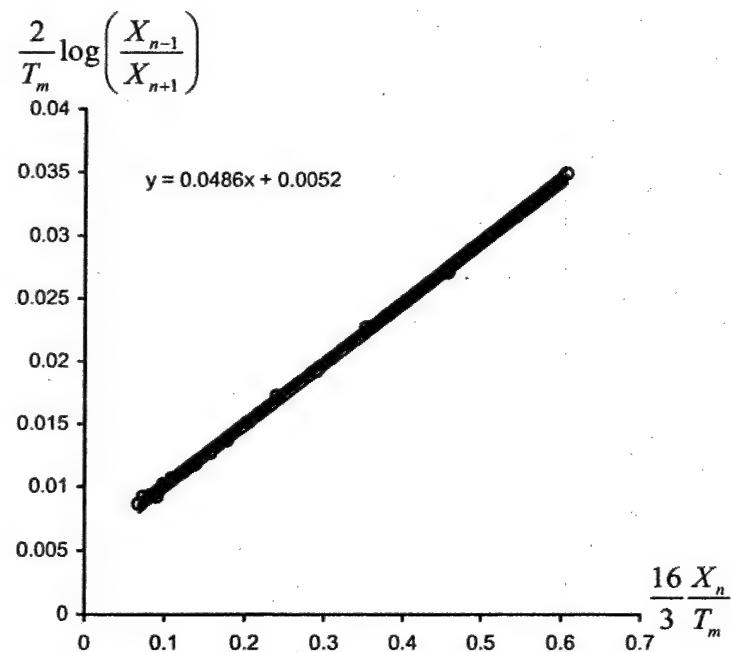
Figure 8.7 Determining coefficients p_1 and p_2 for the surge free decay test with all mechanisms included. 20 m/s constant winds.

The combined system had linear and quadratic damping coefficients which were similar to the individual tests. The differences were not large. The difference in the quadratic damping term p_2 is attributable to data scatter in the results of surge response with viscous drag only. Overall, the combination of the two damping mechanisms appears to match the results expected from the single damping mechanism tests. All remaining tests include both viscous drag and linear damping from the wind turbine.

8.3 Sway Damping

In this research the 1.5 MW Baseline wind turbine is a HAWT with its nacelle aligned with the x-axis. Therefore, sway motion is the horizontal motion of the floater in the plane of the rotor. This type of motion will have a much less significant effect on inflow to the turbine than surge motion. Therefore, the damping effect of the wind turbine is expected to be lower in the sway mode of motion.

A simulated free decay test was conducted by loading the model in the positive y-direction and then removing the load. The response of the model was then generated. The results of the sway free decay test were plotted in Figure 8.8. The mean offset in the y-direction was caused by torque on the rotor.

80
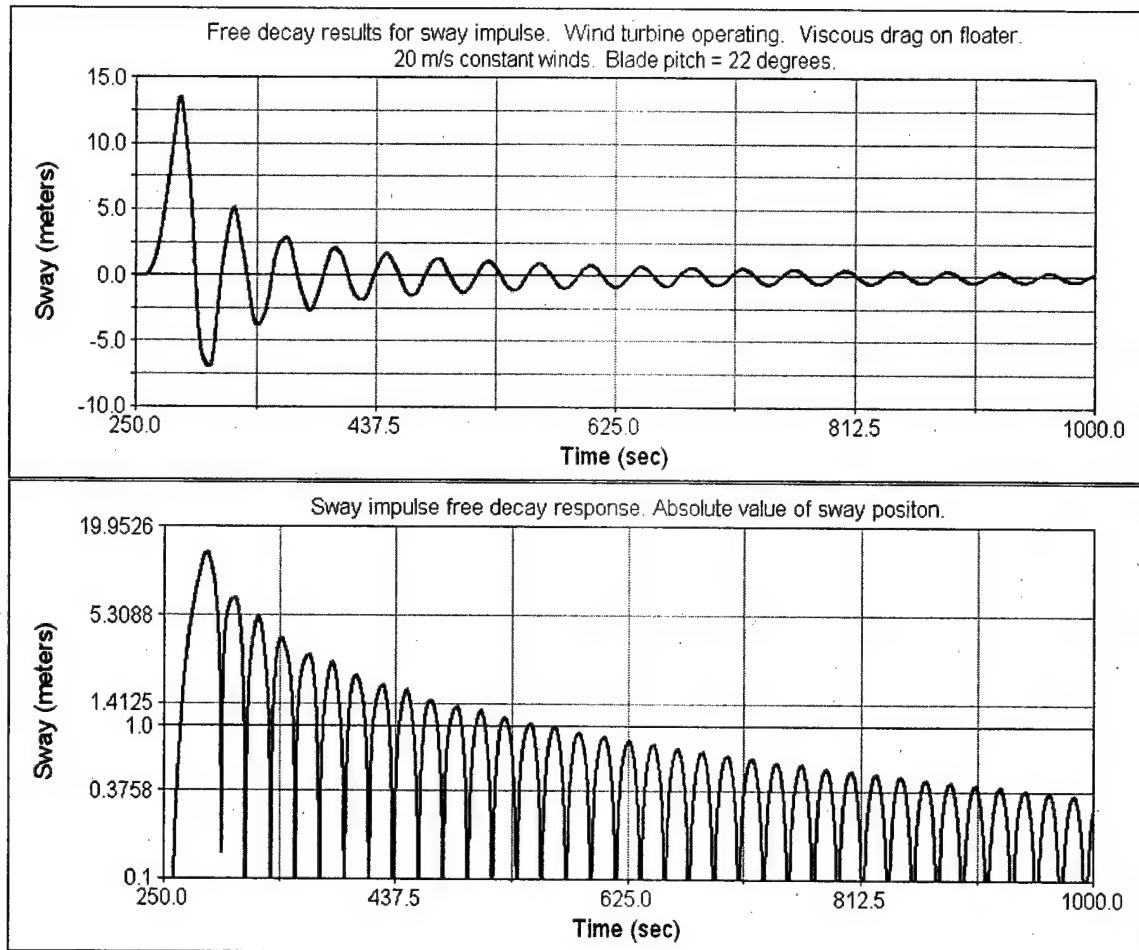
Figure 8.8 Sway free decay test with both linear and quadratic damping effects. Wind turbine operating in 20 m/s constant winds.

Next the coefficients for the linear and quadratic damping terms were determined. The values found for p_1 and p_2 are 0.0454 and 0.0015 respectively. Figure 8.9 is a plot of the data points used to determine the two coefficients. The quadratic damping coefficient p_1 is approximately the same as the value found for the surge damping. This is expected since the floater is moving in sway is nearly identical to the floater moving in sway.

The linear damping coefficient in sway was found to be approximately 30 percent of the surge coefficient for the same initial conditions. The sway linear damping coefficient is less than the surge coefficient since the motion of the structure does not affect the wind inflow to the wind turbine as much as surge motion. This difference in linear damping resulted in the sway oscillations taking longer to damp out than those of the surge test.

81

$$\frac{2}{T_m} \log\left(\frac{X_{n-1}}{X_{n+1}}\right)$$
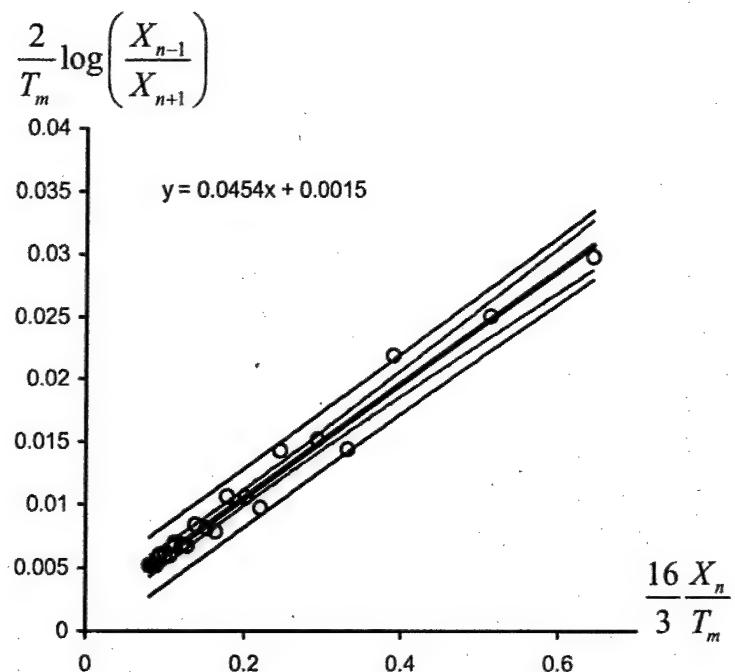
Figure 8.9 Determining p_1 and p_2 for the sway free decay test.

8.4 Heave Damping

Vertical motion of the floating wind turbine is damped out by a combination of changes in wind turbine loading and viscous drag on the floater. The natural frequency for the floating wind turbine in heave is higher than for the other two modes of translational movement (surge and sway). The response of the system to the heave free decay test is therefore characterized by short periods with small amplitudes of oscillation.

In order to determine the heave damping coefficients a free decay test was conducted with the wind turbine operating in 20 m/s constant winds. The blade pitch was fixed at 22 degrees. The floater model was loaded in the positive z-direction and then released. The simulated results were then determined. The frequency of the damping response was 4.44 seconds which agreed with the period predicted using linear theory of 4.45 seconds. The heave position was plotted with respect to time in Figure 8.10.

82
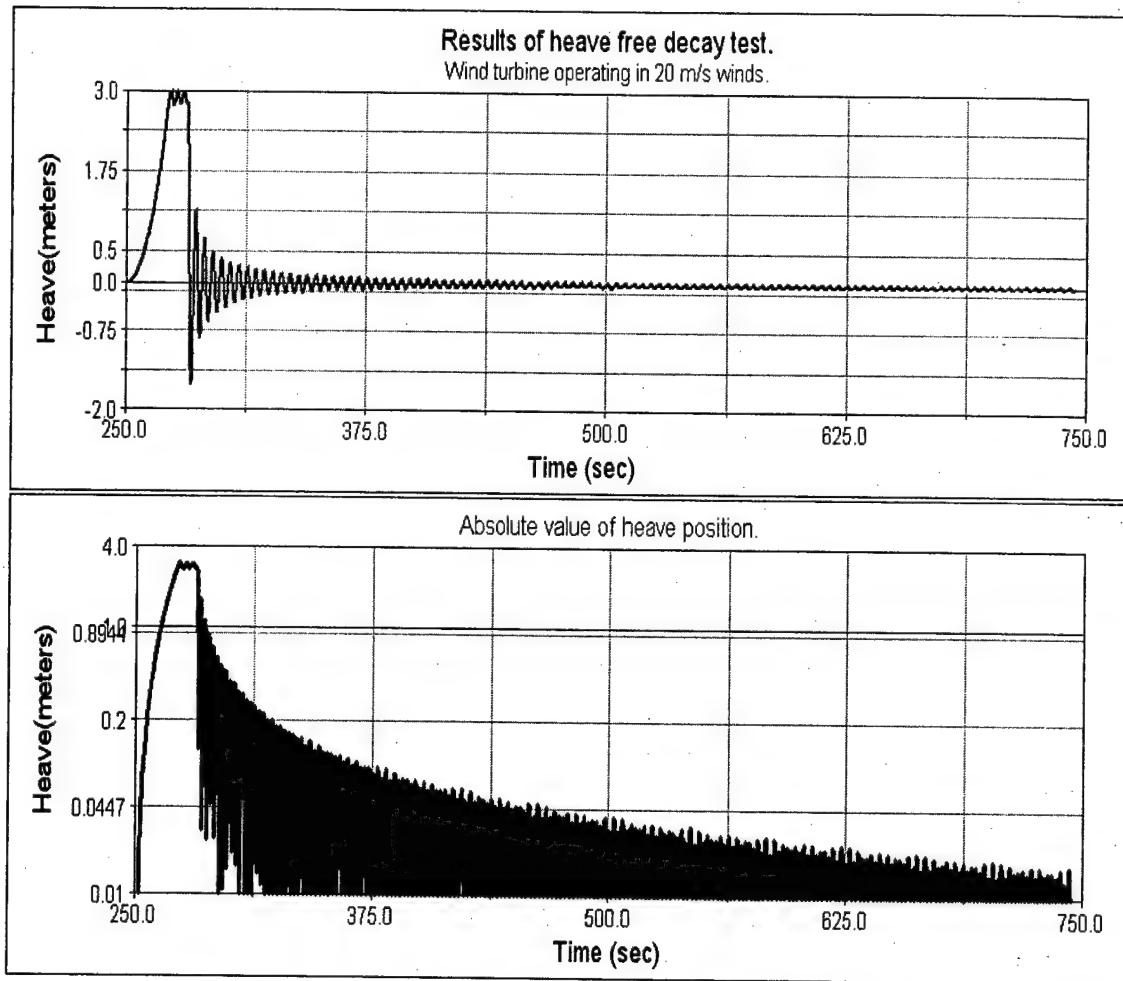
Figure 8.10 Heave free decay test with both linear and quadratic damping effects. Wind turbine operating in 20 m/s constant winds.

The linear and quadratic coefficients were determined from the free decay results. The data points used in this determination were plotted in Figure 8.11. Linear regression of the data resulted in a value of .0039 for p_1 and .244 for p_2. The quadratic damping (p_2) due to viscous drag is relatively large in heave mode of motion. The linear drag coefficient is same order of magnitude as that of the sway mode of motion. Since heave and sway motion a both moving the rotor normal to the wind flow is anticipated that the damping effect of the wind turbine be similar for the two modes of motion.

83

$$\frac{2}{T_m}\log\left(\frac{X_{n-1}}{X_{n+1}}\right)$$
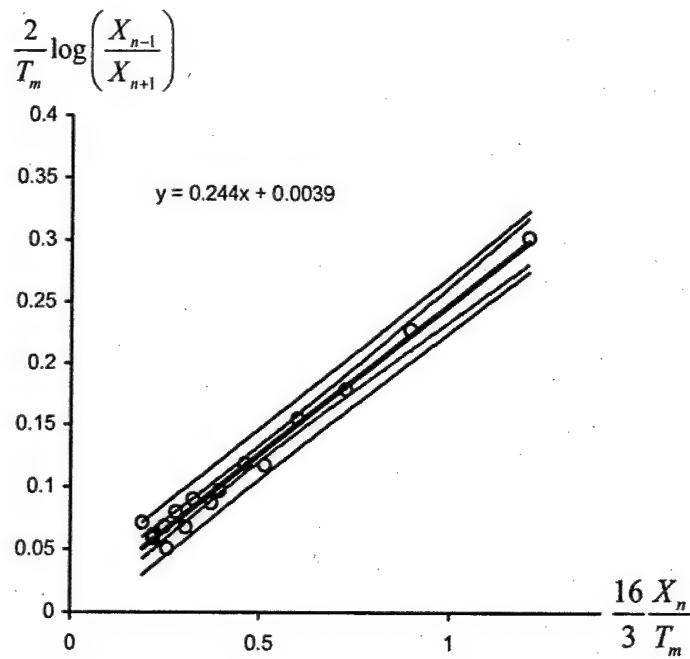
Figure 8.11 Determining p_1 and p_2 for the heave free decay test.

8.5 Roll Damping

The three rotational modes of motion (roll, pitch, and yaw) are coupled to other modes of motion by hydrodynamic effects or by gyroscopic moments generated when the rotor is moved from its plane of rotation. These cross-coupling effects make it more difficult to extract the damping characteristics of the floating wind turbine system than the translational modes of motion. Translational motions in the horizontal directions (surge and sway) have relatively large magnitudes. The cross-coupling from the rotational motions (pitch and sway) do not cause large changes in the horizontal motions. However, the cross-coupling between the translational modes to the rotational modes does have a large effect on the rotational motion of the system in pitch and sway. The result of this behavior is that extracting the damping coefficients for these rotational modes is more difficult.

The first rotational motion that was examined was roll. In roll the structure pivots around an x-axis. This motion did not change the plane of rotation of the rotor. So gyroscopic loads where not generated by the roll motion. The roll motion was cross-coupled to the sway mode of motion. Oscillating displacements in roll caused loading hydrodynamic loading that resulted in sway motion. The sway motion altered the roll oscillations of the structure during the free decay test. The roll position did not oscillate about a fixed point during the free decay test (see Figure 8.17). The period for the roll response was 10.9 seconds which is comparable to the predicted value of 10.8 seconds.

84
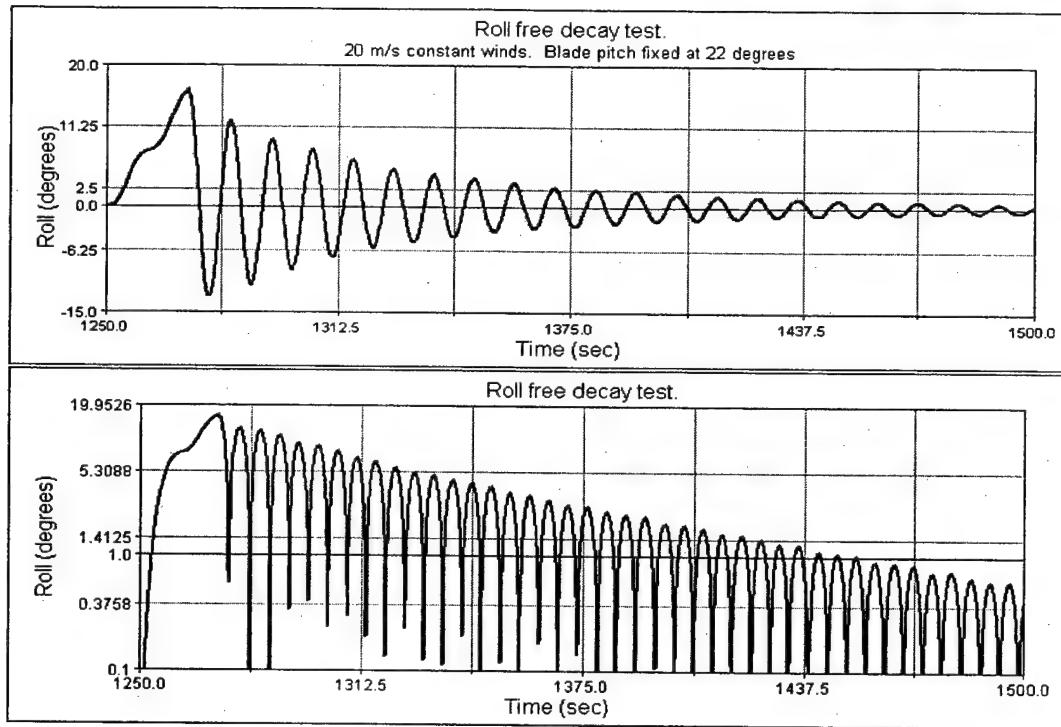
Figure 8.12 Roll damping free decay test. Wind turbine operating in 20 m/s winds. Blade pitch fixed at 22°.

The interaction between roll and sway can be seen on the logarithmic plot of the data. The absolute values of amplitude do not have a smooth trend. The result of this behavior is data scatter during the determination of the p_1 and p_2. Figure 8.13 shows the data points extracted from the free decay test. The values for the linear and quadratic damping coefficients are 0.0285 and 0.0015 respectively.
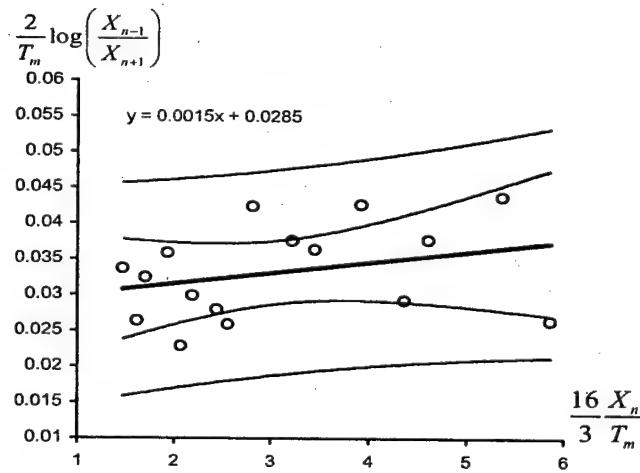
Figure 8.13 Determining p_1 and p_2 for roll free decay test.

85

8.6 Pitch Damping

The floater rotates about a y-axis when it pitches. This motion acts to move the rotor directly into and away from the wind flow, assuming that the nacelle and wind both are aligned with the x-axis. It is intuitively obvious that the damping affect of the turbine will be very large when compared to most of the other modes of motion. This is due to the fact that these other modes don't cause large changes in the inflow to the turbine.

The damping effect of the wind turbine was so large that it made determining the linear and quadratic damping coefficients difficult. As shown in Figure 8.14, the pitch motion of the floater due to the free decay test rapidly damped out. After only four cycles the pitch motion was dominated by cross-coupling with the surge mode of motion (frequency of motion changed to natural frequency of surge.)

Pitch free decay test.
20 m/s constant winds. Blade pitch fixed at 22 degrees.
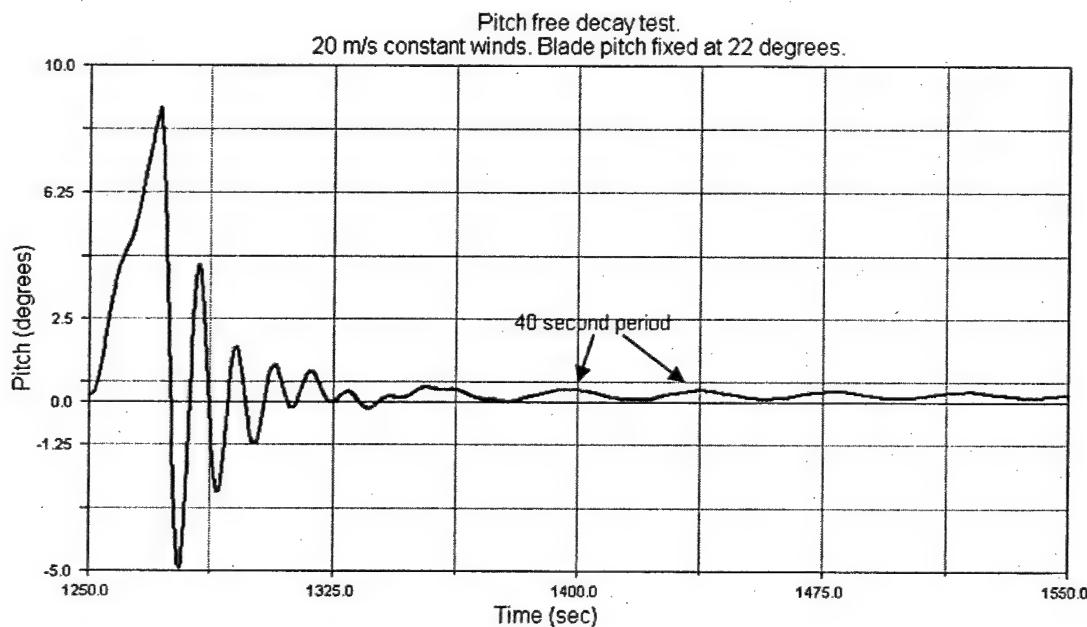
Figure 8.14 Pitch free decay test. 20 m/s constant winds. Blade pitch fixed at 22 degrees.

The pitch damping due to the wind turbine was so strong that only four data points could be obtained to perform the least squares procedure (see Figure 8.15). This number is less than optimal for determining the damping coefficients. The strong linear damping of the system prevented an accurate measurement of the viscous damping term. The values for the damping coefficients found from the linear regression technique were: $p_1 = 0.1665$ and $p_2 = -0.0195$. The value for p_2 is negative. We know that the viscous drag coefficient should be equal to that of roll since the system is symmetrical and should have similar viscous damping properties. Therefore, it is assumed that the value for p_2 is 0.0015 to match the roll viscous drag.

86
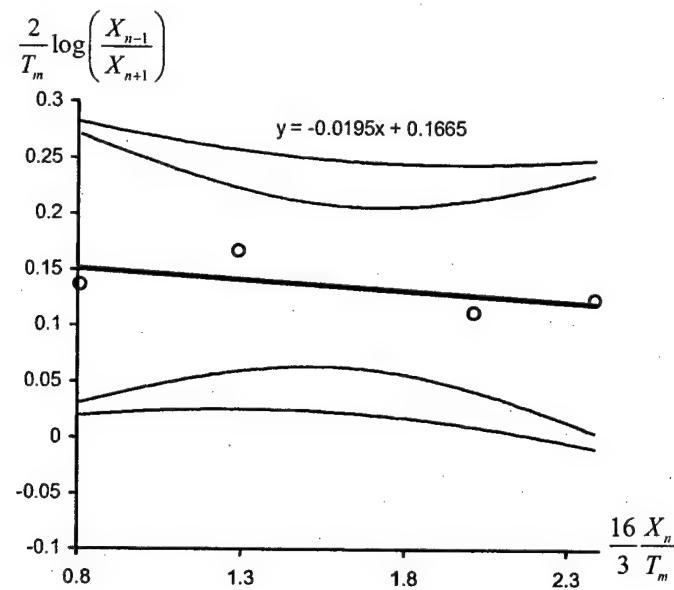
Figure 8.15 Determining p_1 and p_2 for pitch free decay test.

8.7 Yaw Damping

Yaw damping of the system consists of both linear and quadratic effects. The linear damping occurs when a moment is produced on the rotor opposing the yaw motion due to changing aerodynamic forces. As the system yaws, the relative wind speed increases on one side of the rotor and decrease on the other. The difference in relative wind speeds results in a net moment in the opposite direction of the yaw motion. The viscous damping comes from the spokes. As the floater yaws, drag forces develop on the spokes. These forces act to counter the system rotational motion.

It was difficult to conduct a yaw free decay simulation on the design selected for the damping tests. When the system was displaced and then released, it did not simply oscillate in the yaw mode (see Figure 8.16). Observation of other modes of motion showed that the system was being excited into other modes of motion by the yaw motion. The frequency of the oscillations was also not constant. The yaw damping loads are very large and probably the root cause. This behavior is exaggerated greatly when the wind turbine is secured and a free decay test conducted (see Figure 8.17). The cross-coupling between roll and sway can be seen by observing the tail end of the roll curve. The excited roll motion damps out (shorter period) but the structure continues to roll due to sway motion (longer period).

87
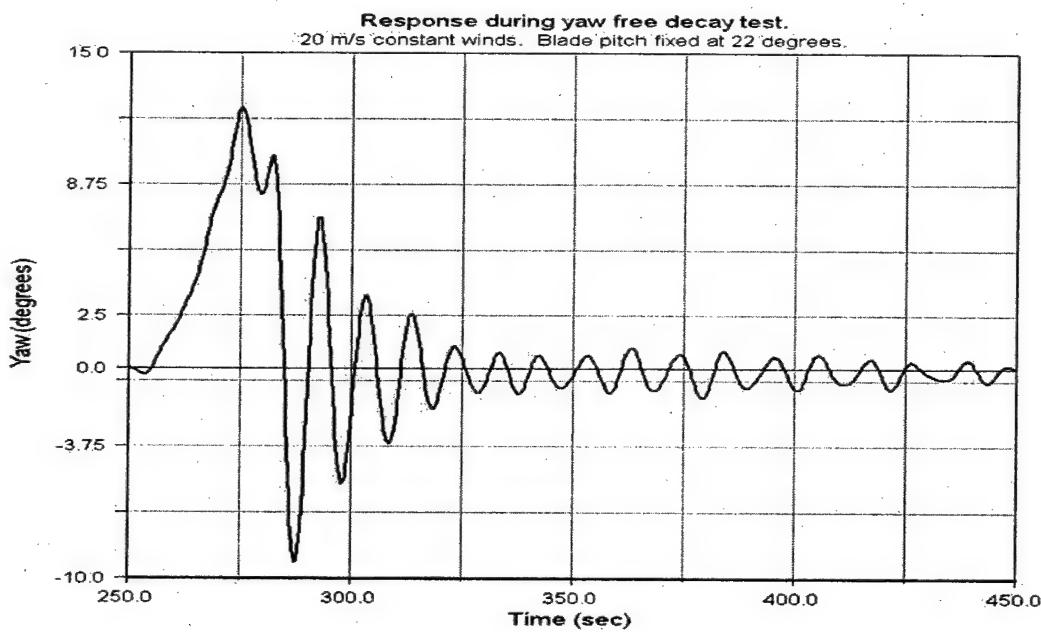
Figure 8.16 Yaw free decay test with system free to move in all modes.
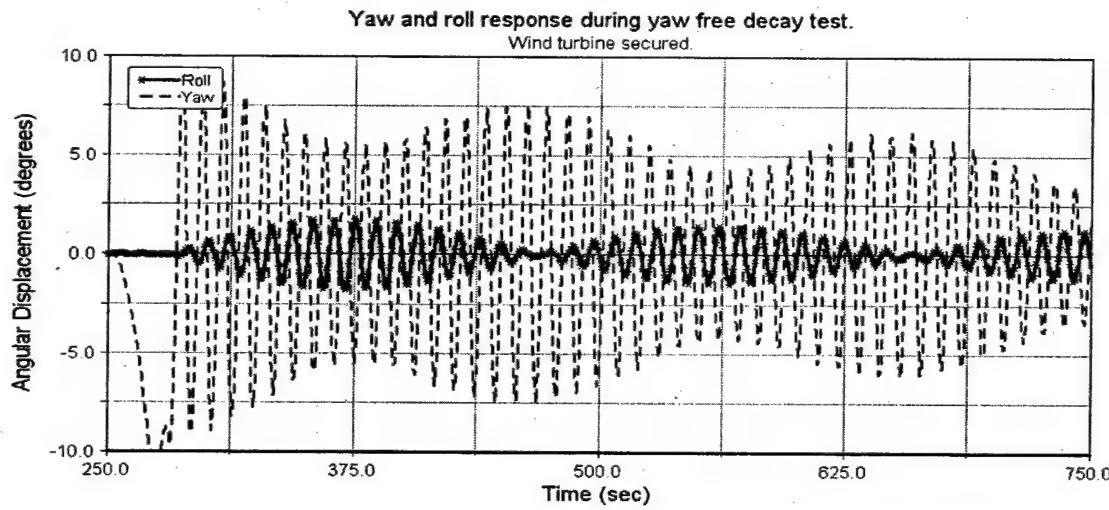
Figure 8.17 Graph of yaw and roll for free decay test with wind turbine secured.

The problems with determining the yaw damping coefficients were overcome by isolating the system so that it only moved in the yaw mode of motion. This was accomplished by creating a joint in the bottom of the floater that attached it directly to ground. This joint only allowed motion about the z-axis. A free decay test was conducted and the damping coefficients found for the modified model (Figure 8.18). The motion of the system damped out rapidly due to the large moments generated by the spokes and rotor. The period of the system response was found to be 10.4 seconds which is close to the period predicted by linear theory (10.5 seconds).

88
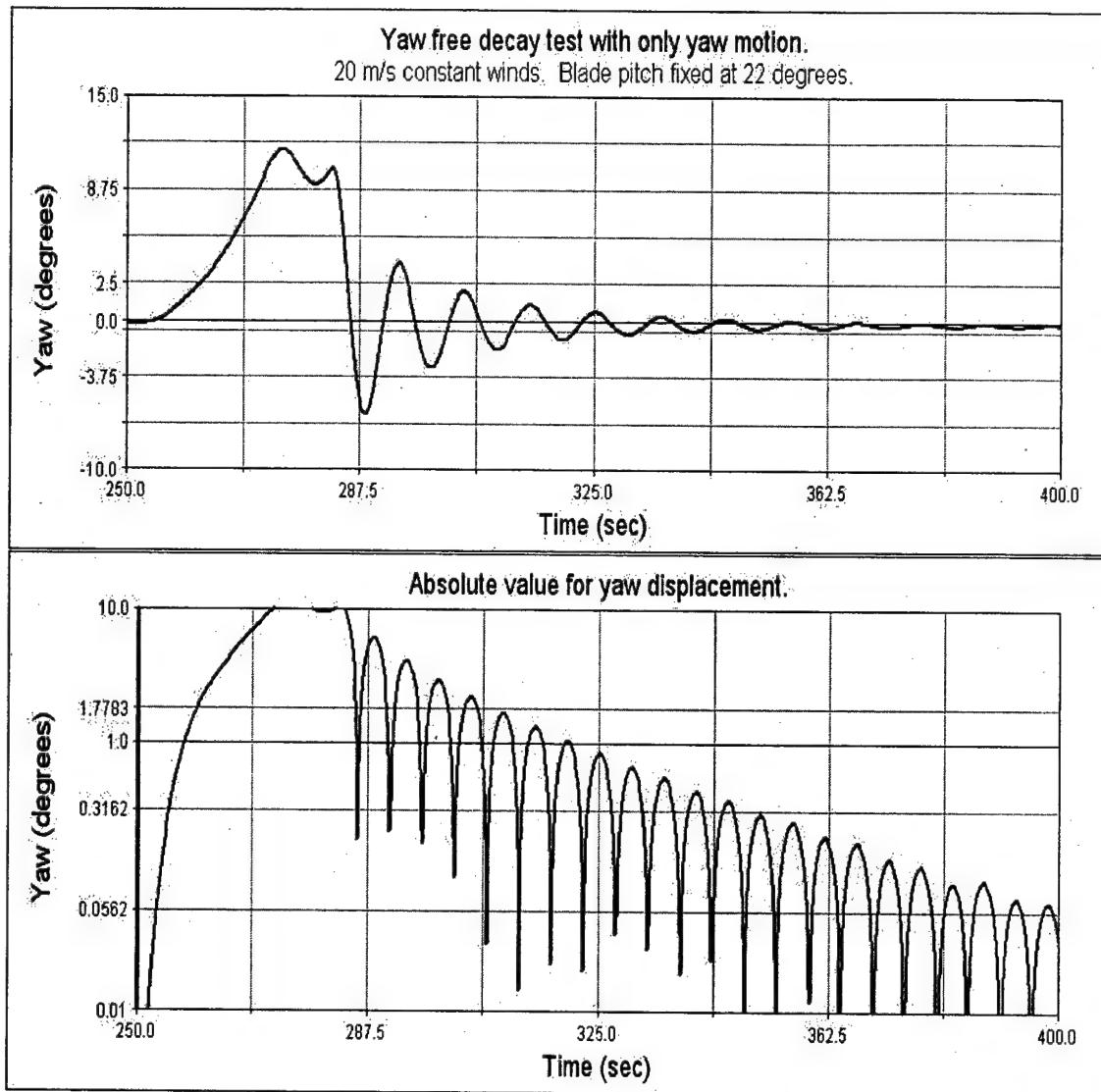
Figure 8.18 Free decay response with only yaw motion. Wind turbine operating in 20 m/s winds.

The wind turbine dominated the yaw damping of the system. This is evident by observing how the absolute value of yaw response decays with time in Figure 8.18. The decay appears to be nearly linear on the log plot, which is the expected behavior for a system with a strong linear damping mechanism. The values for p_1 and p_2 were extracted from the response record of the modified system (Figure 8.19). The values were found to be .0715 for p_1 and .0327 for p_2.

89

$$\frac{2}{T_m}\log\left(\frac{X_{n-1}}{X_{n+1}}\right)$$

$$y = 0.0327x + 0.0715$$

$$\frac{16}{3}\frac{X_n}{T_m}$$
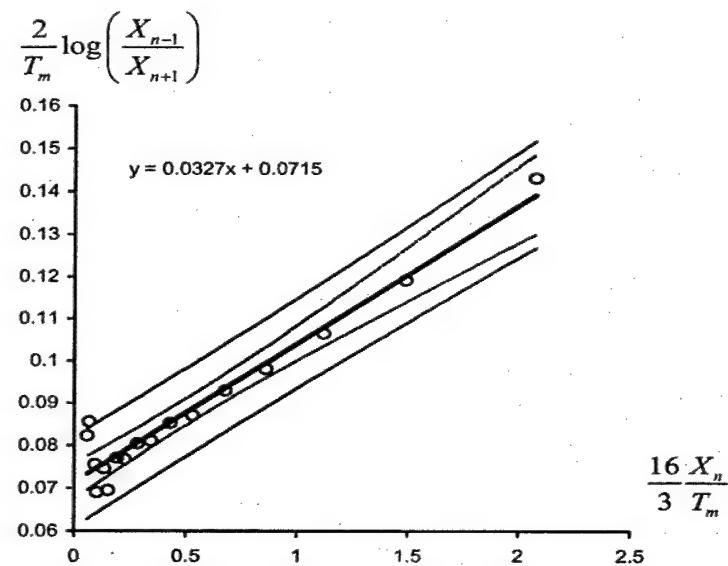
Figure 8.19 Determining p_1 and p_2 for yaw free decay test.

A mechanism for coupling yaw motion of the system to other modes of motion exists. A gyroscopic moment is produced about the x-axis when the spinning rotor is forced to change its orientation. This excites a response in the roll mode. The equation governing this behavior is discussed in 3.2.1. A separate yaw test was run with 40 meter spokes instead of 20 meters to examine this behavior. Using this modified floater design allowed for yaw free decay tests to be conducted without the need to isolate the floater motion to the yaw mode only. The effect of gyroscopic cross-coupling between yaw and roll was simulated. As shown in Figure 8.20 this coupling mechanism is relatively weak.
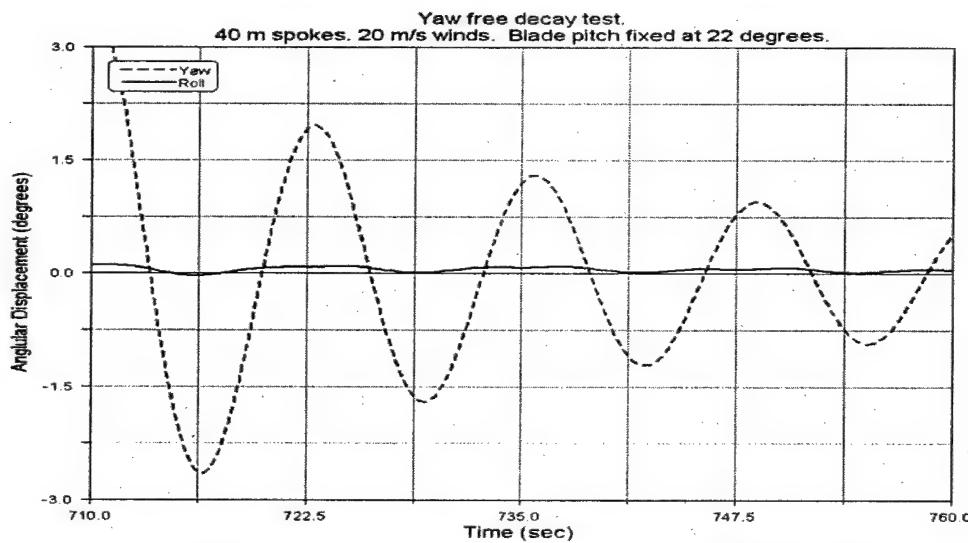
Figure 8.20 Yaw and roll cross-coupling during yaw free decay test.

90

8.8 Surge and Sway Damping in Normal Operating Conditions

For the damping tests previously described the wind turbine was assumed to operate in a wind environment near the cutout speed for the machine. This is the type of environment that will generate extreme wave events and therefore the associated damping characteristics of the system are very important. The normal operating conditions of the wind turbine are winds in the region of 5-12 m/s. The blade pitch at these wind speeds will be much lower than the 22° at which most of the previous damping coefficients were determined.

As discussed earlier blade pitch affects the damping of the system. The surge damping coefficient was shown to increase as blade pitch was reduced (see Table 8-3). However the effect this change in blade pitch had on the sway damping coefficients was not discussed. The damping characteristics of the floating wind turbine in the surge and sway modes of motion were evaluated in order to determine the system damping in the normal operating region. Free decay tests were performed on the simulation model in both surge and sway with hub height wind speeds of 7 m/s. The control system maintained the blade pitch remained fixed at 2.6° throughout both tests since this was the optimum angle for energy absorption for this wind speed.

Due to flexibility and height of the tower the motion of the nacelle may not coincide with that of the floater. The nacelle impulse responses for the two tests are included with the floater surge and sway responses. Figure 8.21 is a graph of the two free decay test results. The motion of the nacelle follows that of the floater in both tests. The initial amplitudes of the nacelle surge and sway response are larger than that of the floater due to the effects of pitch and sway moving the tower top.

It should be noted that the offset between the nacelle and floater surge position is due to the system having a mean pitch of 1.5° caused by the wind turbine loading. A close observation of the sway response for the nacelle (lower graph) reveals small oscillations superimposed on the larger sway motion. These smaller oscillations have a periodicity of 10.8 seconds and correspond to the roll motion of the system. There is no corresponding motion in the surge graphs due to the fact that the pitch damping of the wind turbine is so strong that the system only experienced negligible pitch motion (<.25°) during the free decay test. The effects of pitch are only seen in the first two oscillations of the surge free decay test and this motion is 180° out of phase with the surge motion (offset between floater and nacelle became smaller.) The damping coefficients for these tests are given in Table 8-4. The damping coefficients for the nacelle in sway could not be determined due to interference from roll mode of motion.

91
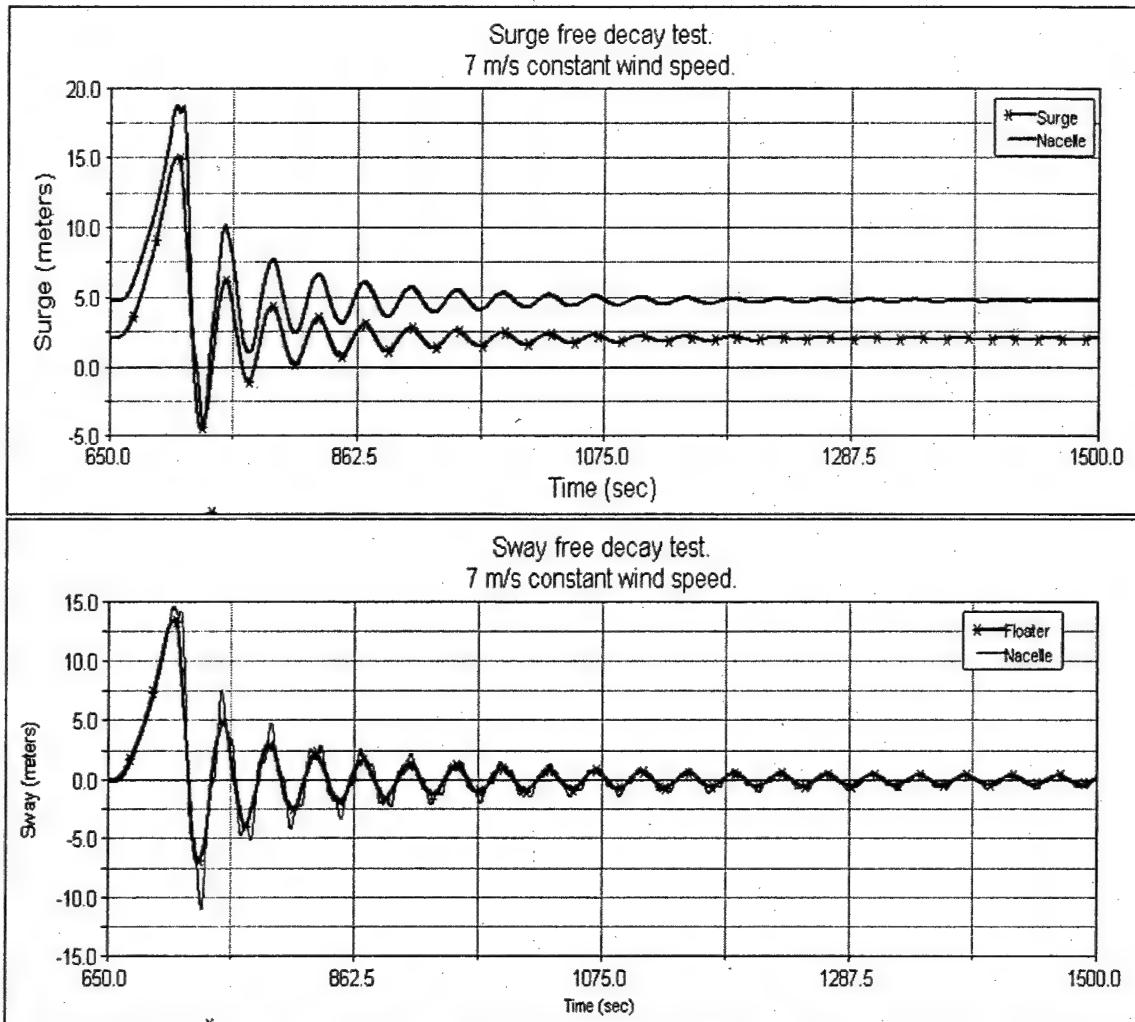
Figure 8.21 Surge and sway free decay response for system operating with 7 m/s winds. Both floater and nacelle positions are plotted.

Table 8-4 Surge and sway damping coefficients for normal operating conditions. Hub height wind speed = 7 m/s.

Test / Component	P_1	P_2
Surge / Floater	.0099	.048
Surge / Nacelle	.0101	.043
Sway / Floater	.0007	.0451

92

8.9 Summary of Single Mode Damping Tests

The free decay tests for the individual modes of motion showed how the floating wind turbine system damped out excited motions. Over fifty free decay tests were conducted in the process of evaluating the system model and determine the damping coefficients. Not all of the modes could be completely isolated from each other. For example the surge/pitch and sway/roll interactions. When one of these modes was excited, the cross-coupled mode was also excited. The cross-coupling made some of the data evaluations difficult since there were changes in the oscillation of the motion being analyzed.

Two tests could not be evaluated fully to determine either one or both of the associated quadratic and linear damping coefficients. The linear pitch damping mechanism was very strong and attenuated the pitch motion after only a few cycles. This fact combined with the cross-coupling with surge hampered the data collection for the pitch free decay test. While the wind turbine was operating, only a rough estimate of the pitch linear damping coefficient could be obtained. The floater is identical with respect to roll and pitch and therefore the roll quadratic damping coefficient was also assigned to the pitch mode of motion.

For the design chosen for the damping tests, it was not possible to perform a yaw free decay test on the system with the system free to move in other modes of motion. The system was constrained to oscillate in the yaw mode only and a free decay test conducted. Coefficients were then determined for the yaw mode of motion. In later tests, longer spokes were found to make the system oscillate in yaw in a stable manner which would have allowed free decay data to be gathered.

It is difficult to extract direct comparisons between the linear and quadratic damping coefficients. However, some general characterizations can be made. For a system configured as in the test case the following appears to be true. The wind turbine was found to have a large effect on the systems damping properties. The wind turbine was the major damping mechanism for both pitch and yaw. Viscous drag was the major damping mechanism in the translational modes of motion: surge, sway, and heave.

The wind turbine had a damping effect even when it was moved across its plane of rotation (roll and sway). The free decay tests where wind speed was 20 m/s the sway linear damping coefficient was 30 percent of the surge mode of motion. The roll linear damping coefficient was determined to be roughly 25 percent of the pitch coefficient. These results show that having an operational wind turbine increases the overall damping of the floating structure no matter which mode is being excited. The results of the individual free decay tests are given in Table 8-5.

93

Table 8-5 Linear and quadratic damping coefficients determined from free decay tests.

Test Description	Linear Damping p_1	Quadratic Damping p_2
Surge, wind turbine secured	-0.0019 †	0.0392
Surge, constant 20 m/s winds, blade pitch = 22°	0.0052	0.0486
Sway, constant 20 m/s winds, blade pitch = 22°	0.0015	0.0454
Heave, constant 20 m/s winds, blade pitch = 22°	0.0039	0.244
Roll, constant 20 m/s, blade pitch = 22°	0.0285	.0015
Pitch, constant 20 m/s, blade pitch = 22°	0.1665	.0015 ‡
Yaw, constant 20 m/s, blade pitch = 22°, yaw motion only	.0715	.0327
Surge free decay, 7 m/s winds, blade pitch= 2.6°, Floater	.0099	.048
Surge free decay, 7m/s winds, blade pitch= 2.6°, Nacelle	.0101	.043
Sway free decay, 7 m/s, blade pitch= 2.6°, Floater	.0007	.0451

† negative value attributed to data scatter. ‡ substituted roll value of p_2 for pitch.

The effect of blade pitch on system damping was investigated. The pitch angle of the rotor blades was shown to have a large effect on the linear damping coefficient for the system. The tests were only performed for surge. But, the results can be applied to the other modes that the wind turbine affected also. This property could be incorporated into a control algorithm that would control blade pitch in order to damp out oscillations of the system before they become dangerous.

The surge and sway damping properties of the system in the region of normal operations (7 m/s winds) were evaluated. It was shown that the linear damping coefficient at this wind speed is less than 10 percent the value of the surge linear damping coefficient. At 20 m/s the sway linear damping coefficient was 30 percent of the surge coefficient. At the lower wind speed the blade pitch angle is only 2.6° instead of 22°. This change in blade pitch also resulted in the surge linear damping coefficient being 90 percent higher for the case with the smaller blade pitch.

8.10 Multiple Mode System Damping

One of the advantages of the analysis method used in this research is the ability to simulate complex event and gather meaningful data about the system response. How different modes of motion interact during an event that involves more than one excitation load. In an effort to determine the system behavior during this type of event, free decay tests involving three loading simultaneously were conducted.

Cross-coupling occurs one of three ways. First is hydrodynamic cross-coupling. As the floater moves in one mode, the velocity and acceleration of the body creates counteracting forces and/or moments that excite another mode into motion. During a free decay test this behavior is characterized by the driving mode moving at its natural frequency and the cross-coupled mode also oscillates at this frequency. The second mechanism is associated with wind turbines: gyroscopic moments. With the nacelle aligned with the x-axis, moving the wind turbine in either pitch or yaw will excite a cross coupled response from another rotational motion. The equation governing this behavior is discussed in 3.2.1. As discussed in the section on yaw damping, gyroscopic moments weakly couple two rotational motions.

The final cross-coupling mechanism is mechanical. Some rotation of the structure cause the base of the floater to translate because the rotation point is not located at the base of the floater, it is above the waterline. This mechanism can be seen by close observation of how the heave mode damps out with surge or sway causing oscillations at their natural frequency. Also, as the structure surges or sways, the lines pull the floater down into the water. The high frequency heave oscillations continue as the structure translates horizontally and the instantaneous mean heave position changes with time.

There are six possible modes to excite. As previously discussed pitch/surge and roll/sway are cross-coupled. Therefore, any excitation of one of the pairs will excite the other. Several tests were run and two are discussed in this section. The first used a combined load which included surge, heave, and yaw. In the second test the system was loaded in the sway, yaw, and negative heave modes. The loading curves are for the two tests are plotted in Figure 8.22 and Figure 8.23.

At the 710 seconds the excitation forces were secured and the free decay test commenced. Figure 8.24 and Figure 8.25 are graphs of the system response. The graphs show how the individual modes damp out with time and interact with each other. A simulation was conducted with the wind turbine secured in order to further determine the effect its operation has on the system (see Figure 8.26).

95
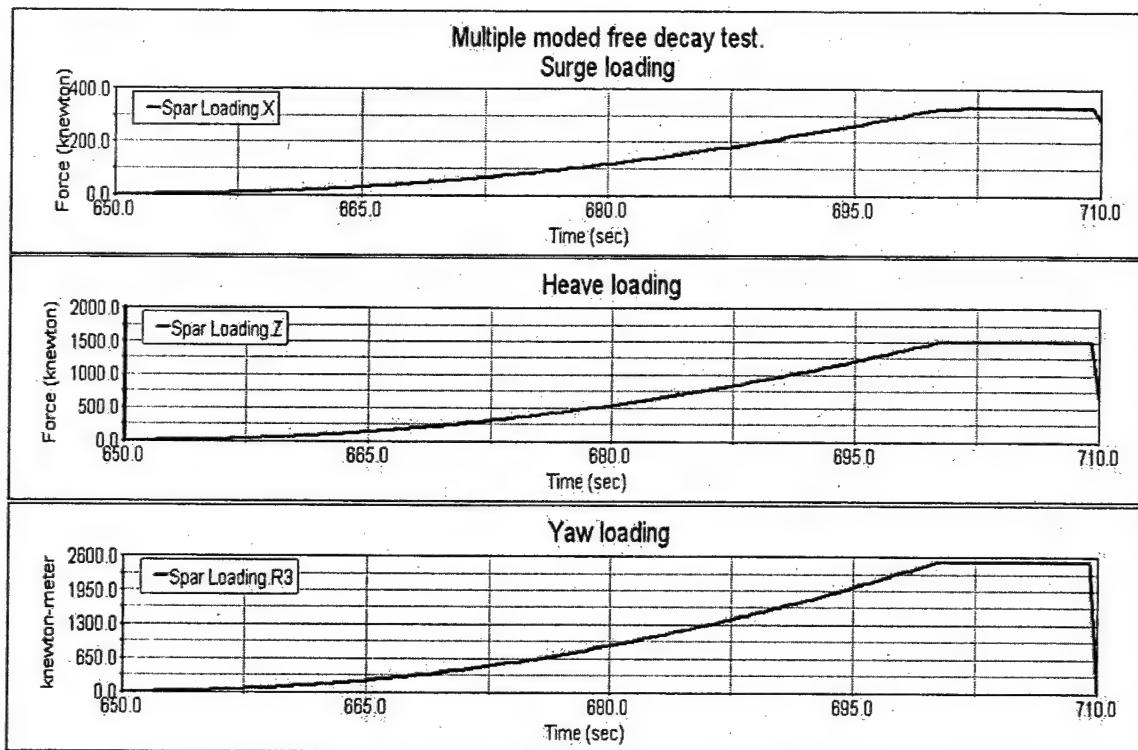
Figure 8.22 Multiple load free decay test number 1. Surge, heave, and yaw loading.
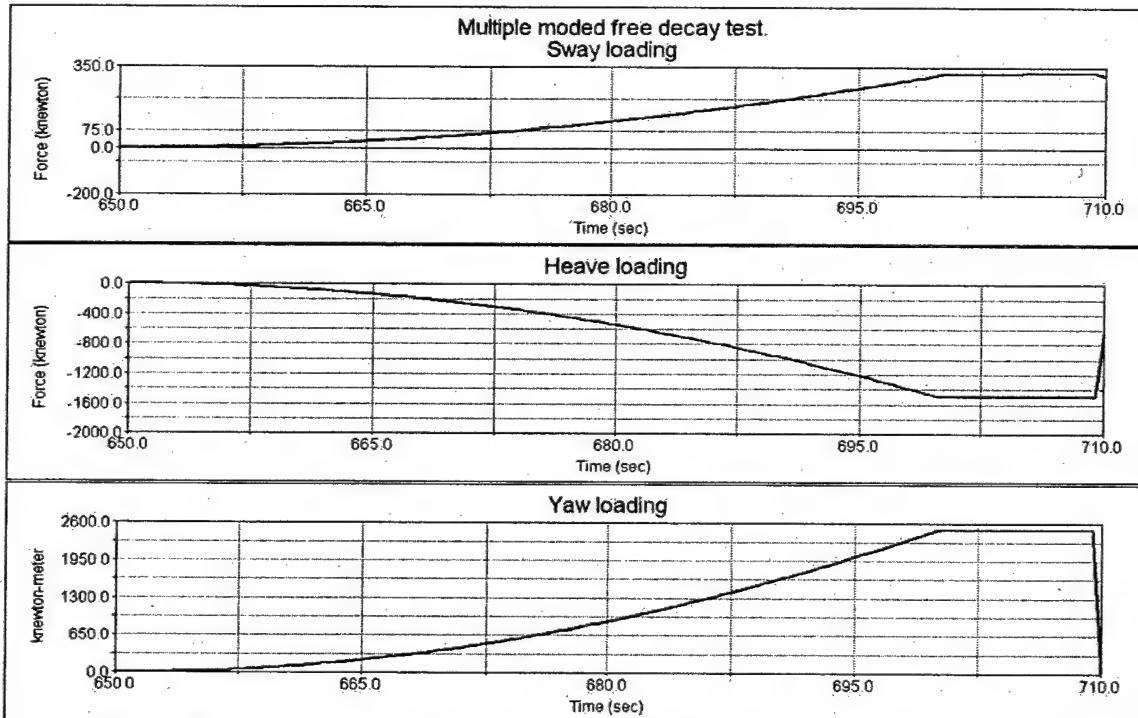
Figure 8.23 Multiple load free decay test number 2. Sway, heave, and yaw loading.
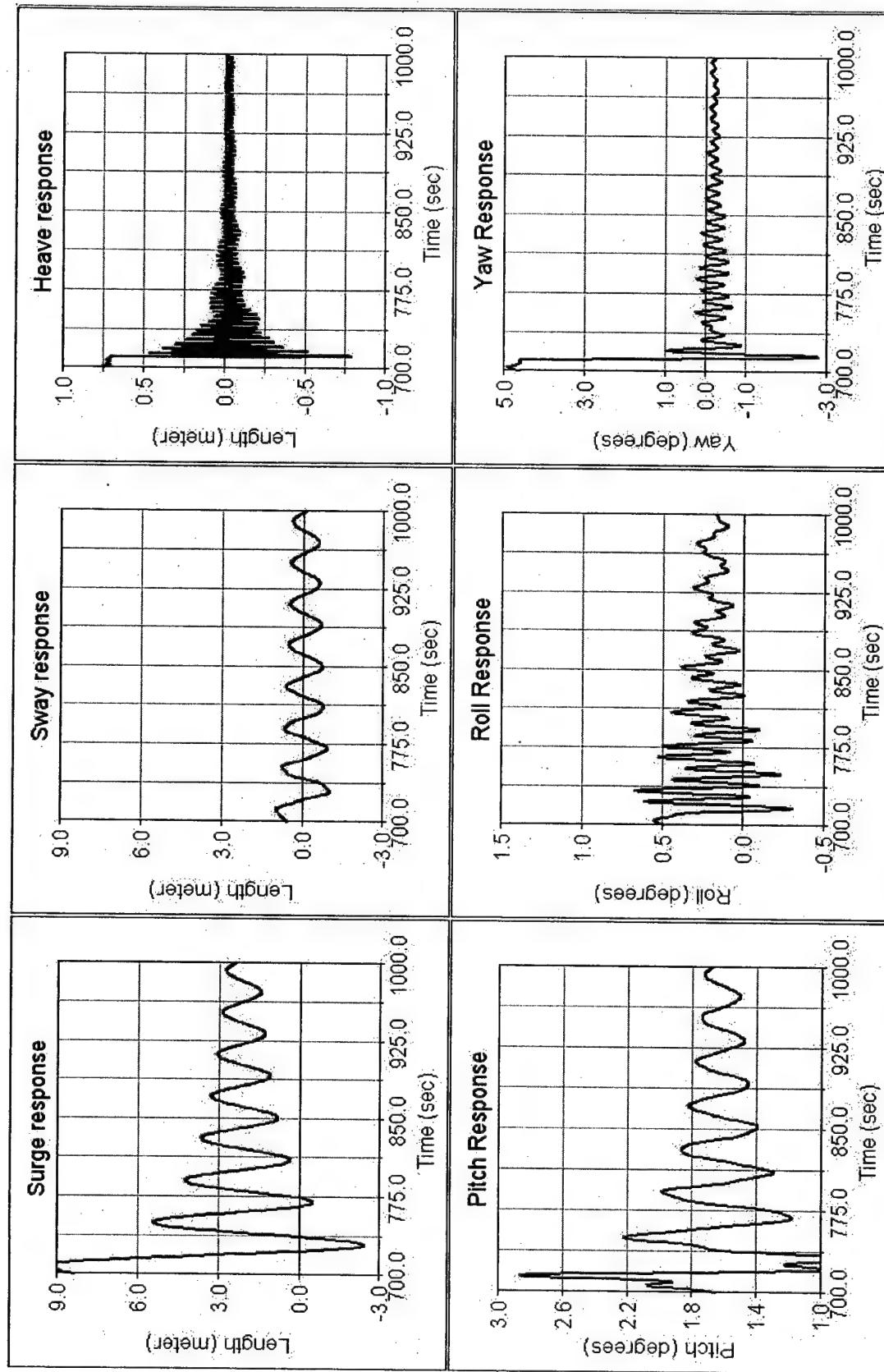
Figure 8.24 Response of six modes of motion to multiple loadings test one.
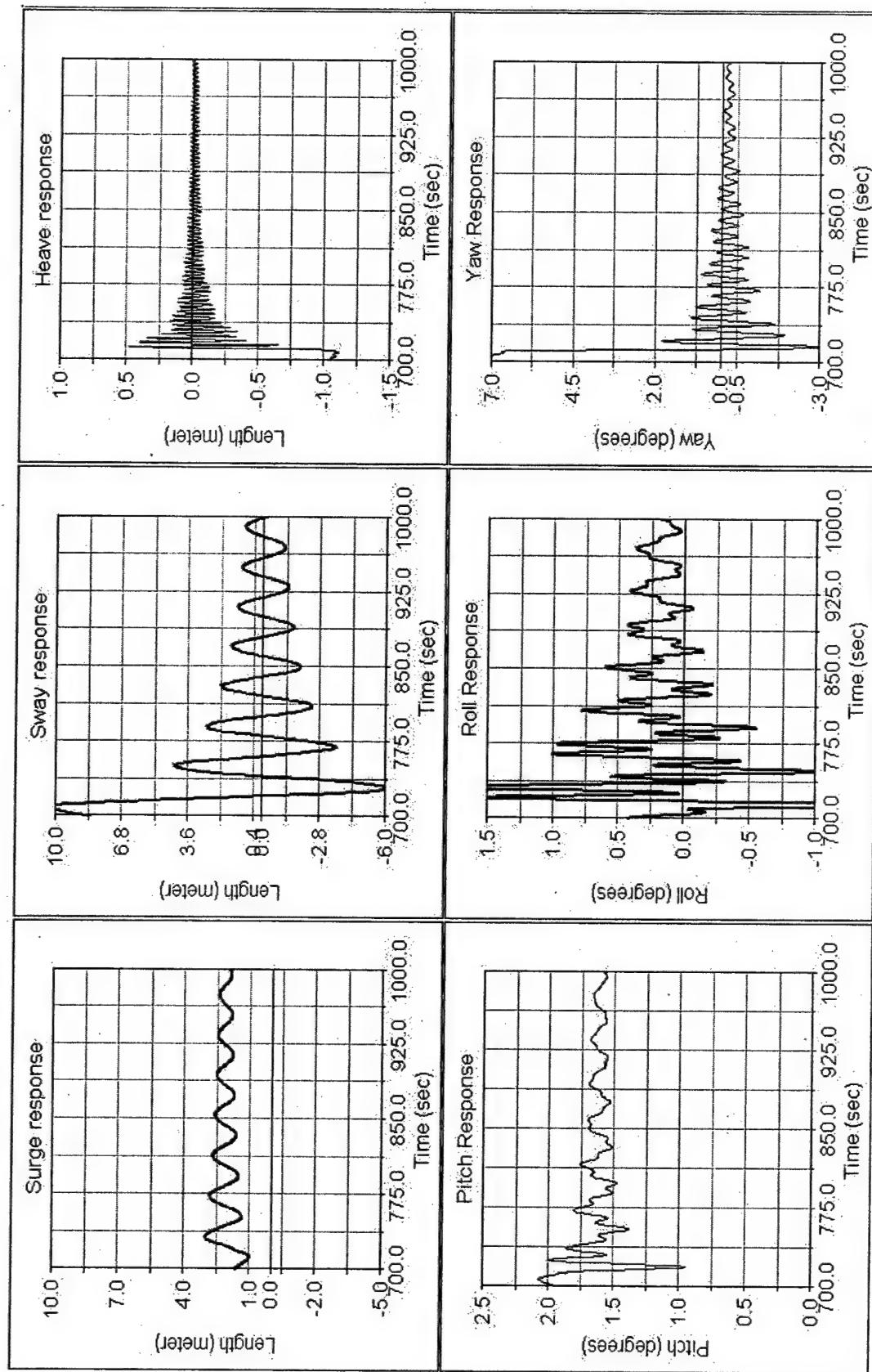
Figure 8.25 Response of six modes of motion to multiple loadings test two
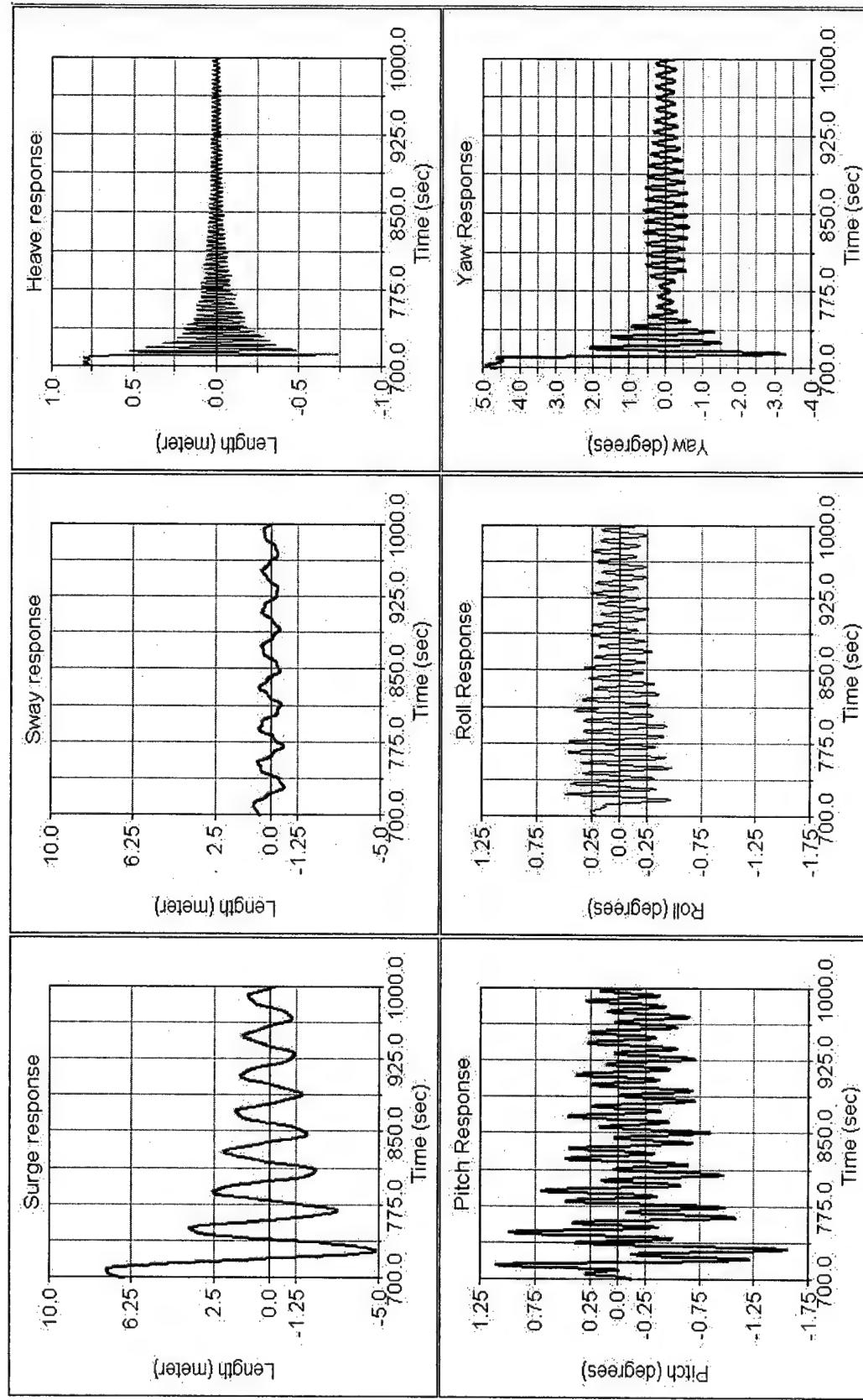
Figure 8.26 Multiple loading free decay response with no wind turbine. Surge, heave, and yaw.

99

The previous graphs show the response of the system to multiple system loadings. Two simulations with the wind turbine and one simulation with the wind turbine secured were conducted. The following observations were made. The cross-coupling between the translational motions surge and sway were coupled with pitch and roll respectively. This cross-coupling was by far the strongest seen.

Another cross-coupling was that between surge and sway motion with heave motion. As described previously, the system moves like an inverted pendulum. When the system surges or sways, it also sinks down into the water a small amount. This affected the heave record during its damping. A slow oscillation approximately 40 seconds in length can be seen on close observation of the heave record. So the overall heave motion appears to be a high frequency oscillation (heave natural frequency) superimposed on the surge / sway response.

The cross-coupling between the modes of motion appeared to have no measurable effect on the natural periods observed. Cross-coupled systems oscillated with their own natural period, the period of the system they were coupled with, or both natural periods simultaneously. No unexpected cross-coupling mechanisms were discovered.

When the wind turbine was secured all modes took longer to attenuate. The largest effect of securing the wind turbine was that the amplitudes of the pitch and roll motions were much larger. The oscillations for these rotational modes were dominated by the cross-coupling to the surge and sway modes of motion. The wind turbine damped out the high frequency rotational motions associated with the oscillation of at the pitch and roll natural frequencies very rapidly. The pitch and roll motions then oscillated at the natural frequencies of surge and sway. The lower frequency motions resulted in smaller changes in wind inflow and hence lower damping forces for the translational motions.

100

9 Operational Evaluation of System

The floating wind turbine system must be able to operate in a random wind and wave environment in excess or twenty years with a low probability of failure for major components like the blades and tethers. The most probable cause of failure would be fatigue. One of the goals of this research was to understand how mounting the wind turbine on a floating base affects its operation. This was accomplished by comparing the wind turbine loads for the same wind turbine mounted on land and the floating base.

The floating support provides some flexibility to the system that is not present in conventional wind turbines. This flexibility can act to reduce the magnitude of excitation loads due to wind events. The base therefore can reduce the severity of a wind induced event. However, in most instances where there are strong winds over an ocean environment there are also waves. The waves force the system to move in various modes of motion. This forced motion resulted in increase wind magnitudes into the rotor which resulted in extra loading on the wind turbine. The forced oscillations also produced additional inertial loads. These loads were highest when the system was supported by flexible lines that allow some pitch motion. When stiffer lines were used and pitch motion reduced, wind turbine loading was also reduced.

9.1 Description of Analysis Model

The floater used in the damping numerical simulations was also used for the operational simulations. Polyester lines were used in the damping tests to increase the amplitudes of oscillation to improve data gathering and analysis. The flexibility provided by those lines resulted in some natural periods for the system which were not ideal for a structure moored in an ocean environment. The lines were changed to have a maximum extension of 4.5% instead of 14%. The type of line that would have this elongation property is also a synthetic line made of High Modulus PolyEthylene (HMPE), which also has a high strength to weight ratio.

Changing the elongation characteristic of the tethers changed the restoring coefficients for the pitch, roll and heave modes of motion. Hence, the natural frequencies for these modes also changed. The natural periods of all modes (except yaw) were either above or below the values for which waves were known to have large spectral densities. The yaw natural frequency was not a concern since a majority of the submerged structure consists of vertical cylinders which do not generate yaw

moments in waves. The wave induced yaw moments on the spokes were very small due to the water depth at which they were attached. The wind turbine was the major source of excitation for the system in yaw. Changing the yaw natural period was deemed unnecessary. The following two tables detail the parameters and calculated properties of the system model used in the operational evaluation.

Table 9-1 Dimensions and properties of floater used in operational tests.

Spar Diameter	10 m	Line Diameter	104mm
Spar Length	12 m	Number of Lines	1 / spoke
Tower Diameter	8 m	Line Minimum Break Load	743 tonnes
Tower Draft	5 m	Maximum Line Extension	4.5 %
Spoke Length	20 m	Line Length (un-stretched)	180.76 m
Spoke Width	1 m	Water Depth	200 m
Buoyant Spokes	No	Structure Thickness	2.53 cm

Table 9-2 Calculated attributes of the floating wind turbine used in the operational tests

Mass of Floater	210435.4 kg	Center of Gravity (system) CG	16.98 m
Buoyant Mass	1228424.6 kg	Center of Buoyancy CB	-10.89 m
Total Mass of System	411494.5 kg	CG - CB	27.87 m
Reserve Buoyancy	198.5 %	Surge Natural Period	39.02 sec
Initial Line Stress	235.4 MPa	Heave Natural Period	2.74 sec
Breaking Line Stress	857.7 MPa	Pitch / Roll Natural Period	5.88 sec
Center of Gravity (floater)	-13.82 m	Yaw Natural Period	10.51 sec

9.2 Test Descriptions

Wind turbine designs are proven to be satisfactory by evaluating their ultimate and fatigue strength characteristics. The magnitude and periodicity of loading events govern the fatigue life of the system. For some system components fatigue failure is the dominant mechanism. Other components are more susceptible to failure due to exceeding the ultimate yield strength of the component. Both of these strength criteria can be evaluated using the appropriate aero-elastic time domain model. The governing document for wind turbine design and safety is IEC 61400-1 [19].

Table 2 in the Structural Design section of IEC 61400-1 listed the design load cases. In order for a wind turbine design to become type certified it must have passed evaluations for all of the applicable load cases. In the course of the operational evaluation of the floating wind turbine system the design load cases were used as guidance for selecting test cases. The goal of this research was not to achieve type certification; therefore not all of the cases were addressed. Actual certification of the floating design is left for future work. Evaluations of the floating platform were obtained by evaluating a specific load case with the wind turbine mounted on the floater and a wind turbine with a fixed base. In accordance with section 12.1 of Guideline DG01 [29] the following loads were evaluated during the numerical simulations:

- Blade-root flapwise bending moment
- Blade-root edgewise bending moment
- Tower-head torsion
- Low-speed shaft bending moments (2 directions)
- Low-speed shaft torque (rotor torque)
- Tower-base bending moments (2 directions)

The first operational tests which were conducted involved simulating the operation of the two systems (floater and fixed) at three different wind speeds. For these tests the wind turbine was operating in speed regulate (blades pitch to maintain rotor speed). The wind profiles used in the simulations were generated with SNWind (NWTC design code). Wind profiles were generated using the power law equation (9.1). For offshore wind turbines Germanischer Lloyd (GL) recommended using a power law exponent $\alpha = 0.11$ (GL-Regulation [14]).

$$V(z) = V(z_r) \cdot \left(\frac{z}{z_r} \right)^{\alpha} \tag{9.1}$$

where $V(z)$ is the wind velocity at height z. $V(z_r)$ is the wind speed at the reference height z_r.

The ultimate strength test which was chosen for evaluation was the Extreme Operating Gust (EOG). This wind load response was evaluated using the guidance of IEC 61400-1 [19]. For the purposes of testing the 1.5 MW Baseline wind turbine was assumed to be a IEC Class II-A wind turbine. Table 1 of section 6 in IEC 61400-1 gives the basic parameters that apply for the difference classes of wind turbines. This class of wind turbine has a reference velocity (V_{ref}) of 42.5 m/s and a turbulence intensity (I_{ref}) of 0.16. The hub height gust has a periodicity of once per year and a gust magnitude (V_{gust}) given by:

$$V_{gust} = Min \left\{ 1.35(V_{e1} - V_{hub}); \quad 3.3 \left(\frac{\sigma_1}{1 + 0.1(\frac{D}{\Lambda_1})} \right) \right\} \tag{9.2}$$

where

Standard deviation of turbulence: $\quad \sigma_1 = I_{ref}(0.75 V_{hub} + b); \quad b = 5.6 m/s$

One year extreme wind speed: $\quad V_{e1} = 1.12 V_{ref} \left(\frac{z}{z_{hub}} \right)^{0.11}$

Longitudinal turbulence scale parameter: $\quad \Lambda_1 = \begin{cases} 0.7z & z \le 60m \\ 42m & z \ge 60m \end{cases}$

The test wind record is found using the gust velocity to modify the wind velocity as follows:

$$V(z,t) = \begin{cases} V(z) - 0.37 V_{gust} \sin(3\pi t / T)(1 - \cos(2\pi t / T)) & for \; 0 \le t \le T \\ V(z) & otherwise \end{cases} \tag{9.3}$$

The extreme operating gust was generated for a hub height wind velocity of 7 m/s. This gust was used as the wind input for a 10 minute simulation.

The systems response to extreme wave events was tested. Extreme waves are generally produced by extreme winds. For this case the wind speed was above the rated cutout speed for the 1.5 MW baseline wind turbine. The wind turbine model was generated for a shutdown condition. The wind turbine was secured and the rotor blades were set at 90° to minimize wind loads. This mitigated the

104

wind loads on the structure. The system was subjected to an extreme wave group with two different wave incident angles.

The amplitudes of extreme waves can be using a probabilistic approach which is described in Sclavounos [31]. Assumptions are made in order to determine the amplitude for the extreme wave simulations. The amplitude of the extreme wave is called the design peak ($\hat{y}$). For these analyses, the design peak is assumed to be the amplitude of largest wave passing the floating structure during a three hour time period. For a given spectrum described by a significant wave height ($H_{1/3}$) and average period (T_0) the design peak for the time interval (T) is found using the following equations:

$$\text{Design Peak: } \hat{y} = \sqrt{2\ln\left(\frac{n}{\alpha}\right)}\ \sigma$$

$$\text{Number of Peaks: } n = \frac{T}{T_0}$$

$$\text{Reliability: } \alpha \equiv \Pr\left(y > \hat{y}\right)$$

$$\text{Standard Deviation: } \sigma \cong \frac{H_{1/3}}{4}$$

(9.4)

Where α is the reliability parameter which is chosen to be a small value to indicate the low likelihood of the design peak being exceeded during the given time interval. The value used in these analysis was $\alpha = 0.01$. The probability of the design peak being exceeded in the three hour period is therefore 1 percent.

The value for the design peak was determined using the wave spectrum which corresponded to the reference wind speed which resulted in the hub height wind speed exceeding the cutout speed for the machine. The two wave incidence angles were assumed to be 0° and 30°. These simulations were ten minutes in length. During the test the wave elevation was ramped up to the design peak, held for one cycle, and then ramped down.

9.3 Normal Power Generation Cases

The purpose of the operational simulation tests were to determine the effects mounting a wind turbine on a tension leg floating platform has on the wind turbine. Also the effects on the mooring lines had to be evaluated. Numerical simulations were conducted with different wind and wave conditions. The loads at various points in the wind turbine of the floating system were compared to the loads on an identical wind turbine with a fixed base. The wind environments are the same for both the floating and fixed wind turbine.

Three reference wind speeds were chosen: 7 m/s, 11 m/s, and 15 m/s at a reference height of 10 meters. The ocean waves for the tests were assumed to be generated by the winds. The wave characteristics were chosen to match the reference wind speed. The wave spectrum was model as a Pierson-Moskowitz type with a significant wave height ($H_{1/3}$) and a mean wave period (T_1). The values for $H_{1/3}$ and T_1 were extrapolated from Table 6.1 of Newman, 1997 [28].

Table 9-3 Environmental conditions for power generation cases. Reference height for wind - 10 m. Wave spectrum used - Pierson-Moskowitz.

Test #	Wind Inputs		Wave Inputs		
	Reference Wind Speed (m/s)	Mean Wind Speed (hub) (m/s)	Sea State	Significant Wave Height -$H_{1/3}$ (m)	Mean Wave Period – T_1 (seconds)
1	7	8.67	3	1.2	4.344
2	11	13.63	4	2.4	6.19
3	15	18.59	6	5.0	8.688

For the first three cases both the wind and waves were directed along the positive x-axis. Each of the first three simulations had a length of one hour. The random seeds used to generate the wind and wave records were changed for each case. The data collected during each run was processed using a program called Crunch (NWTC design code). This program was used to obtain statistical and fatigue data from the time records of wind turbine and line loading. The statistical data consisted of [3]:

- Minimum
- Mean
- Maximum
- Maximum range
- Standard deviation

106

During normal operations wind and waves loads cause the floater to move. Some modes of motion are more affected than others. Figure 9.1 is an example of the floater response in a random wind and wave environment. The solid red lines represent the response with both wind and waves. The blue dotted lines represent the response of the floater with only wind acting on the system. By comparing the two sets of responses, it can be seen that waves have a great effect on heave response. The thrust produced by wind on the rotor results in surge and pitch motion. As previously discussed surge motion is coupled with pitch motion. The surge motion is mechanically cross-coupled with heave motion. Horizontal motion causes set-down. Yaw motion is primarily caused by wind acting on the rotor blades.
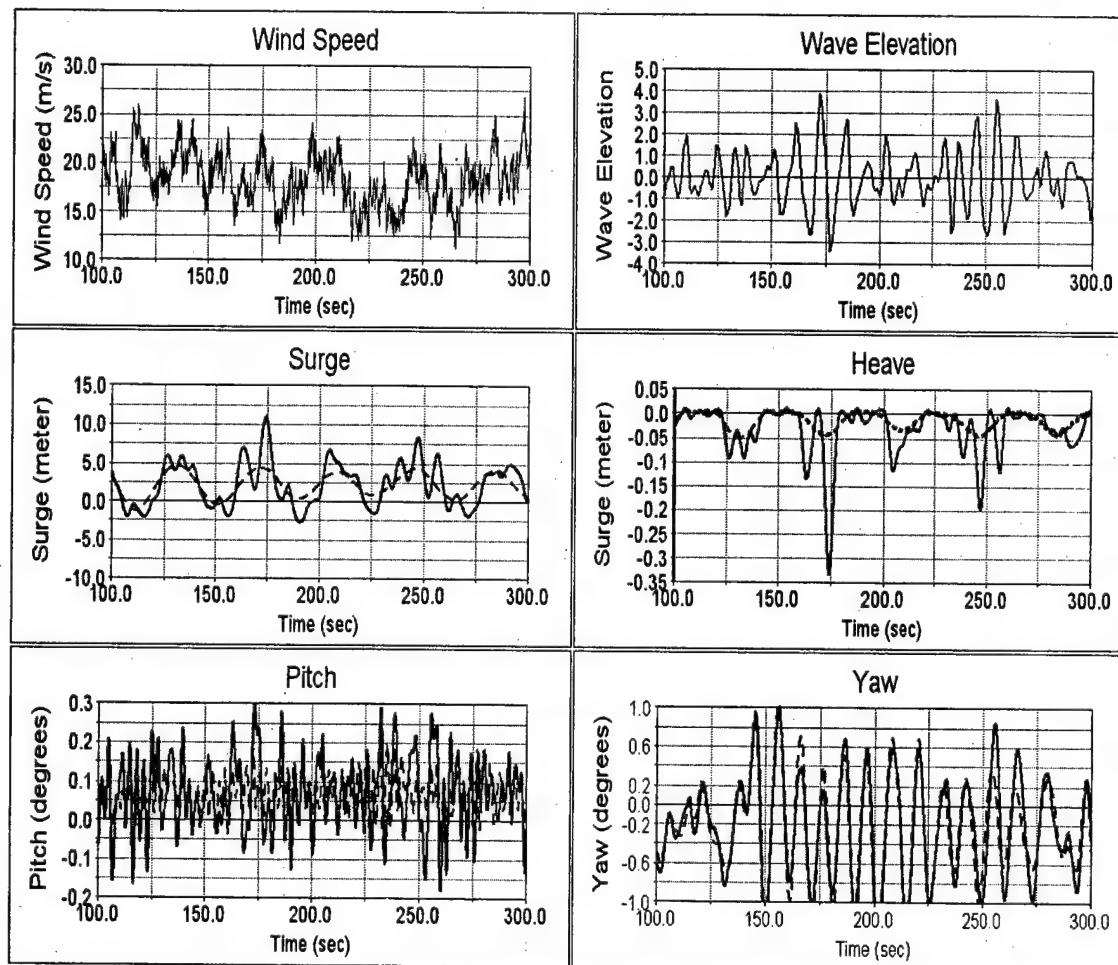
Figure 9.1 Example of floater response to random wind and waves. Reference wind speed 15 m/s. Sea State 6.

107

9.3.1 Wind Turbine Results

The results presented in this section seek to contrast the differences between the loading on a fixed base wind turbine and a floating wind turbine. Failure of a component can occur when maximum yield strength is exceeded or a fatigue limit is passed. First a comparison of the maximum loading for the floating and non-floating variants is made. The eight loadings listed in the previous section were collected for the hour long simulations and their maximum (positive or negative) values charted for the three different wind and wave conditions (see Figure 9.2 to Figure 9.4). The following abbreviations were used on the charts and the following discussions for the loads:

TwrBsMxt: tower base moment (x-axis)

TwrBsMyt: tower base moment (y-axis)

RootMxb2: blade-root edgewise bending moment (blade 2)

RootMyb2: blade-root flapwise bending moment (blade 2)

YawBrMzn: tower-head torsion

LSSTipMys: low-speed shaft bending moment (y-axis)

LSSTipMzs: low-speed shaft bending moment (z-axis)

LSShftMxa: low-speed shaft torque

The charts show which loadings were most affected by mounting the wind turbine on a floating base and subjecting it to excitation by waves. In general the floating wind turbine had higher maximum values for the eight loading values. However, two of the parameters were higher for the fixed base wind turbine. These two loads (RootMxb2 and LSShtMxa) were higher for the fixed base wind turbine in the first case with reference wind equal to 7 m/s. All of the maximums were greater for the floating system in the tests two and three.

The bending moment at the tower base showed the largest difference between the two wind turbines. The system was allowed some slight movement in the roll and pitch modes when the wind turbine was mounted on the floating base. With the wind and waves directed along the x-axis, large pitching moments developed and pitch deflection occurred. The pitching motion of the structure tilted the tower and generated large additional moment at the tower base.

A summary of the three tests is presented in Table 9-4. The percentage difference between the floater and fixed base values for the eight loads are listed. These values are the percentage of the fixed base loading. Negative values represent the cases where the fixed base maxima were greater. Both the low-speed shaft tip bending and blade root bending moments showed large increases their maxima.
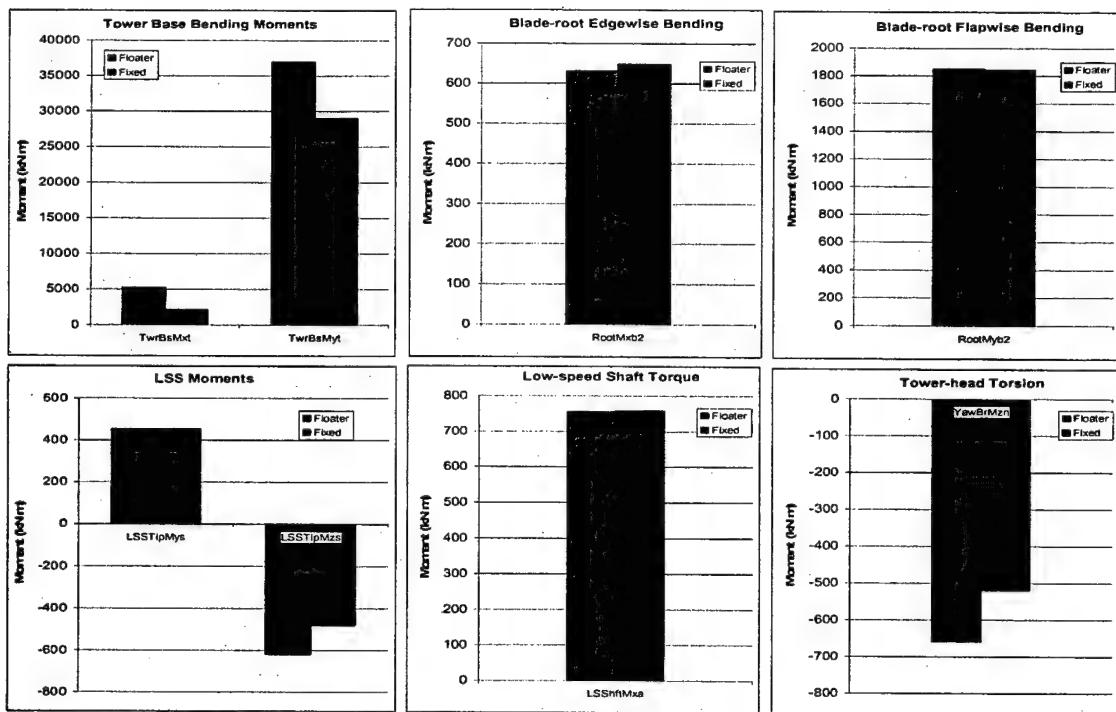
Figure 9.2 Comparison of maximum loading for fixed base and floating wind turbine for test 1.
Reference wind speed = 7 m/s. Sea state = 3.
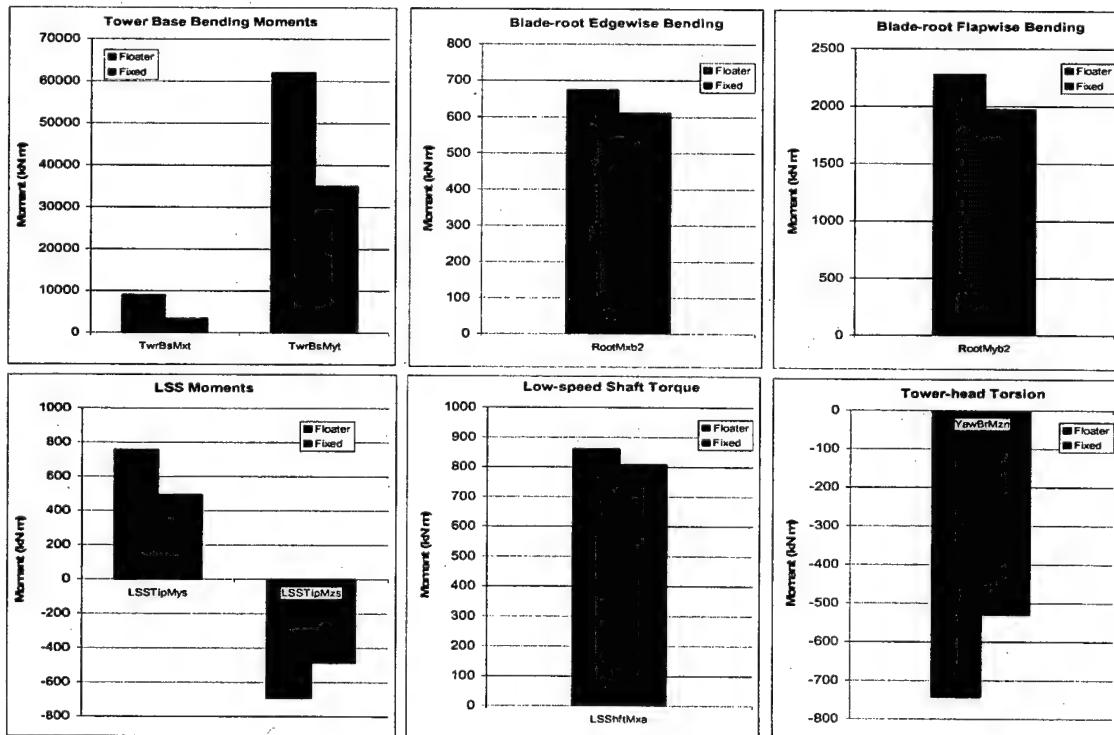
Figure 9.3 Comparison of maximum loading for fixed base and floating wind turbine for test 2.
Reference wind speed = 11 m/s. Sea state = 4.

109
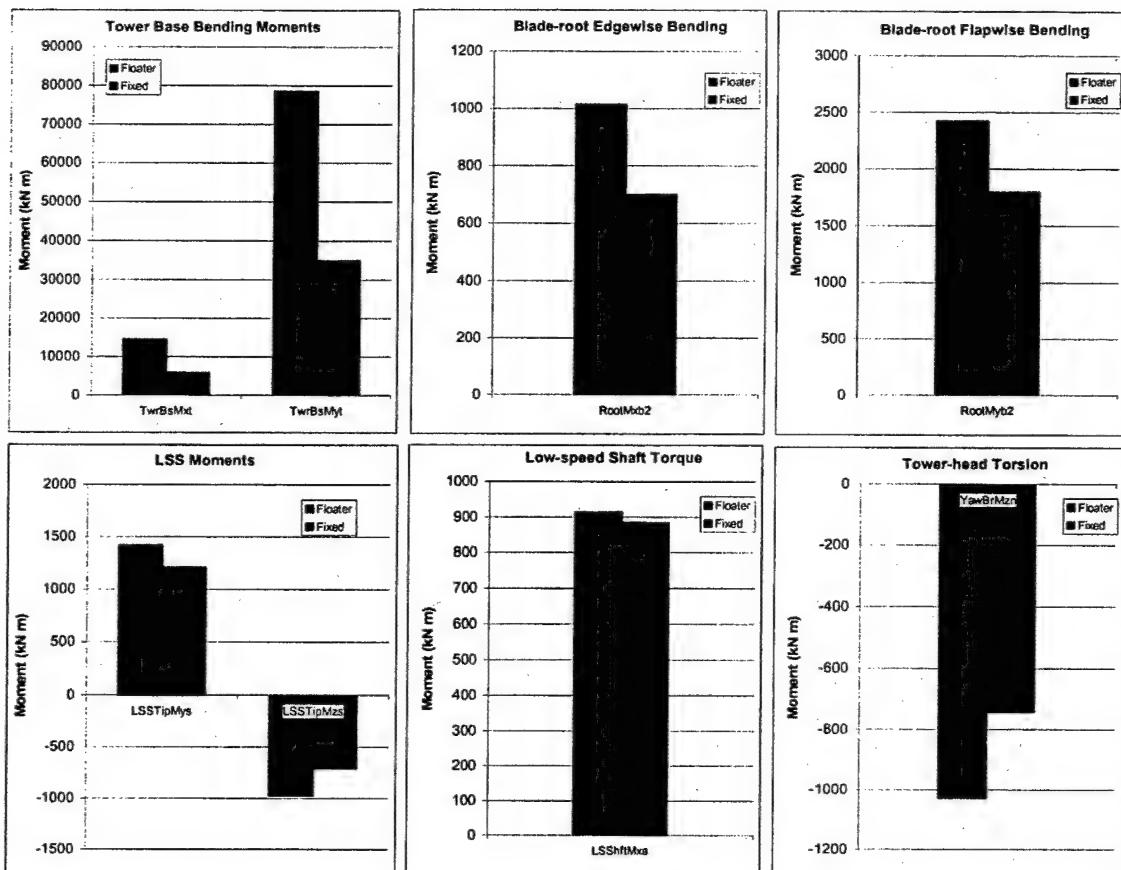
Figure 9.4 Comparison of maximum loading for fixed base and floating wind turbine for test 3.
Reference wind speed = 15 m/s. Sea state = 6.

Table 9-4 Summary of maximum loading for three operational tests. Percentages represent the
difference between fixed base wind turbine and floating wind turbine. Negative values indicate fixed
base maximum load was higher than the floater load for the same wind conditions.

LOADING	Test 1	Test 2	Test 3
Tower Base Bending (x-axis)	140.7%	164.9%	145.1%
Tower Base Bending (y-axis)	27.6%	77.1%	124.0%
Blade-Root Edgewise Bending	-2.6%	10.4%	44.9%
Blade-Root Flapwise Bending	0.3%	15.4%	34.8%
Low-Speed Shaft Tip Bending (y-axis)	-0.2%	53.3%	17.0%
Low-Speed Shaft Tip Bending (z-axis)	29.0%	43.0%	37.5%
Low-Speed Shaft Torque	-0.3%	6.6%	3.3%
Tower-Head Torsion	26.9%	40.2%	38.6%

110

The largest percentage difference was between the fixed and floating values for tower base moment about the x-axis. The actual values for the maxima for this load are low relative to the other tower base load. The percentage differences for the blade-root bending moments and the tower base bending moment about the y-axis increased as the environmental conditions went up.

The effect on wind turbine fatigue due to the floating support can be evaluated by determining the rainflow cycle counts or raw cycles for the oscillating loads. These rainflow cycle counts are obtained by analyzing the time history for the six simulations using the Crunch post-processor. The cyclic loads are separated into bins. Each bin holds the number of oscillations which have a given range. The width of the bin defines the ranges of cyclic loads which are counted. The cycle counts can be used to determine the effect on the fatigue life of the wind turbine components. Therefore, the cycle counts can be used to compare the fatigue of the fixed base and floating wind turbines.

The results of the rainflow cycle counts for the six simulations are shown in the following charts. Each graph shows the twenty bins and the number of cycles in each for the fixed and floating base wind turbines. The floating support has more extreme oscillations than the fixed base support. From a design standpoint the increased cyclic loading on the blade-roots and low-speed shaft are a cause for concern. A wind turbine which could be used for the fixed base machine would probably be unacceptable for the floating system. Once again the largest differences in loading are in the tower base bending moments which could be compensated for by extra structural support in the lower portions of the tower.
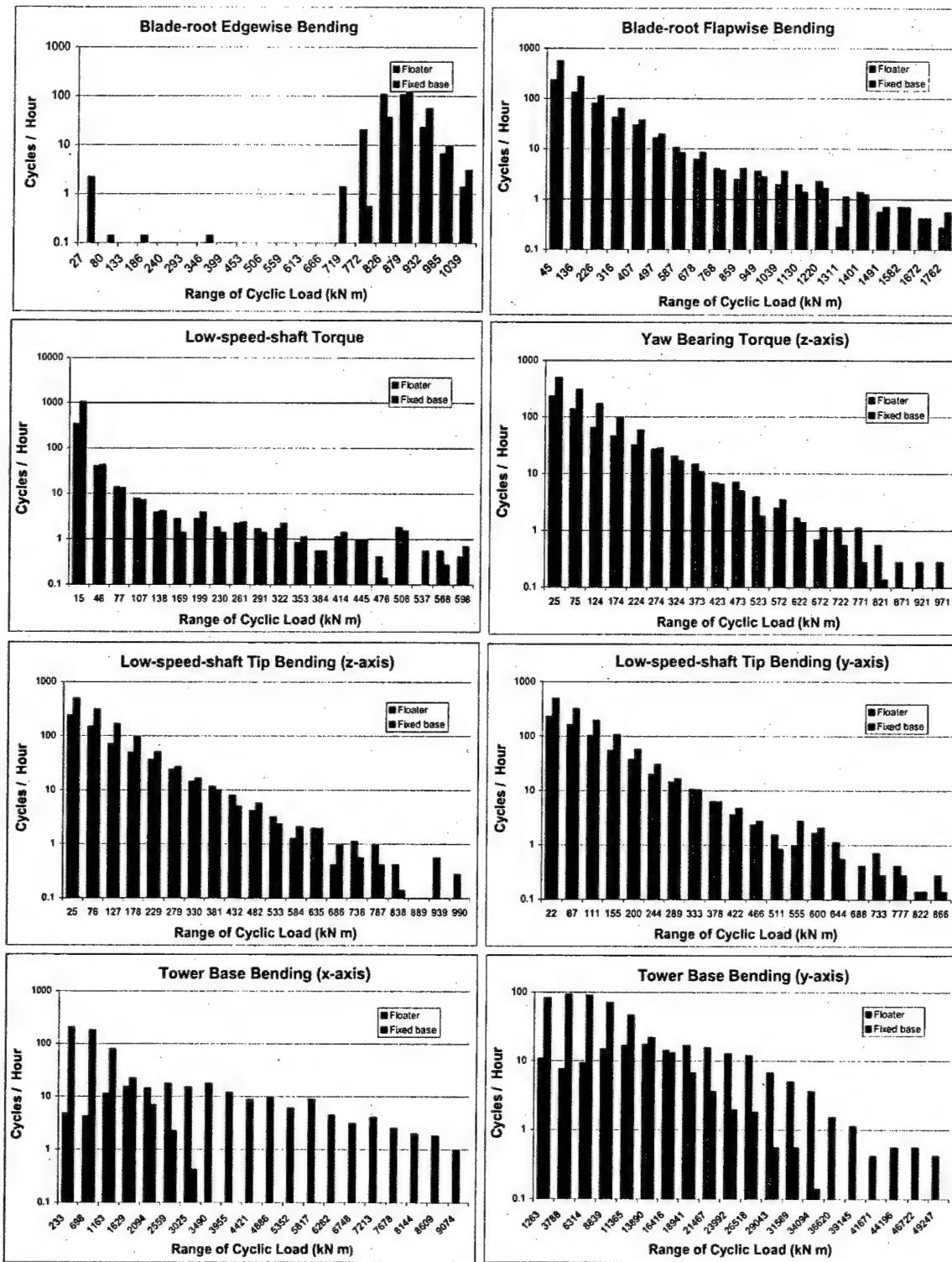
Figure 9.5 Rainflow cycle counts for test 1 fixed base and floating wind turbine. Reference wind speed = 7 m/s. Sea state 3.
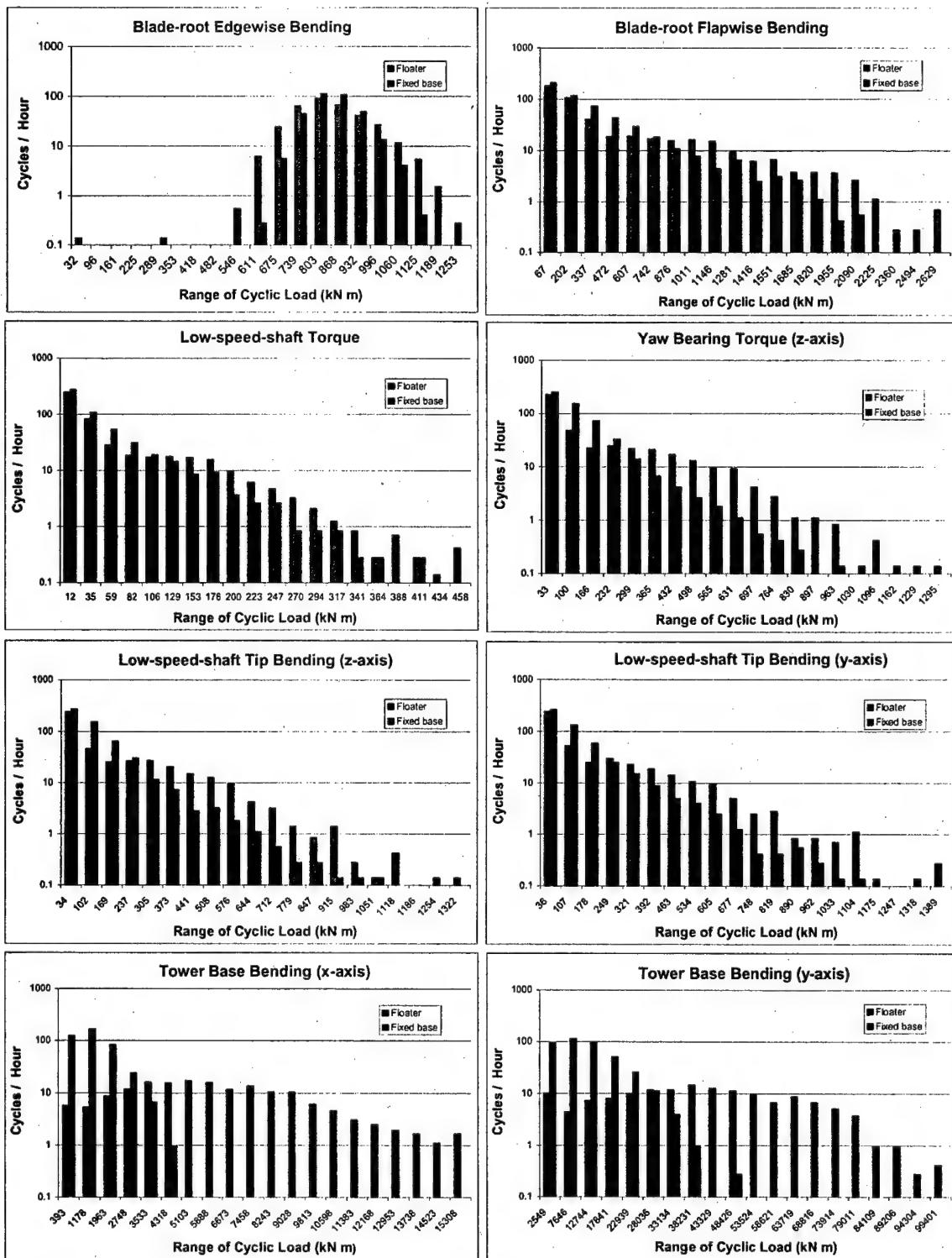
Figure 9.6 Rainflow cycle counts for test 2 fixed base and floating wind turbine. Reference wind speed = 11 m/s. Sea state 4.

113
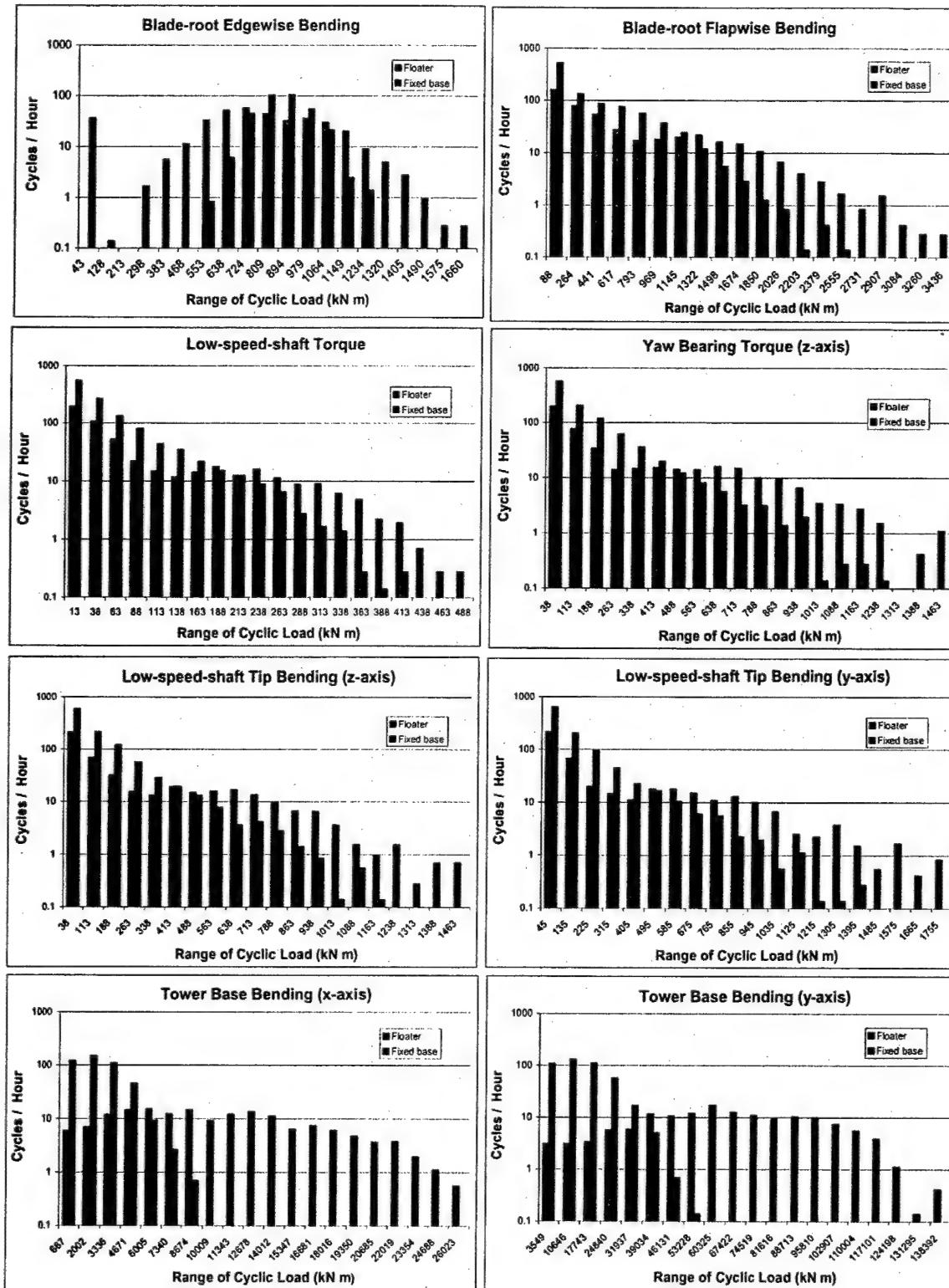
Figure 9.7 Rainflow cycle counts for test 3 fixed base and floating wind turbine. Reference wind speed = 15 m/s. Sea state 6.

114

9.3.2 Comparisons of Wind Turbine Power Production

Understanding how mounting a wind turbine on a floating support structure affects the machines power output is important. If changing the way it was mounted dramatically altered the power output, the system would be unfeasible. This was found not to be the case with the system tested in the three sets of operating conditions.

The power output for the fixed base and floating wind turbines was compared by determining the average power output for each of the three operational tests. It was unclear what the cause of this reduction in power was. Several parameters for each test were reviewed. The most likely cause is the flexibility of the system allowed some of the power that would normally be transferred to the generator to be passed on to the floating support. The motion of the floater absorbs a small portion of the energy that would have been transferred to the generator. Observation of the sway and roll modes of motions showed motion which had to have been excited by the wind turbine since the waves were directed along the x-axis. This motion was damped by viscous drag on the floater. The damping due to drag on the structure is an energy loss. Another reason for the power loss could be the increased pitch and yaw motion of the rotor due to the motion of the floater. As shown in Table 9-5, the maximum reduction in power was only 1.1 percent.

Table 9-5 Average power output for fixed base and floating wind turbine for the three operating conditions.

Test #	Fixed Base Average Power Output (kW)	Floater Average Power Output (kW)	Change in Power Output (%)
Test 1	740.3	733.4	-0.9%
Test 2	1373.8	1365.1	-0.6%
Test 3	1380.0	1364.8	-1.1%

9.3.3 Tether Results

A majority of the restoring forces and moments for the floating system came from the tethers. As previously discussed pitch and roll moments caused the largest changes in line tension. The first three tests cases used a single 104 mm synthetic line on each spoke. The reserve buoyancy of the system resulted in a static line tension of approximately 30 percent of the ultimate stress for the chosen lines. When the wind and waves aligned with the x-axis the highest stresses were experienced on line number 3 (on negative x-axis). Lines 1 and 3 absorbed the pitching moments acting on the system.

Figure 9.8 is a graph showing a 100 second record of line stress for the three sets of environmental conditions. This graph shows that the oscillations in the line stress increase in severity as the wind speed and sea state increase. The graphs for line number 1 and 3 look similar except that they are opposite in sign. Line 3 stress increases and line 1 stress decreases for positive pitching moments.
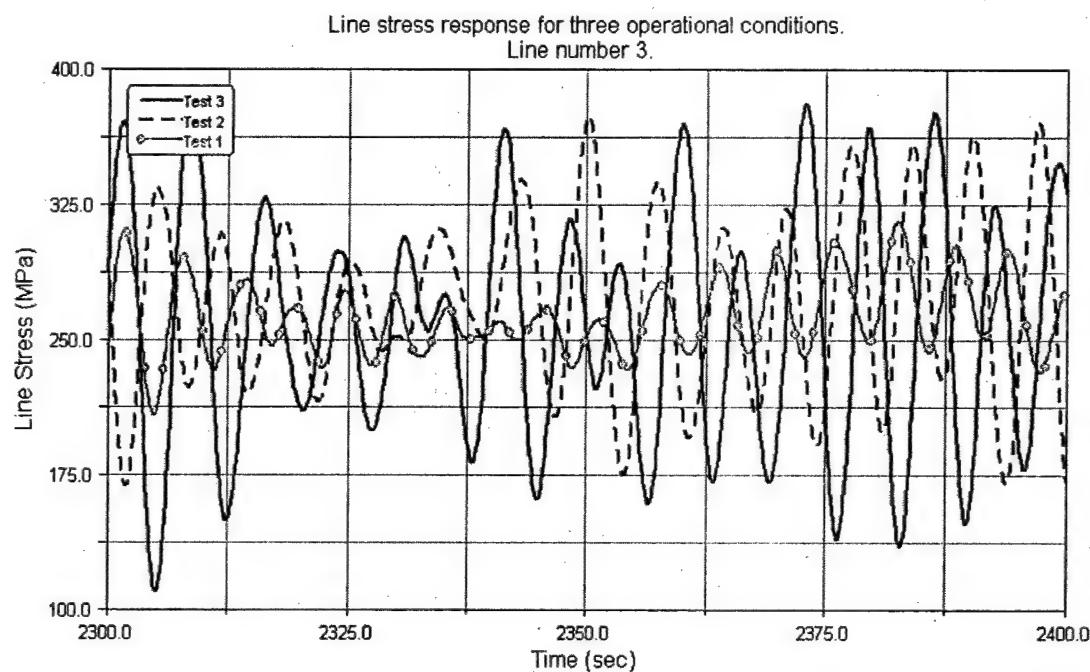
Figure 9.8 Line stresses for three operational conditions for the weather (upwind) line.

The time records of the line stress were analyzed in order to evaluate the effect of the three test conditions on the tethers. The statistical results were recorded in Table 9-6. As expected the maximum line stresses increased as the environmental conditions worsened. The maximum line stress for the three operational cases was 433.5 MPa, which was approximately 50 % of the breaking stress.

116

Table 9-6 Line stress statistics for operational tests 1, 2, and 3.

	Test 1			Test 2			Test 3		
	Minimum Stress (MPA)	Mean Stress (MPA)	Minimum Stress (MPA)	Minimum Stress (MPA)	Mean Stress(MPA)	Maximum Stress (MPA)	Minimum Stress (MPA)	Mean Stress (MPA)	Maximum Stress (MPA)
Line1	139.2	204.9	270.2	79.2	204.1	328.1	30.8	214.0	386.3
Line2	223.7	237.3	250.7	215.1	238.4	259.7	200.6	239.5	279.9
Line3	200.0	267.3	332.4	132.0	268.1	392.2	79.7	258.1	433.5
Line4	222.1	234.9	247.3	208.1	233.8	254.3	192.7	232.6	272.5

The tethers were made of a high modulus polyethylene material which is reported to have better fatigue properties that steel wire ropes [8]. Some test data was found that backed up this claim. But no comprehensive tension – tension fatigue life graphs were found for the high modulus polyethylene. It was decided that a conservative estimation of the fatigue loading of the tethers could be obtained by using the fatigue graphs associated with steel wire ropes. Using the dimensions and fatigue properties allowed the equivalent damage due to fatigue loading to be calculated for the three one hour simulations. Damage was assumed to accumulate linearly for each oscillating load using an equation take from Annex G of 61400-1 [19]:

$$Damage = \sum_i \frac{1}{N(S_i)} \qquad (9.5)$$

where S_i is the load range for cycle i, and $N(S_i)$ is the number of cycles to failure for the load range S_i. The values for S_i are obtained from the load range values of the rainflow cycle bins. The number of cycles to failure is derived from the fatigue life cycle graph. The equivalent damage for each of the three tests is found by combining the damage from every cycle in the bins. A value of damage of 1.0 or higher means failure is predicted. The damage values for lines 1 and 3 during the second and third tests are the highest (see Table 9-7). The life of the chosen lines could be extremely low (< 25 hours for lines 1 and 3 in test 3) in high wind and sea conditions and would therefore be unacceptable.

Table 9-7 Total damage due to fatigue for lines 1-4 during tests 1, 2, and 3.

Test #	Line 1	Line 2	Line 3	Line 4
Test 1	1.94E-05	1.77E-09	2.15E-05	1.45E-09
Test 2	2.81E-03	3.27E-08	3.84E-03	2.65E-08
Test 3	4.04E-02	1.34E-06	4.26E-02	8.85E-07

9.4 Design Modification

The results of the first three operational tests showed that the floating design resulted in increased loading on the wind turbine. The fatigue life of the wind turbine was also shown to be adversely affected. These problems could be mitigated by design changes. Although design optimization was not a goal for this research, it was decided that a single change would be made to the system to demonstrate how the loading properties of the system could be adjusted to overcome problems.

The first step in this design iteration was to determine the most likely cause for a majority of the increased load on the wind turbine components. It was found that the most of the increase in load on the tower base was due to the structure pitching, by comparing the pitch angle response of the floater to the tower base bending moment (y-axis). A positive pitch angle resulted in a positive bending moment (see Figure 9.9). Other wind turbine loads were also found to be largely affected by either pitch angle or rate of pitch.
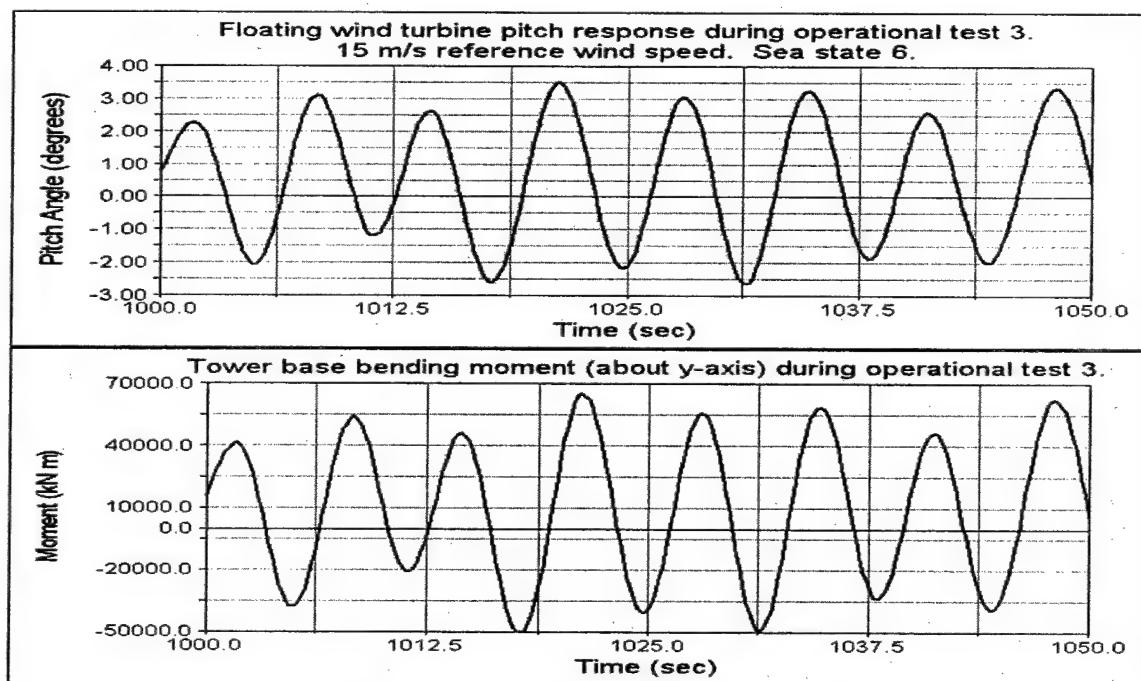
Figure 9.9 Graph of pitch angle and tower base bending moment (y-axis) for operational test 3.

The next step was to decide which design parameter to change in order to reduce the pitch motion of the floater. The three parameters which had the largest effect on pitch motion were the type of lines selected, number of lines, and spoke length. Either of these parameters could be changed to achieve the desired result of reduced wind turbine loading. The number of lines was increased to three per spoke and lines with a higher stiffness were used. The maximum elongation was changed from 4.5%

118

to 2.0%, which is consistent with another type of high modulus polyethylene line [9]. This change resulted in a system which was much stiffer in the pitch mode of motion with natural periods of pitch of 2.3 seconds. Operational test 3 was repeated for the new design. The surge, pitch, and heave responses for both designs were plotted in Figure 9.10. Three of the wind turbine loads were also plotted for both designs. The largest load reduction was the y-axis tower bending moment. Limiting the tower angle reduced the gravity induced moment at the base of the tower. The reduced pitch motion improved the systems behavior for all eight wind turbine loads (see Table 9-8).
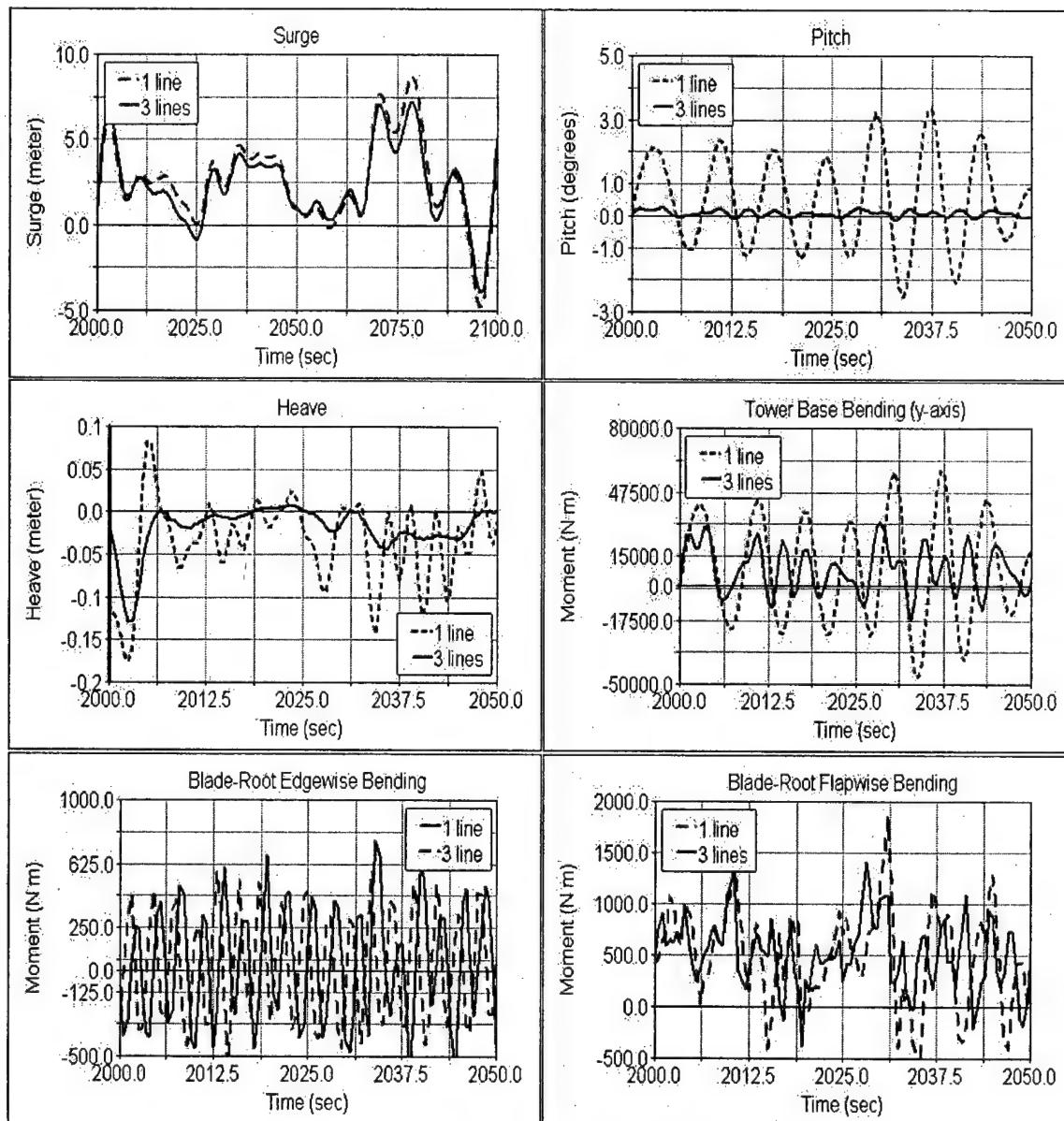
Figure 9.10 Surge, heave, and pitch response and wind turbine loads for 1 and 3 lines per spoke for operational test 3 conditions.

119

Table 9-8 Comparison of fixed base and floating wind turbines for 1 and 3 lines per spoke. The reference wind speed was 15 m/s. Sea state 6. The values represent the percentage difference between the two floating variants and the fixed base wind turbine maximum loading values.

LOADING	Fixed Base Loading (kN·m)	1 Line / Spoke		3 Lines / Spoke	
		Loading (kN·m)	Delta (%)	Loading (kN·m)	Delta (%)
Tower Base Bending (x-axis)	5956.0	14600.0	145.1%	6604	10.9%
Tower Base Bending (y-axis)	35060.0	78550.0	124.0%	45390	29.5%
Blade-Root Edgewise Bending	700.5	1015.0	44.9%	741.9	5.9%
Blade-Root Flapwise Bending	1797.0	2422.0	34.8%	1866	3.8%
Low-Speed Shaft Tip Bending (y-axis)	1213.0	1419.0	17.0%	1325	9.2%
Low-Speed Shaft Tip Bending (z-axis)	486.6	669.1	37.5%	467.9	-3.8%
Low-Speed Shaft Torque	884.0	913.4	3.3%	843	-4.6%
Tower-Head Torsion	741.2	1027.0	38.6%	752.5	1.5%

As shown in Figure 9.11, the fatigue loading of the wind turbine was greatly reduced. Increasing the stiffness in pitch resulted in smaller pitch motions and angular velocities. The total effect of these changes reduced the range of cyclic load for the wind turbine. The results of the numerical simulation indicated that some of the loadings had lower cyclic loads than the fixed base wind turbine even with sea state 6 seas acting on the floater. The flexibility of the system in surge was not significantly affected by the change of lines. The system surged when wind loading events occurred and thereby relieved some of the loads on the wind turbine. The reduction in wave induced pitch motion (since system was more stiff in the pitch mode) dramatically reduced the loads on the wind turbine.

The increased number of lines improved the fatigue results for the tethers. The maximum value for total damage was 1.9 E-7 instead of 4.3E-2. This change would greatly increase the fatigue life of the lines. The maximum line stress for the three line design was 126.6 MPa while the single line design had a maximum stress of 433.5 MPa. The results of this test showed that design changes could be used to overcome adverse loading conditions on the wind turbine and lines. The improved design was used in all subsequent tests.

120
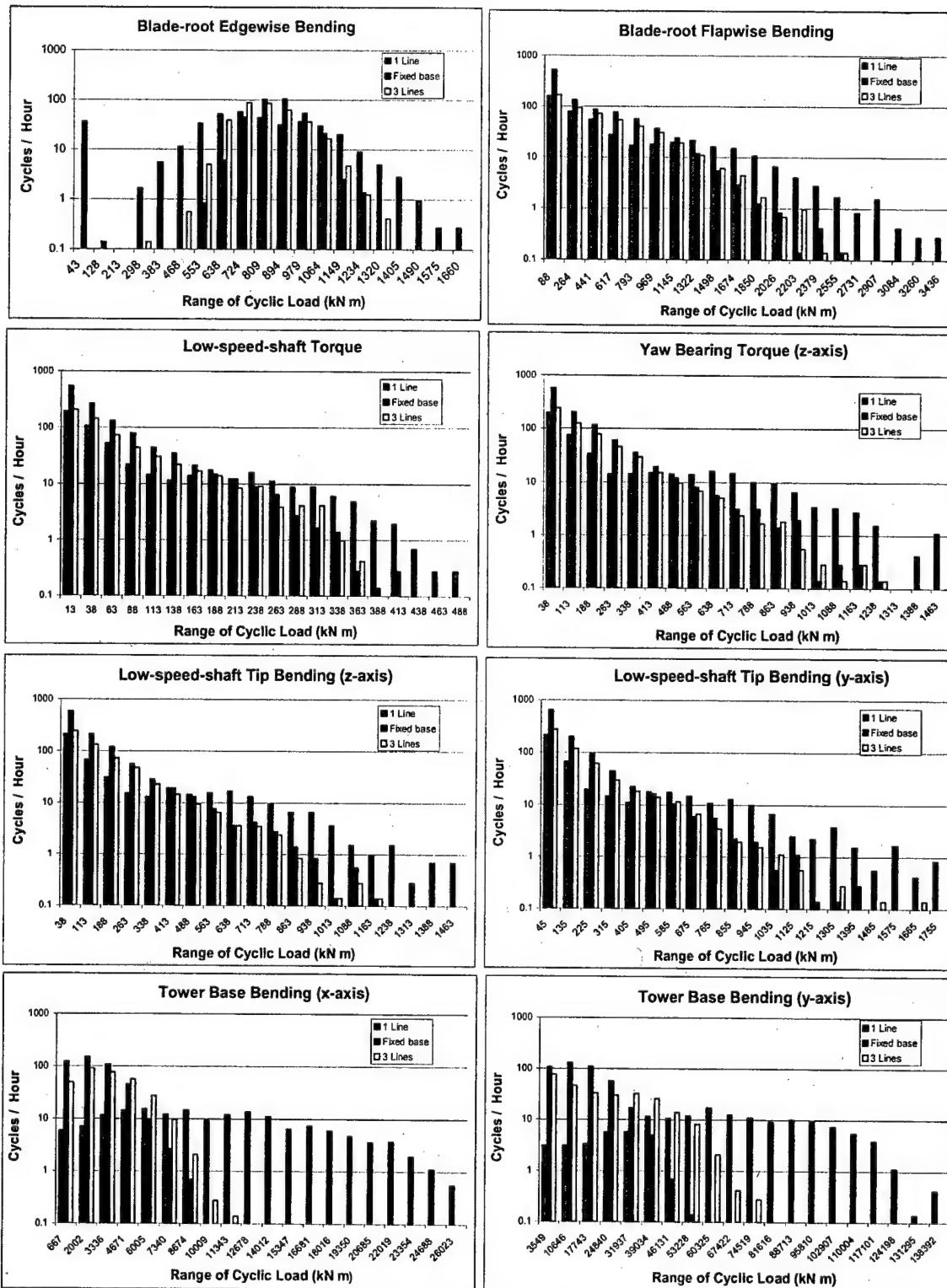
Figure 9.11 Rainflow cycle counts for fixed base, floating support (1 line), and floating support (3 lines) during operational test 3. 15 m/s reference wind speed. Sea state 6.

9.4.1 Design Verification

While the results of a single simulation may be enough to determine the unsuitability of a design, one simulation is not adequate to prove the acceptability of a design. The environmental inputs can vary greatly between different simulations. The random number generators used to produce the wind and wave records determine the environmental inputs for the floating wind turbine system. A single test is insufficient and several simulations must be conducted before a design can truly be proven adequate.

The response of the modified floating wind with three tethers per spoke was further tested using operational test 3 conditions (sea state 6 and 15 m/s reference winds). Five floating and five fixed base simulations were conducted using different random seeds to generate the input wind records and wave spectrums. Each simulation was ten minutes in length. Table 9-9 is a summary of the ten simulations. The maximum loading values for all but the tower base bending moments were higher for the fixed base than the floating support results. This general behavior is not shown in the single one simulation. During the one hour simulation wave loading was the driving factor behind the maximum loading on the floating wind turbine since most of floating loadings were highest for the floating support. The value of running multiple tests was therefore demonstrated since the results of the single test showed maximum loading values being higher for the floater being higher than the fixed base for four additional loads.

Table 9-9 Comparison of mean and maximum loading values for 5 fixed base and 5 floating support 10 minute simulations using operational test 3 conditions.

Loading	Mean Loading			Maximum Loading		
	Fixed (kN m)	Floater (kN m)	Delta (%)	Fixed (kN m)	Floater (kN m)	Delta (%)
Tower Base Bending (x-axis)	1223.4	1260.5	3.0%	5790.0	6075.0	4.9%
Tower Base Bending (y-axis)	7302.9	7393.7	1.2%	41720.0	53180.0	27.5%
Blade-Root Edgewise Bending	36.9	38.0	2.8%	1254.0	1009.0	-19.5%
Blade-Root Flapwise Bending	503.7	504.1	0.1%	2060.0	2022.0	-1.8%
Low-Speed Shaft Tip Bending (y-axis)	253.5	250.8	-1.0%	1318.0	1239.0	-6.0%
Low-Speed Shaft Tip Bending (z-axis)	89.9	92.4	2.8%	846.2	614.3	-27.4%
Low-Speed Shaft Torque	677.6	675.4	-0.3%	1010.0	932.5	-7.7%
Tower-Head Torsion	128.1	130.8	2.1%	862.0	636.3	-26.2%

Running multiple tests using different random seeds for the environmental inputs showed how a stiff support system on the floater can result in lower maximum operating loads than a fixed base wind turbine. This effect of wave loading on the maximum loading values for all but the tower base bending moments was mitigated by the fact that the stiffer tethers did not allow the waves to induce excessive motion of the nacelle due to pitch / roll. The flexibility of the floating system in surge and sway relieved some of the wind stresses placed on the system.

The fatigue response of the system was also determined for the ten simulations. The rainflow cycle counts were determine for each of the tests. Then the results of the five floating and five fixed base test were combined into two rainflow cycle records for the two wind turbine base conditions (see). Higher numbers of cycles at the higher loading values will result in decreased component life. As shown in Figure 9.12, both of the tower base bending moments will have higher fatigue for the floating wind turbine. The loading values for the other six components were shown to be very similar for both the fixed and floating cases. The additional loading on the system had very little effect on the cyclic loading on the parts at the tower top.
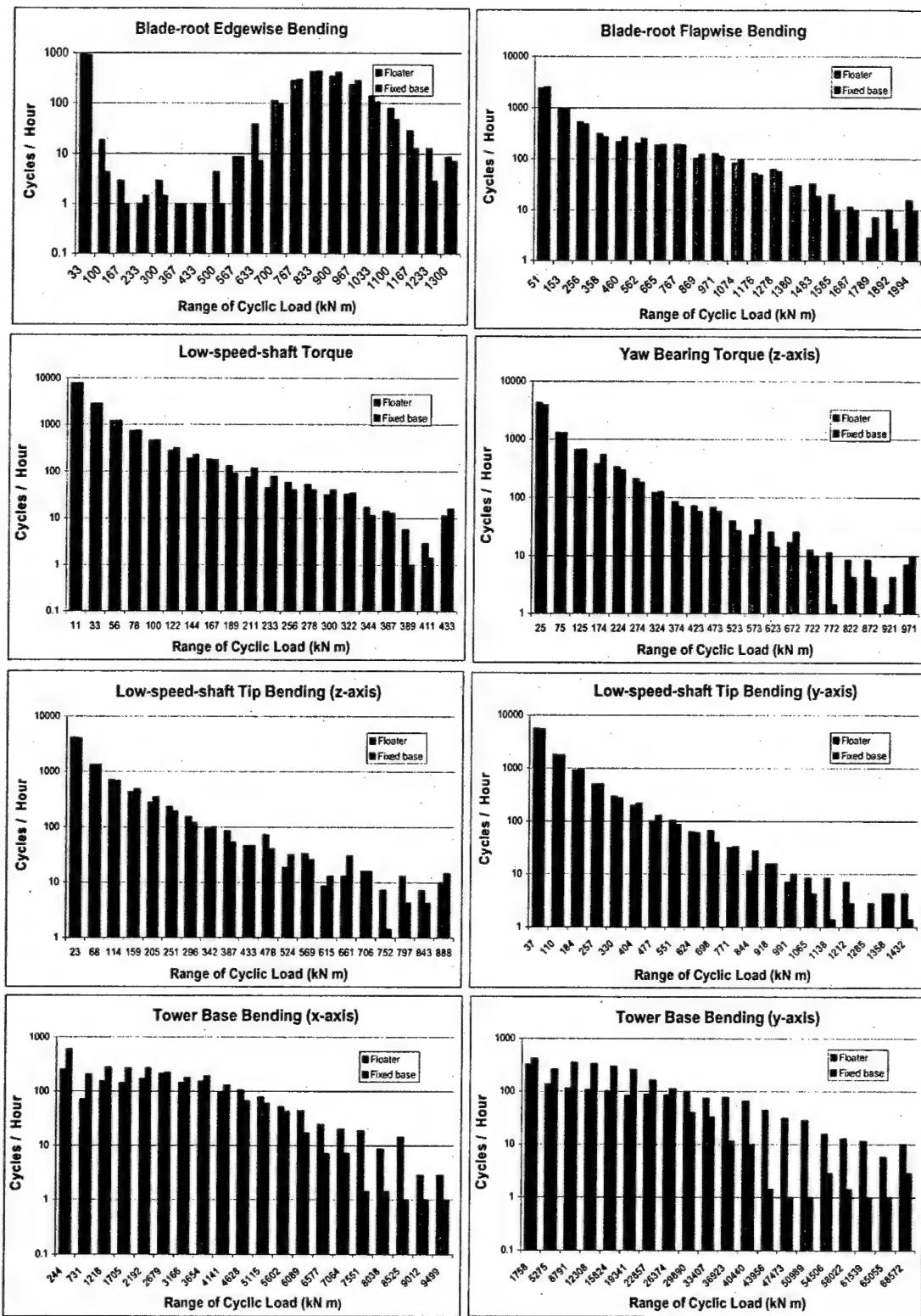
Figure 9.12 Combined rainflow cycle counts for five floating (3 lines per spoke) and five fixed base simulations. Simulation times = 10 minutes. Sea state 6 and 15 m/s reference winds.

124

9.5 Extreme Wind Loading Case

The response of the system to an abnormal wind event can be evaluated using the Extreme Operating Gust (EOG) described in section 9.2. During the EOG event the wind inflow to the rotor initially dips down, then rises sharply to the peak wind velocity, followed by another dip, and finally comes back to the original wind speed. This event occurs over a 10 second period. The hub height wind record used in this testing is shown in

Figure 9.13. This wind record was generated using the IECWind program from the National Wind Technology Center.
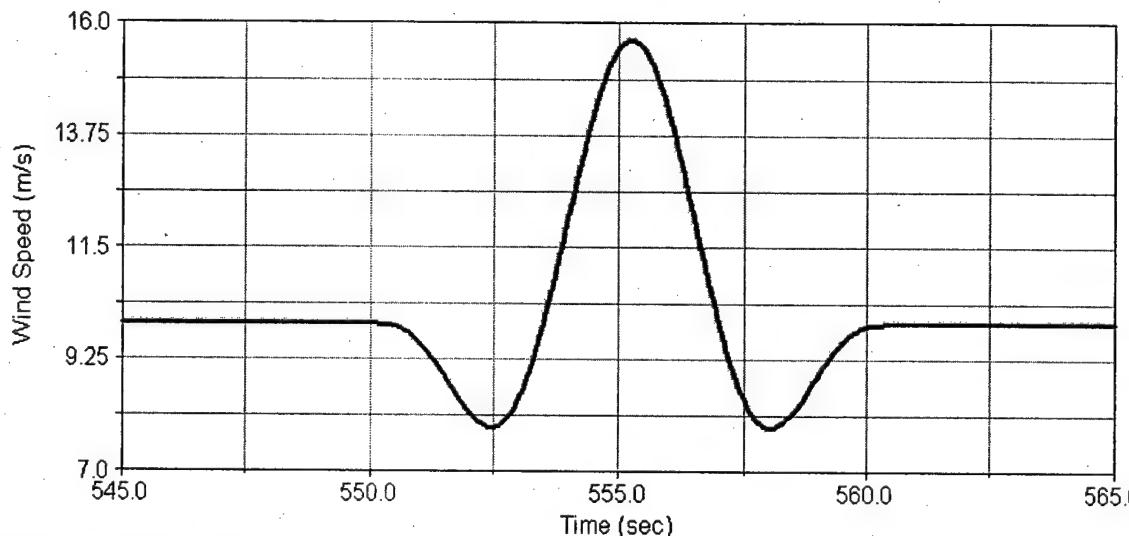
Figure 9.13 Wind velocity record during Extreme Operating Gust for a class II-A wind turbine with a rated speed of 10 m/s and cutout speed of 25 m/s.

Numerical simulations were conducted on the system for four different cases. First the fixed based wind turbine was evaluated. Next, a floating wind turbine with no incident waves was subjected to the EOG. Finally, two tests with sea state 3 waves and the EOG were conducted. The second wave test used the same wave spectra as the first sea state 3 test with the phase angles for the spectrum bands shifted by 180 degrees. This phase shift resulted in the wave excitation forces on the floater being likewise shifted by 180 degrees.

As shown in Figure 9.14, mounting the wind turbine on a floating base changes the maximum values of loading during the extreme operating gust event. Most of the values for loading were higher for the floater that the fixed base wind turbine. But in most cases the differences were small. The waves acting on the floating base were seen to affect the values for maximum loading.

125
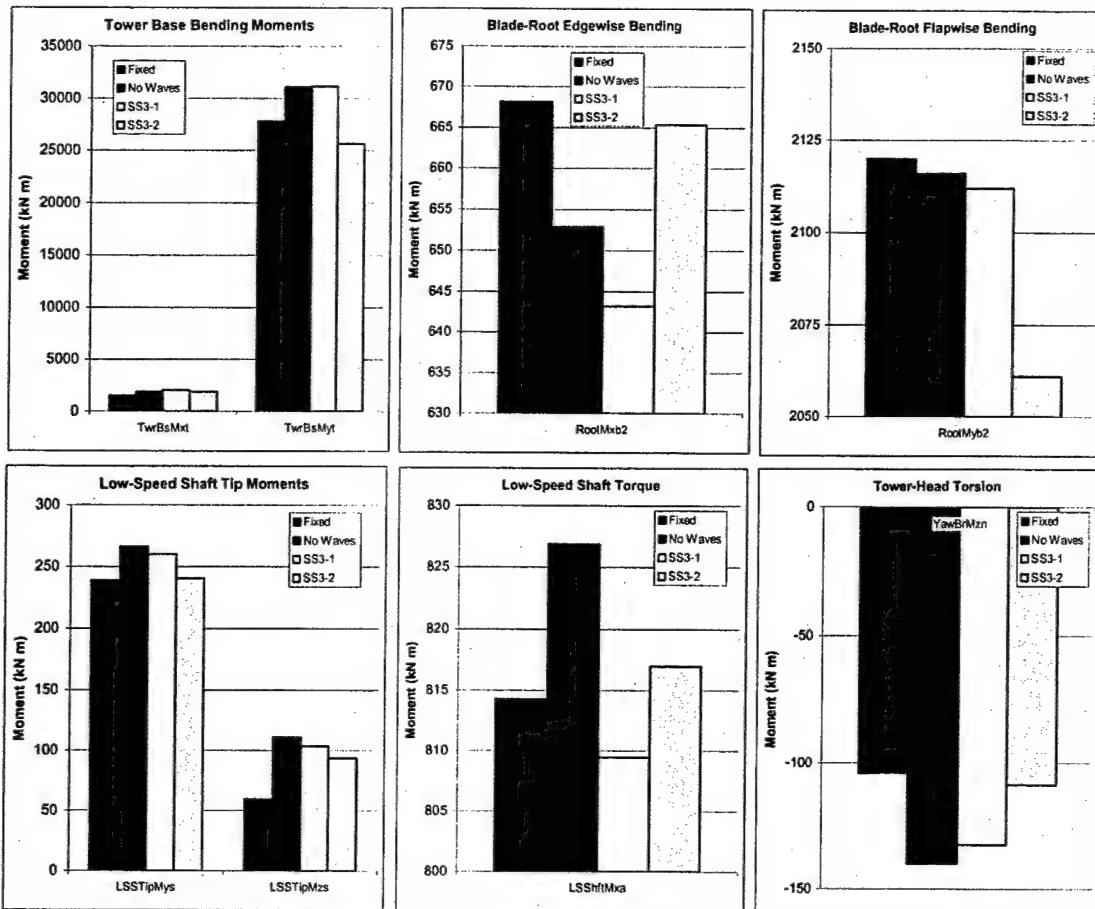
Figure 9.14 Load comparisons for extreme operating gust. Four cases: fixed base, floating with no waves, floating with sea state 3-1st case, and floating with sea state 3-2nd case (phase shifted 180°).

In general, loading values for the floating wind turbines were higher than the fixed base wind turbine. However, some of the loading values were lower for the floating wind turbine. All of the blade-root moments were slightly lower for the floating turbine than the fixed turbine. The largest differences were between the values of low-speed shaft tip bending moments (see Table 9-10). But, the values are low compared to the moments of the shaft tip about the y-axis and therefore are not very troubling.

Waves acting on the floater produced forces and moments on the system. In the first test the wave loads acted in the opposite direction as the wind loads during the 10 second period of the EOG. Wave loads acted in the same directions as wind loads during the second test. This factor resulted in six of the eight wind turbine loads being lower for the second test being lower that the first sea state 3 test. Comparison of the EOG results with those of operational test 3 (see Table 9-8) shows that that the EOG event is not a limiting case for the floating wind turbine system.

126

Table 9-10 Summary of maximum loading for three operational tests. Percentages represent the difference between fixed base wind turbine and three floating wind turbine cases: no waves, sea state 3, and sea state 3 (shifted by 180°). Negative delta values indicate fixed base loading was higher.

LOADING	Fixed Base Loading (kN·m)	No Waves		SS3 -1st		SS3-2nd	
		Loading (kN·m)	Delta (%)	Loading (kN·m)	Delta (%)	Loading (kN·m)	Delta (%)
Tower Base Bending (x-axis)	1532	1909	24.6%	2063	34.7%	1889	23.3%
Tower Base Bending (y-axis)	27820	31100	11.8%	31180	12.1%	25640	-7.8%
Blade-Root Edgewise Bending	668	653	-2.3%	643	-3.7%	665	-0.4%
Blade-Root Flapwise Bending	2120	2116	-0.2%	2112	-0.4%	2061	-2.8%
Low-Speed Shaft Tip Bending (y-axis)	239	266	11.3%	260	8.9%	241	0.8%
Low-Speed Shaft Tip Bending (z-axis)	-30	-75	145.6%	-68	122.5%	-46	50.7%
Low-Speed Shaft Torque	814	827	1.5%	810	-0.6%	817	0.3%
Tower-Head Torsion	-104	-140	34.5%	-132	27.3%	-109	4.5%

The load imparted by the extreme operating gust was transferred to the tethers. The wind transients were directed along the x-axis and therefore generated surge forces and pitching moments. Lines attached to the upwind spoke (line 3) had the highest line stresses during the EOG tests. None of the line stresses exceeded 15 percent of the breaking stress for the lines. The lines all remained in tension throughout all of the tests.

9.6 Extreme Wave Loading

The final simulations dealt with how the system responded to large amplitude waves while the wind turbine was shutdown. This state would be associated with extreme wind conditions which prevent normal wind turbine operations. The floating wind turbine was assumed to have an operational requirement that necessitated securing the wind turbine once the sea state reached a certain level. It was important to understand how the system responds to extreme waves when in this condition. The response of the system to an extreme wave event was evaluated with the wind turbine secured with the hub height wind speed greater than the cutout speed of the wind turbine. The reference wind

speed (at 10 meters above the water) which corresponded to this hub wind speed was 20 m/s. According to Table 6.1 of Newman, the sea state would be approximately 7 for winds of 20 m/s. The Pierson-Moskowitz sea state 7 spectrum is characterized by a significant wave height $H_{1/3} = 8.9$ meters and a average period $T_0 = 10.7$ seconds. These values were used in (9.4) to determine the design peak $\hat{y} = 10.68$ meters. This value was used to generate the wave group for the two test cases (see Figure 9.15).
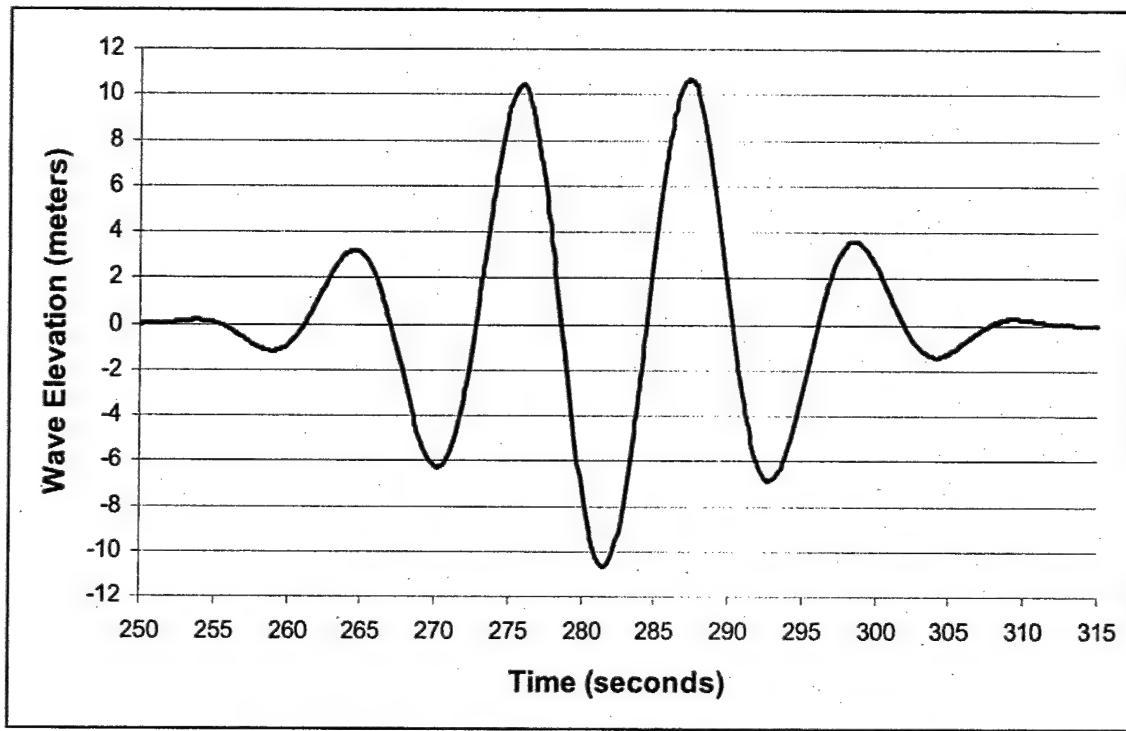
Figure 9.15 Wave elevation record for extreme wave tests.

The extreme wave is the largest wave expected to pass the floating wind turbine during a three hour period. The value used for $\hat{y}$ had a reliability factor of $\alpha = 0.01$, meaning that there was only a one percent chance of the actual highest wave exceeding the value of $\hat{y}$. The maximum wave amplitude during the test was 10.68 meters. When the trough of the wave passed the floater, the entire submerged portion of the tower and approximately 5 meters of the spar were temporarily above the surface of the water. This led to the generation of large nonlinear loads on the floater. To show this behavior, the combined horizontal force on the submerged portion of the tower and the spar was plotted in Figure 9.16. The horizontal forces in the positive x-direction were larger than those in the negative x-direction due to the non-linear effects of the wave passing the tethered floater.

128
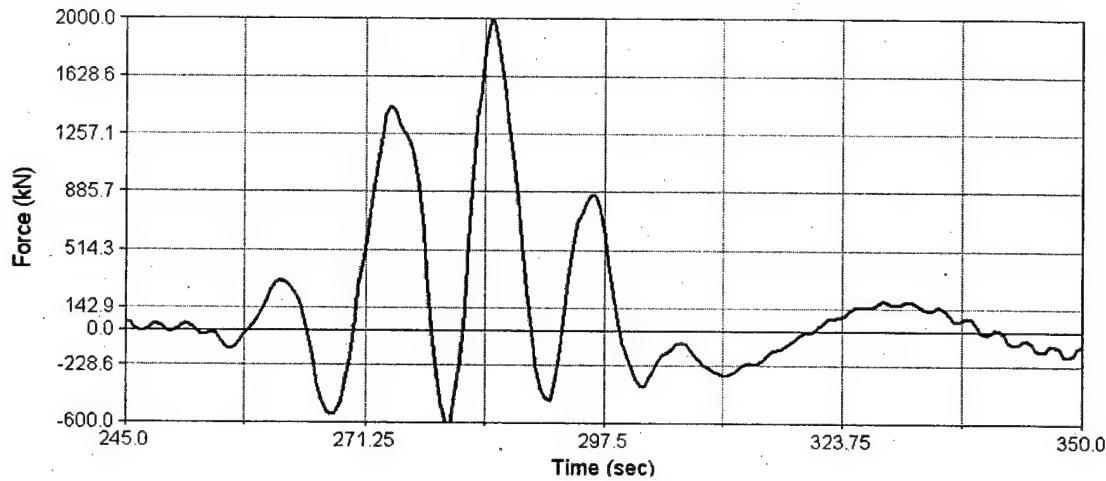
Figure 9.16 Horizontal wave loading of submerged tower and spar during extreme wave test 1.
Incident wave angle = 0°.

The effect of the wave loading on the system was determined for two wave incident angles: 0° and 30°. The other loading on the system was due to random winds which had an average hub height velocity of 25.3 m/s. The winds were directed along the positive x-axis. The wind record also reflected the fact that y and z wind velocity components were present. The combination of wind and wave loading on the system produced loads on the various wind turbine components. A baseline test was also run with the floater fixed in position for comparison purposes. The baseline wind turbine loads were then compared to the loads from the two floating cases. The baseline system was only acted on by wind. For all cases the rotor was fixed in position with the blades pitch = 90° to minimized wind loads. The maximum values for the three tests are charted in Figure 9.17.
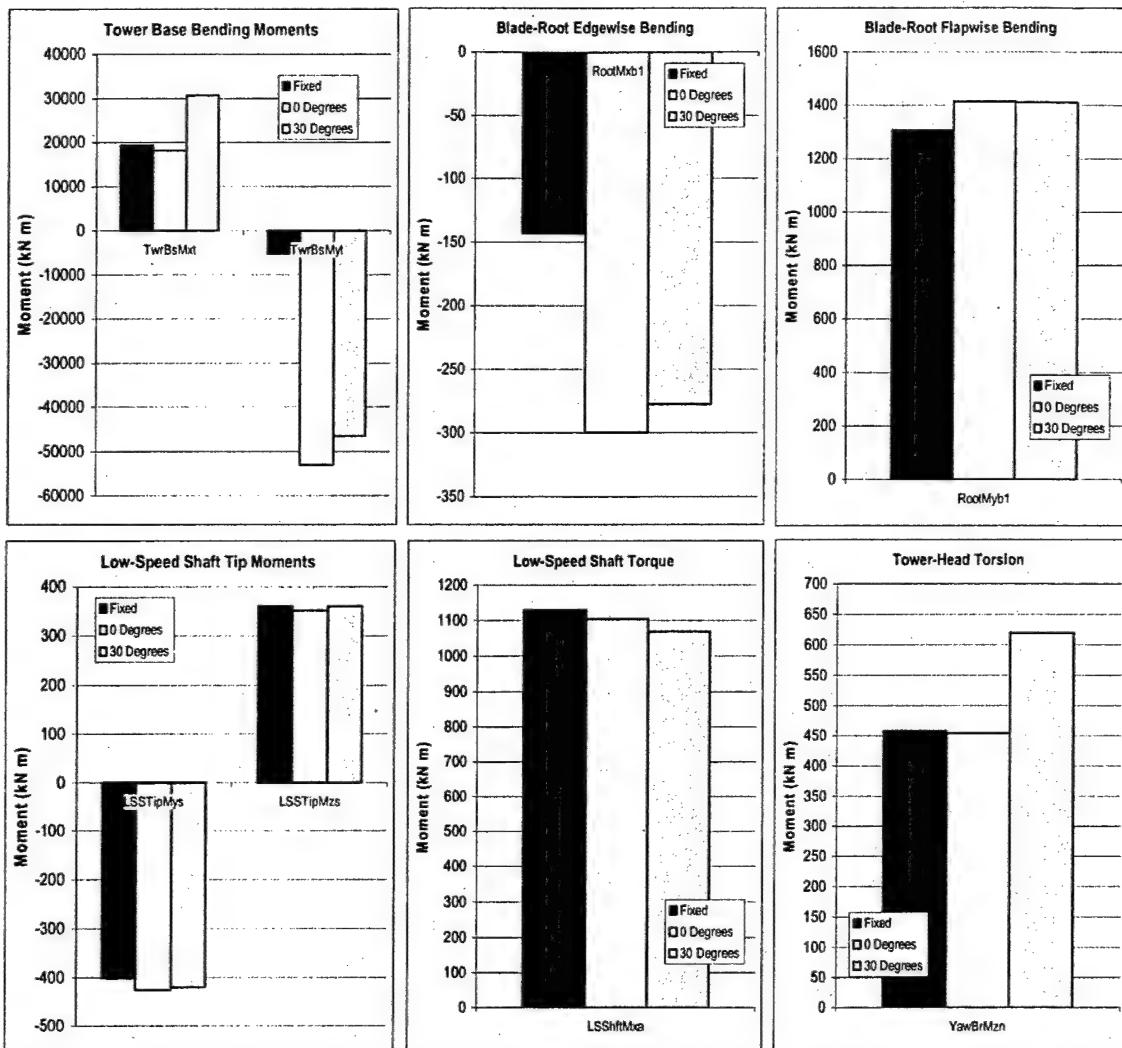
Figure 9.17 Maximum wind turbine loads during extreme wave tests. Wind turbine secured. Blade pitch = 90°. Reference speed of 20 m/s. Incident wave amplitude = 10.68 m. Incident wave period = 11.62 seconds. 1) Fixed base (only wind loading), 2) floating (incident wave angle = 0°), and 3) floating (incident wave angle = 30°)

The extreme wave events caused translational and rotational motion of the system. In some cases, these motions increased the loading on the wind turbine components. In a few instances the ability of the floater to move when the blade elements were acted on by the wind reduced the component loading values. Once again the largest differences in loading were between the fixed and floating support tower base bending moments. The tower moment about the y-axis when the waves were directed along the x-axis (0°) was over nine times the value of the fixed base case with only wind loading on the feathered rotor blades.

130

The wind turbine in these tests is in a different configuration during the extreme wave tests, therefore the wind loading on the system is very different from the other tests. However, by comparing the values in Table 9-11 with those of Table 9-8 for the three lines per spoke design, it can be seen that only the tower base bending moments for the extreme wave tests are greater than the associated baseline and the sea state 6 operational loading tests. Therefore, with exception of the tower base, exceeding the maximum allowed loading on wind turbine would not be a limiting factor for the chosen extreme wave event. If the system could withstand normal operational, it could also handle the design peak extreme wave.

Table 9-11 Extreme wave loading results. The two extreme wave cases are compared with the loading on the fixed base wind turbine (baseline). Reference wind speed = 20 m/s. Blade pitch = 90°. Maximum wave amplitude =-10.68 m. Wave period = 10.7 seconds.

| Component | Baseline Loading (kN m) | Extreme Wave Tests | | | |
| | | Wave Angle = 0° | | Wave Angle = 30° | |
		Loading (kN m)	Change (%)	Loading (kN m)	Change (%)
Tower Base Bending (x-axis)	19370	18170	-6.2%	30700	58.5%
Tower Base Bending (y-axis)	-5247	-53010	910.3%	-46530	786.8%
Blade-Root Edgewise Bending	333	349	4.8%	382	14.8%
Blade-Root Flapwise Bending	1307	1414	8.2%	1411	8.0%
Low-Speed Shaft Tip Bending (y-axis)	-402	-425	5.9%	-419	4.4%
Low-Speed Shaft Tip Bending (z-axis)	361	352	-2.6%	361	-0.2%
Low-Speed Shaft Torque	1130	1105	-2.2%	1070	-5.3%
Tower-Head Torsion	458	454	-0.9%	620	35.3%

The line configuration for the design which was used in the numerical simulations was relatively stiff. The lines and spokes resisted the pitching moments caused by the wind and waves. As shown in Figure 9.18, even when the system was rapidly translating the mooring system maintained the vertical alignment of floater and tower.

131
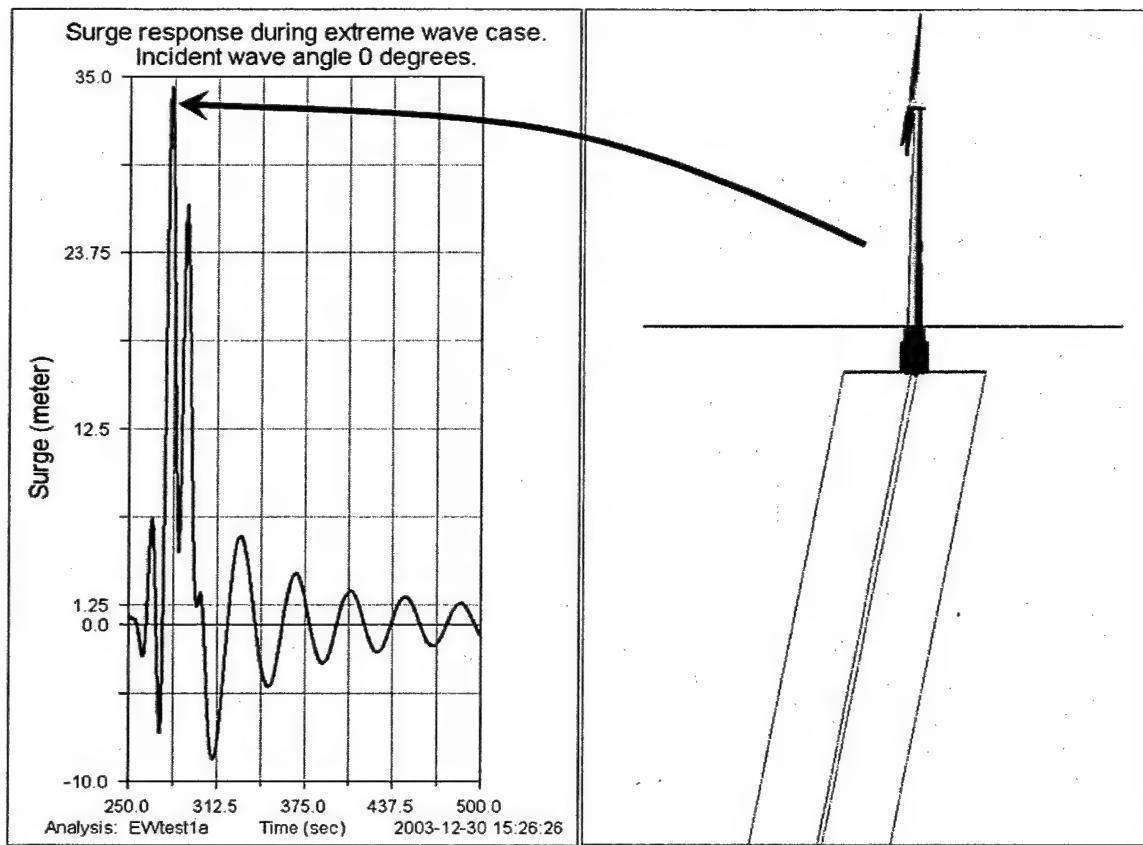
Figure 9.18 Surge response during extreme wave event. Left: graph of surge response. Right: Still image of animation of simulation at time = 279.7 seconds (time of maximum deflection).

The other factor which was evaluated during the extreme wave cases was the line stress. In order for the system design to be acceptable for the chosen environment the lines must not exceed their breaking stress. A safety factor would also be incorporated into the analyses. None of the line stresses exceeded 15 percent of the breaking stress (857.6×10^6 Pa). The minimum line stress during the extreme wave simulations was found to be 76×10^6 Pa. If any of the line stresses had gone to zero during the tests the pitch angle would have increased. Opposite lines absorbed moments placed on the system. Lines 1 and 3 (on the x-axis) resist pitch motion and lines 2 and 4 (on the y-axis) resist roll motion. As shown in Figure 9.19, during the first test the lines stresses for lines 1 and 3 oscillated with line 1 stress increasing as line 3 stress decreased and vice versa. During the first test the waves propagated along the x-axis and therefore created no roll moments. For this reason lines 2 and 4 stresses only had to absorb roll moments produced by wind effects on the blades and inertial loads. During the second test (incident wave angle = 30°), the waves produced both large roll and pitching moments. Lines 1 and 3 absorbed the pitch moments and lines 2 and four absorbed the roll moments, and their line stresses changed accordingly.

132
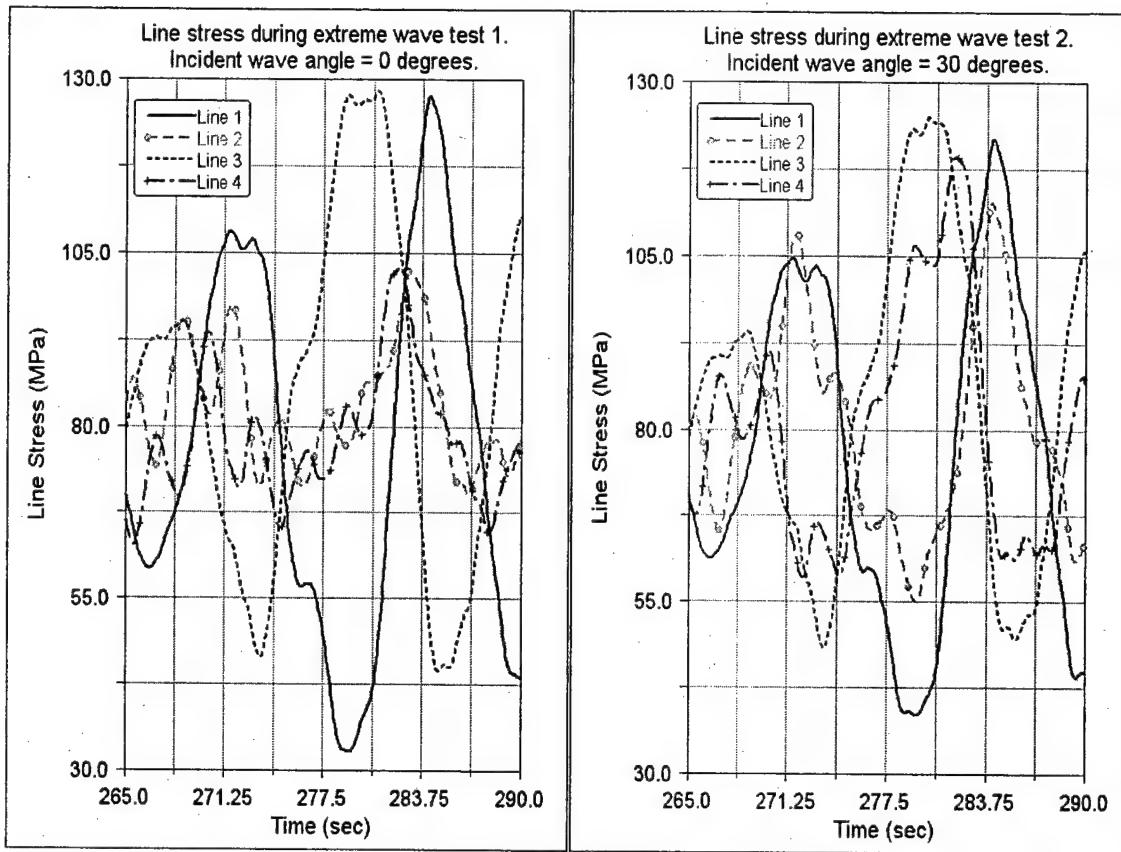
Figure 9.19 Line stress response during extreme wave events. Wave angles = 0° and 30°.

During the extreme wave event which was tested all of the wind turbine components loading values were below those determined during the normal operations test cases. The line stresses caused by the extreme wave events were well below the limitations for the tethers. Also, the lines remained in tension throughout which prevented excessive rotational motion of the system. Therefore, it was proven that the tested extreme wave event would not be a limiting case for this configuration of the floating wind turbine system.

133

10 Conclusions and Future Work

The thesis focused on floating offshore wind turbines. The first goal of the work was to develop a method to analyze a floating wind turbine system. The second goal was to determine a promising design for the floating support which could allow for the safe operation of a wind turbine in realistic wind and wave environments. Determining the dynamic properties of the system was the third goal of this research. The final goal was evaluate the effects of normal operations and extreme wind and wave events on both the wind turbine and tethers.

In order to support a wind turbine and its own weight the floater must have a minimum displacement. The center of gravity of the wind turbine is well above the free surface this leads to a problem with the center of gravity being above the center of buoyancy for floater. This arrangement would be unacceptable and could be overcome by either increasing the size and weight of the floater to bring the system center of gravity down below the center of buoyancy or using tethers to maintain the system in an upright position. The former design would be much larger than the later design and subsequently more expensive. It was assumed that the support system should be relatively stiff in the pitch and roll modes of motion in order not to put undo stresses on the wind turbine portion of the system. Other possible designs which had multiple wind turbines supported on a single floater were deemed to be cost prohibitive and would be subjected to very large wave loads.

The design chosen for analysis in this work was a tension leg spar buoy, which consisted of a vertical cylinder most of the displacement volume and spokes with tethers under tension attaching the floater to the seafloor. This design required smaller displacement volumes and hence lower material costs for the floater than for a design which had the system center of gravity below the center of buoyancy. The use of spokes and tethers under tension creates a support system that has the potential to be very stiff in the pitch and roll modes of motion depending on the type of lines used for the tethers. A design parameter analysis of the system was conducted for the system and is included in Appendix A.

The analysis method used for the floating wind turbine incorporated models of a wind turbine and floater. These two systems were analyzed in a fully coupled manner in the time domain. The wind turbine was modeled using a blade element method. The loads on the individual blade elements were calculated using the AeroDyn subroutine. The loads on the floater were calculated using the *fltr_loads* subroutine. These loadings were determined for the system model using the ADAMS Solver dynamics program. The elastic and damping properties of the wind turbine and tower were

134

incorporated into the ADAMS dynamic model. The dynamic model of the system also included the behavior of the tethers.

The wave loads on the floater were calculated using a combination of equations of GI Taylor and Morrison. The inertial loads on the floater were found using GI Taylor. Viscous drag calculations on the cylinders and spokes on the system were determined by Morrison's equation. These calculations were carried out in the time domain so no linear approximations of drag were required. The operation of the floater loading subroutine was verified for small amplitude waves with linear calculations using a floater which did not include a wind turbine.

Time varying wave elevations produce nonlinear wave forces. These forces result in a mean displacement of the system in the direction of wave propagation. These nonlinear loads are modeled using a linear approximation method described in Faltinsen, 1990 [13].

Numerical simulations were conducted for free decay tests of the system in the different modes of motion. The non-dimensional linear (wind turbine) and quadratic (viscous drag) damping coefficients for the floater and wind turbine were evaluated. Effects of wind speed and rotor blade pitch angle were investigated. The natural periods of the system during the free decay tests corresponded well with those predicted using linear theory.

The wind turbine damping was also shown to be linear. The wind turbine was found to be a very large source of damping for pitch motion. The quadratic damping of the system was the result of viscous drag. Viscous drag dominated the initial damping of the system for most of the free decay simulations. Blade pitch had a large effect on the system damping. This fact could possibly be incorporated into future control systems to change damping behavior of the system.

The effects of normal operating conditions on various components of the wind turbine were evaluated. Three different combinations of reference wind speed and sea state were used. The maximum loading and fatigue response of the floating wind turbine system was compared to that of the same wind turbine with a fixed base. The initial floating design was shown to have increased maximum loading values and markedly reduced fatigue life when compared to the fixed base design. The number and types of lines used to tether the structure were changed to demonstrate how the initial problems could be overcome. The stiffness of the system in pitch and roll was increased by making the tethers stiffer. The altered design showed marked improvements in both maximum loading and fatigue response. This process demonstrated how design optimization could be used to improve system performance.

135

The final tests involved determining the response of the floating wind turbine systems to extreme wind and wave events. The extreme operating gust case described in IEC 61400-1 was performed for both floating and fixed base wind turbines. The maximum loading values for the wind turbine were compared. The maximum loading was determined for an extreme wave event with the wind speed at above the cutout speed for the wind turbine. With one exception, the values for maximum load during the extreme wind and wave tests were found to be less than those determined during the normal operations cases or less than that of the fixed base wind turbine results. The loading of the tower base was identified as the load which had the largest differences between the fixed base and floating support loads.

The some of the behaviors of the tension leg spar buoy predicted by this research could be verified by model testing. Unfortunately, accurately it is not possible to build a scaled model of an operational wind turbine and attach it to a scaled floater. The behavior of the wind turbine would not realistically mimic the response of a large scale machine. However, some useful data could be gathered using scaled models. The best way to prove the viability of the chosen floating support would be to build a prototype and operate it in an offshore environment. Yet, the fully coupled dynamic method developed in this thesis is expected to be accurate since the independent validation of the wind turbine modeling methods (AeroDyn, FAST, and ADAMS) as well as the fundamental wave loading algorithms used in the present research has been performed extensively in earlier studies.

The use of active controls is important for large wind turbine systems. These systems are designed to improve power output and mitigate adverse loading conditions on machine components. When mounted on a floating platform the control systems will have to be adapted to also respond to undesirable loading situations of the tethers. Further research is required to better understand how theses systems might best be utilized for a floating wind turbine system.

In conclusion, the fully coupled dynamic analysis method proved to be a useful tool in the evaluation of a floating offshore wind turbine system. The tension leg spar buoy was shown to be a promising design for supporting wind turbines in water depths that prohibit the use of towers fixed to the sea floor. In the future the design should be further analyzed to include a detailed structural model for the floater. An optimization of the floater configuration would be required in order to minimize the cost and maximize the system performance. The optimized floater design should then be evaluated using the techniques developed in this research. Alternate tether / mooring line configurations should also be investigated.

Appendix A: Parametric Design Issues

It is necessary to understand how changing floater design parameters affect the system response, in order for the floater design evaluated in this research to be adapted for specific wind turbines and environmental conditions. Figure A.0.1 is a diagram of the tension leg spar buoy. The design parameters that are used to describe the floater are:

- spar diameter
- spar length
- submerged tower diameter
- submerged tower draft

- spoke length
- spoke width
- line stiffness
- number of lines per spoke
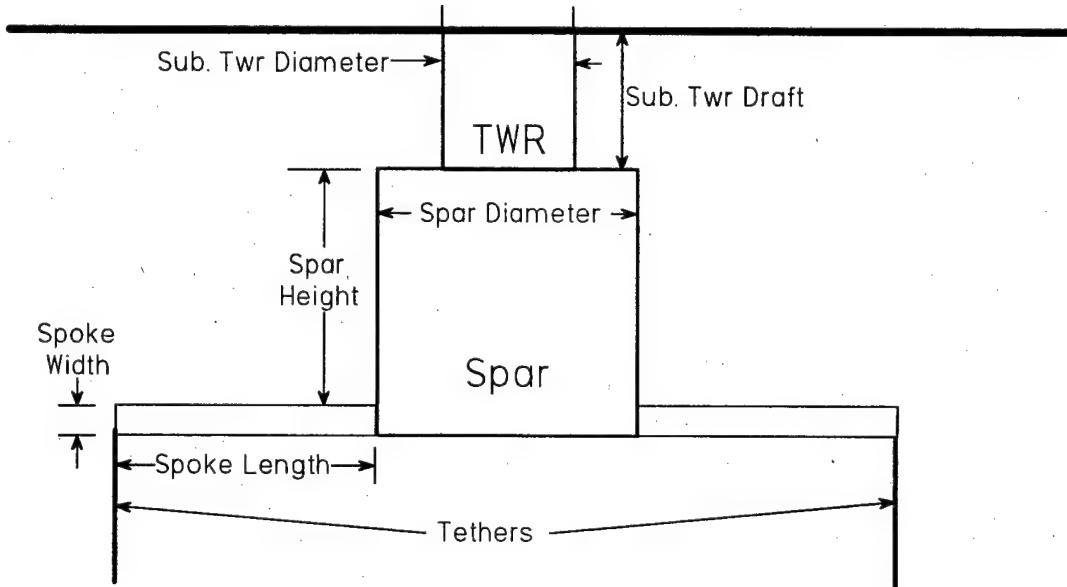
Figure A.0.1 Diagram of Floating Support

The line stiffness is determined by the type of line used (steel, HPME, polyester, etc) and the diameter of the line. The design parameters affect the restoring, damping, and inertia terms in the system equations of motion. Most of the parameters all affect the wave excitation forces acting on the submerged portions of the structure. The water depth has an effect on the restoring coefficients since it drives the length of the tethers.

It is necessary to understand how the floater design can be modified to achieve a desired change in response. The wave environment in which the system must operate is a key design consideration for

137

the system. Changing one floater design parameter can affect the system response in many ways. For example, changing the floater diameter changes the excess buoyancy of the system which changes the natural periods of the system for the surge, sway, and yaw modes of motion. This change has small affects on the roll and pitch restoring coefficients. The amount of wave excitation changes when the floater diameter is changed.

Natural Periods

Frequently, designers are concerned with the natural periods of a system. For waterborne structures it is normal to design the system such that its natural periods lie either about or below the range where wave action might excite resonance. This section examines the affects the design parameters of the floater have on the systems natural periods. The general equations used to determine the natural periods are:

$$T_{natural} = \frac{2\pi}{\omega_{natural}}$$

$$\omega_{natural} = \sqrt{\frac{C}{M+A}}$$

where C is the restoring coefficient, M is the inertia term, and A is the added mass. Due to symmetry of the floater the natural periods for surge and sway are identical and roll and pitch are identical. For the following analysis the design parameters are varied about a reference design. This reference design is the same as that used in the extreme event cases discussed in the previous chapter. Table A-1 and Table A-2 list the properties of the reference system.

Table A-1 Dimensions and properties of floater used in operational tests.

Spar Diameter	10 m	Line Diameter	104mm
Spar Length	12 m	Number of Lines	3 / spoke
Tower Diameter	8 m	Line Minimum Break Load	743 tonnes
Tower Draft	5 m	Maximum Line Extension	4.5 %
Spoke Length	20 m	Line Length (un-stretched)	180.76 m
Spoke Width	1 m	Water Depth	200 m
Buoyant Spokes	No	Structure Thickness	2.53 cm

Table A-2 Calculated attributes of the floating wind turbine used in the operational tests

Mass of Floater	210435.4 kg	Center of Gravity (system) CG	16.98 m
Buoyant Mass	1228424.6 kg	Center of Buoyancy CB	-10.89 m
Total Mass of System	411494.5 kg	CG - CB	27.87 m
Reserve Buoyancy	198.5 %	Surge Natural Period	39.0186 sec
Initial Line Stress	235.4 MPa	Heave Natural Period	1.6591 sec
Breaking Line Stress	857.7 MPa	Pitch / Roll Natural Period	3.3561 sec
Center of Gravity (floater)	-13.82 m	Yaw Natural Period	10.51 sec

The important parameters used in determining the natural periods of systems are the restoring coefficients, the inertia terms of the structure, and the added mass. The following equations are relevant to the discussions of natural periods:

$$C_{11} = C_{22} = \frac{F_{tethers}}{L_{tether}}$$

$$A_{11} = A_{22} = \left(\frac{d^2}{4} \rho_{sw} \pi T \right)$$

$$C_{33} = \frac{4 \cdot E_{tethers} A_{tethers}}{L_{tethers}} + \rho_{sw} g A_{wp}$$

$$A_{33} = \frac{2}{3} \cdot \rho \pi r^3 + 4 \cdot \left(4.754 \cdot L_{spoke} \rho \left(\frac{w_{spoke}}{2} \right)^2 \right)$$

$$C_{55} = C_{44} = 2 \frac{\left(E_{line} \cdot A_{tether} \right)}{L_{tether}} \left(L_{spoke} + \frac{d}{2} \right)^2 + F_{buoy} \frac{T}{2} - m_{total} g (CG_{sys} + T)$$

$$A_{44} = A_{55} \frac{d^2}{12} \rho_{sw} \pi T^3$$

$$C_{66} = \frac{\left(\frac{d}{2} + L_{spoke} \right)^2}{L_{tethers}} \cdot F_{tethers}$$

$$A_{66} = 4 \left(4.754 \cdot \left(\frac{w}{2} \right)^2 \rho \left(\left(L_{spar} + \frac{d}{2} \right)^3 - \left(\frac{d}{2} \right)^3 \right) \right)$$

Spar Diameter

The first design parameter which is evaluated is spar diameter. Changing the spar diameter changes the cross-sectional area of the cylinder, which increases the added mass in every mode except yaw. The restoring coefficients are also affected since the buoyancy of the system changes. The spar diameter is varied from 12 meters to 8 meters and the natural periods determined. The spoke length is changed to keep the lines at the same location relative to the center of the structure.

Figure A.0.2 shows how increasing the diameter causes the surge, sway, and yaw natural periods to decrease. This decrease is due to the fact that the as the diameter increases the amount of reserve buoyancy increases (even though the weight went up also). The restoring coefficients for all three of these modes of motion are dependant on the amount of reserve buoyancy. As the restoring coefficients increase the natural periods decrease.

The pitch, roll, and heave natural periods increase when the spar diameter increases. This is due to the fact that the heave added mass associated with these modes of motion also increases with the spar diameter. And since the restoring coefficients are not greatly affected by the change in diameter (heave restoring increases slightly with increasing diameter), the natural periods increase with the spar diameter.
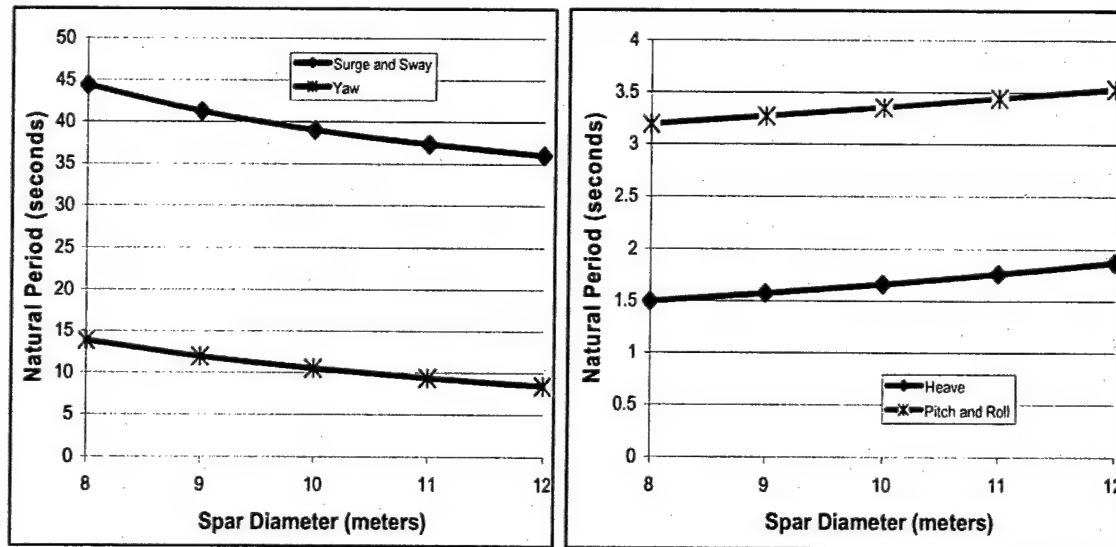
Figure A.0.2 Effect of spar diameter on natural periods.

Spar Height

Spar has a similar effect on the systems natural periods as spar diameter on all of the modes of motion except for heave (see Figure A.0.3). Changing the spar length changes the buoyancy and mass of the system. The buoyancy changes up linearly unlike spar diameter. The added mass terms for surge and sway are affected while yaw added mass is unaffected. The net result of changing the spar length are natural periods of surge, sway, and yaw which decreases less than linearly as length increases.
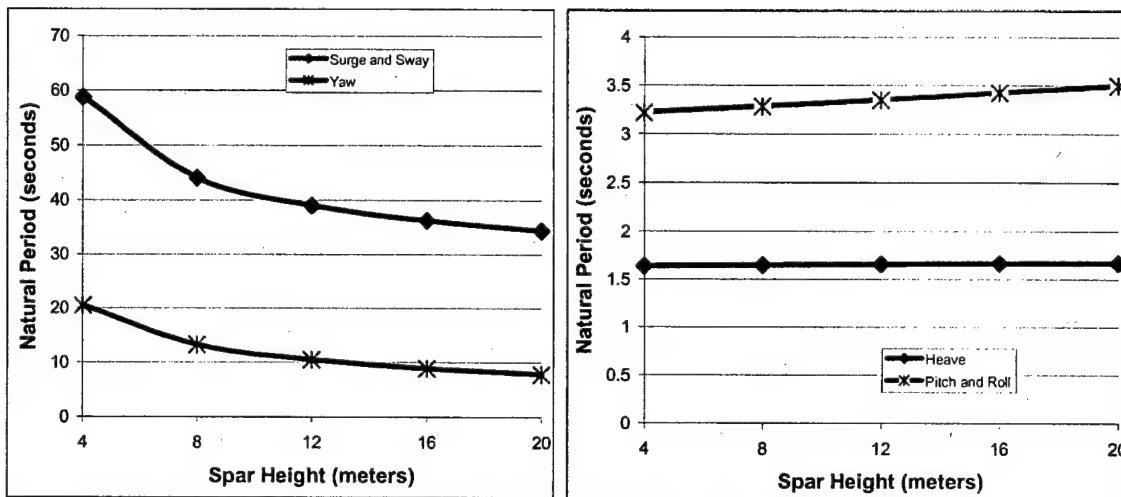
Figure A.0.3 Effects of spar height on natural periods.

Heave is relatively unaffected by changing the length of the cylinder in water depths of 200 meters. The mass of the system increases with spar height, therefore the inertia term gets bigger. Small changes in line length affect the spring constant of the lines and hence the heave restoring coefficient. However, the increase in the inertia term dominates and heave natural period goes up with increasing spar length. The roll and pitch natural periods are more affected by changes in length since the added mass terms go up proportional to the square of the length. The moments of inertia also change. The combined effect of increased inertia and added mass in roll and pitch cause the natural periods to increase for longer spar lengths.

141

Spoke Length

The use of spokes for the tension leg spar buoy increases the stiffness of the system in all three of the rotational modes of motion. As was shown in the previous chapter, the increased stiffness reduced maximum and fatigue loading on the floating wind turbine. Unfortunately, as the spoke length increases challenges arise in mounting very long spokes on a relatively small spar. Design optimization should be used to balance the additional cost of longer spokes to increasing the stiffness of the lines. This decision will be based on the water depth and the size of the machine being supported by the floater.

Since the spokes are modeled as closed box structures, the inertia terms for every mode of motion are affected by changing the spoke length. The added mass terms for all of the modes increase with spoke length. These increases in the inertia and added mass terms cause all of the modes except pitch and roll to increase with spoke length. The yaw restoring coefficient increases with spoke length, but not as much as the added mass and inertia terms increase. A different model of spoke which had less impact on the inertia and added mass terms would result in the yaw natural period decreasing with increasing spoke length.

As shown in Figure A.0.4, the pitch and roll natural periods decrease less than linearly with the increases in spoke length. The spoke length greatly affects the pitch restoring coefficient, which is the dominant term for these modes natural period.
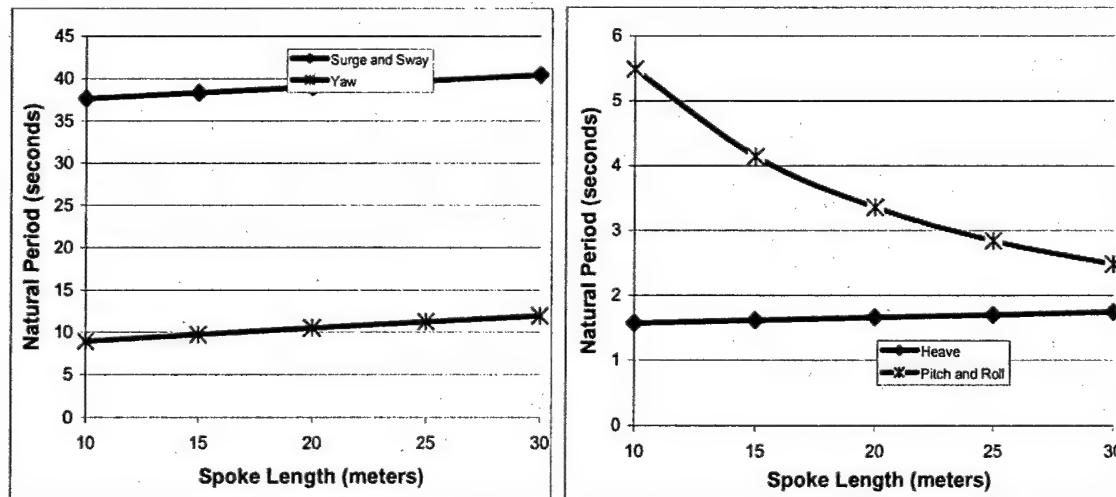
Figure A.0.4 Effect of spoke length on natural periods.

Spoke Width

Spoke width affects all of the modes in a similar manner (see Figure A.0.5). An increase in spoke width increases the mass and moments of inertia of the system. Larger spoke cross-sections have more added mass. The restoring coefficients in surge, sway, and yaw go down as the reserve buoyancy increases. Therefore, these effects combine to increase the natural period with increases in spoke width.
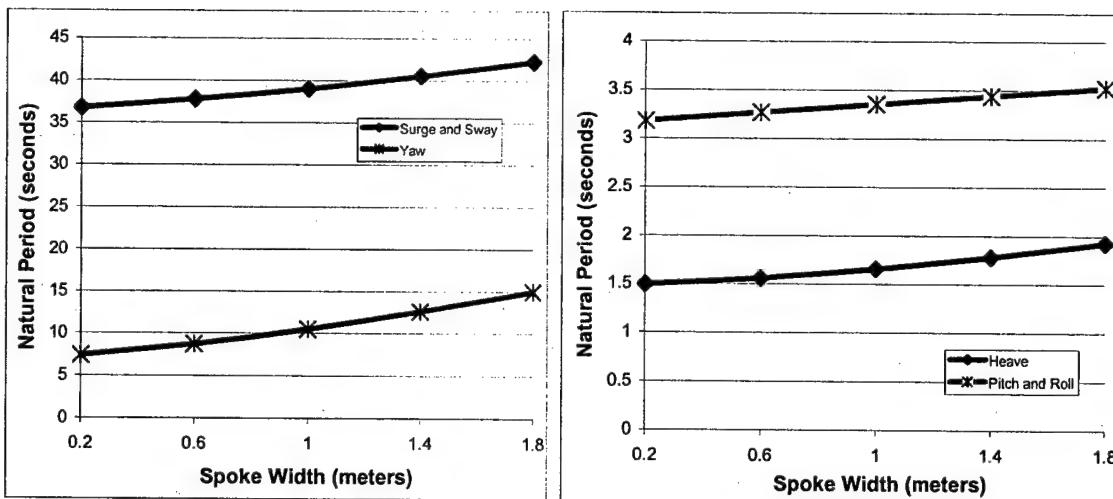
Figure A.0.5 Effect of spoke width on natural periods.

Number of Lines

Changing the number of lines parameter is equivalent to increasing the spring constant acting at the end of each spoke. Changing the line diameter or material type would have similar effects. The surge, sway, and yaw restoring coefficients are constant when lines are changed since they depend on the amount of reserved buoyancy (generates line tension) and the length of the lines. The number of lines has a negligible effect on the inertia properties of the system. Surge, sway, and yaw natural periods are unaffected by the changes in the lines.

Pitch and roll natural periods are greatly affected by the number of lines. For most floater designs the line tension and relaxation components of the pitch and roll restoring coefficients determine a majority of the stiffness (see equation (4.6)). Changing the number of lines affects the restoring coefficients. Therefore, pitch and roll natural frequencies change. Figure A.0.6 is a graph showing how increasing the number of lines reduces the roll and pitch natural periods. Similarly, the heave restoring coefficient changes when the number of lines is changed, this causes the natural period to change.

143
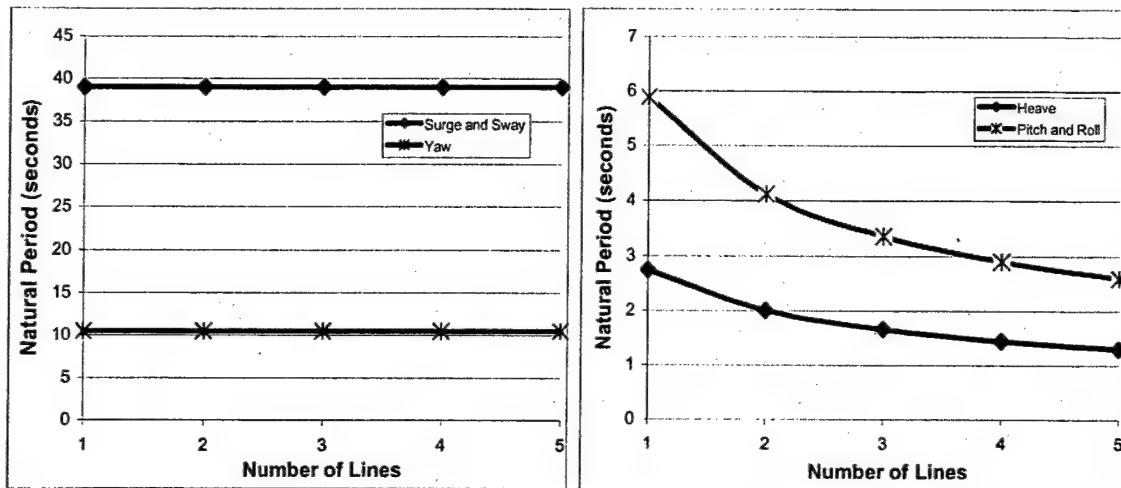
Figure A.0.6 Effect of number of lines on natural periods.

Appendix B: Input file for floater verification test

```
4.0                  ! Floater Diameter ALL UNITS SI
4.0                  ! Tower Diameter
0.0                  ! Depth of tower
10.0                  ! Length of cylinder (Height)
0.0                  ! Height of spokes on cylinder (0 = bottom)
5.0                  ! Length of spokes
1.0                  ! Characteristic width of spokes (square cross-section)
0.0253                  ! Thickness of spar
0.050                  ! Line Diameter (m)
1                  ! Number of lines
200.0                  ! Breaking Load in tonnes   743
0.045                  ! Maximum line Extension
200.0                  ! Water depth
0.0                  ! Wave Direction (degrees)
0.0                  ! Wave Direction Range (+/- this value)
1                  ! Number of Bands (integer value)
.true.                  ! Buoyant spokes
1.0                  ! Wave Amplitude (meter)
0.75                  ! Wave Frequency (rad/sec)
```

=============Line Length Calculations=======================
229.40 190.00 1.0785 Initial Values of KofLine kN/m, Line Length, and L
230.70 188.92 1.0725 Final Values of KofLine kN/m, Line Length, and Lin
=============Calculated Floater Properties=======================

32362.0	Spar Mass
24893.8	Mass Cylinder
2489.4	Mass Spar Plate
0.0	Submerged Tower Mass
16640.3	Mass of Spokes
49002.3	Total Floater Mass
201059.2	Mass of Wind Turbine
49002.3	System Mass
149887.8	Buoyant Mass
100885.5	Reserve Buoyancy
205.88	Percent Reserve Buoyancy
0.0079	Total Area of Lines
230.7	Spring Constant
126.01	Intial Line Stress (MPa)
1.07	Intial Line Stretch

============= System Properties =======================

0.0000	CG of Wind Turbine
-6.6979	CG of Floater
-6.6979	CG of System
-1.0114	BG of System
141537.5	A11 and A22

145

```
  46183.0   A33
14281945.8   A44 and A55
 546258.4   A66
1140080.9   Ixx
1140080.9   Iyy
 451478.0   Izz
  5208.9   C11 and C22
1049673.8   C33
27364352.8   C44 and C55
  36462.2 C66
```

==================== Natural Frequencies of Floater System ====================

0.1653	Surge and Sway Natural Frequencies (rad/sec)
3.3208	Heave Natural Frequency(rad/sec)
1.3321	Roll Natural Frequency(rad/sec)
1.3321	Pitch Natural Frequency (rad/sec)
0.1912	Yaw Natural Frequency (rad/sec)

==================== Natural Periods of Floater System ====================

38.0015	Surge and Sway Natural Period (sec)
1.8921	Heave Natural Period (sec)
4.7169	Roll Natural Period (sec)
4.7169	Pitch Natural Period (sec)
32.8675	Yaw Natural Period (sec)

Appendix C: 1.5 MW Baseline FAST Input File

```
------ FAST INPUT FILE -------------------------------------------------
FAST certification Test #13: WindPACT 1.5 MW Baseline with many DOFs with VS and VP and FF turbulence.
Model properties from "InputData1.5A08V07adm.xls" (from C. Hansen) with bugs removed. Compatible with FAST v4.3.
--------------------- SIMULATION CONTROL ------------------------------------
False    Echo       - Echo input data to "echo.out" (switch)
  2      ADAMSPrep  - ADAMS preprocessor mode {1: Run FAST, 2: use FAST as a preprocessor to create an ADAMS model, 3: do
both} (switch)
  2      AnalMode   - Analysis mode {1: Run a time-marching simulation, 2: create a periodic linearized model} (switch)
  3      NumBl      - Number of blades (-)
1000.0   TMax       - Total run time (s)
 0.05    DT         - Integration time step (s)
--------------------- TURBINE CONTROL ------------------------------------
  2      PCMode     - Pitch control mode {0: none, 1: power control, 2: speed control} (switch)
  5.0    TPCOn      - Time to enable active pitch control (s)
  1      VSContrl   - Variable-speed control {0: none, 1: simple VS, 2: user-defined VS}  (switch)
1800.0   RatGenSp   - Rated generator speed for simple variable-speed generator control (HSS side) (rpm) [used only when VSContrl=1]
 0.002456 Reg2TCon   - Torque constant for simple variable-speed generator control in Region 2 (HSS side) (N-m/rpm^2) [used only
when VSContrl=1]
  1      GenModel   - Generator model {1: Simple, 2: Thevenin, 3: User Defined} [used only when VSContrl=0] (-)
True     GenTiStr   - Method to start the generator {T: timed using TimGenOn, F: generator speed using SpdGenOn} (switch)
True     GenTiStp   - Method to stop the generator {T: timed using TimGenOf, F: when generator power = 0} (switch)
9999.9   SpdGenOn   - Generator speed to turn on the generator for a startup (HSS speed) (rpm)
  0.0    TimGenOn   - Time to turn on the generator for a startup (s)
9999.9   TimGenOf   - Time to turn off the generator (s)
9999.9   THSSBrDp   - Time to initiate deployment of the HSS brake (s)
9999.9   TiDynBrk   - Time to initiate deployment of the dynamic generator brake [CURRENTLY IGNORED] (s)
9999.9   TTpBrDp(1) - Time to initiate deployment of tip brake 1 (s)
9999.9   TTpBrDp(2) - Time to initiate deployment of tip brake 2 (s)
9999.9   TTpBrDp(3) - Time to initiate deployment of tip brake 3 (s) [unused for 2 blades]
9999.9   TBDepISp(1) - Deployment-initiation speed for the tip brake on blade 1 (rpm)
9999.9   TBDepISp(2) - Deployment-initiation speed for the tip brake on blade 2 (rpm)
9999.9   TBDepISp(3) - Deployment-initiation speed for the tip brake on blade 3 (rpm) [unused for 2 blades]
9999.9   TPitManS(1) - Time to start override pitch maneuver for blade 1 and end standard pitch control (s)
9999.9   TPitManS(2) - Time to start override pitch maneuver for blade 2 and end standard pitch control (s)
9999.9   TPitManS(3) - Time to start override pitch maneuver for blade 3 and end standard pitch control (s) [unused for 2 blades]
9999.9   TPitManE(1) - Time at which override pitch maneuver for blade 1 reaches final pitch (s)
9999.9   TPitManE(2) - Time at which override pitch maneuver for blade 2 reaches final pitch (s)
9999.9   TPitManE(3) - Time at which override pitch maneuver for blade 3 reaches final pitch (s) [unused for 2 blades]
 23.0    BlPitch(1) - Blade 1 initial pitch (degrees)
 23.0    BlPitch(2) - Blade 2 initial pitch (degrees)
 23.0    BlPitch(3) - Blade 3 initial pitch (degrees) [unused for 2 blades]
 23.0    B1PitchF(1) - Blade 1 final pitch for pitch maneuvers (degrees)
 23.0    B1PitchF(2) - Blade 2 final pitch for pitch maneuvers (degrees)
 23.0    B1PitchF(3) - Blade 3 final pitch for pitch maneuvers (degrees) [unused for 2 blades]
--------------------- ENVIRONMENTAL CONDITIONS ----------------------------
9.80665 Gravity     - Gravitational acceleration (m/s^2)
--------------------- FEATURE SWITCHES ------------------------------------
True     FlapDOF1   - First flapwise blade mode DOF (switch)
True     FlapDOF2   - Second flapwise blade mode DOF (switch)
True     EdgeDOF    - First edgewise blade mode DOF (switch)
False    TeetDOF    - Rotor-teeter DOF (switch) [unused for 3 blades]
True     DrTrDOF    - Drivetrain rotational-flexibility DOF (switch)
True     GenDOF     - Generator DOF (switch)
False    TiltDOF    - Nacelle-tilt DOF (switch)
False    YawDOF     - Yaw DOF (switch)
True     TwFADOF1   - First fore-aft tower bending-mode DOF (switch)
True     TwFADOF2   - Second fore-aft tower bending-mode DOF (switch)
True     TwSSDOF1   - First side-to-side tower bending-mode DOF (switch)
True     TwSSDOF2   - Second side-to-side tower bending-mode DOF (switch)
True     CompAero   - Compute aerodynamic forces (switch)
False    CompNoise  - Compute aerodynamic noise (switch)
```

```
---------------------- INITIAL CONDITIONS ------------------------------------
  0.0    OoPDefl   - Initial out-of-plane blade-tip displacement, (meters)
  0.0    IPDefl    - Initial in-plane blade-tip deflection, (meters)
  0.0    TeetDefl  - Initial or fixed teeter angle (degrees) [unused for 3 blades]
  0.0    Azimuth   - Initial azimuth angle for blade 1 (degrees)
 20.0    RotSpeed  - Initial or fixed rotor speed (rpm)
 -5.0    NacTilt   - Initial or fixed nacelle-tilt angle (degrees)
  0.0    NacYaw    - Initial or fixed nacelle-yaw angle (degrees) *********************8
  0.0    TTDspFA   - Initial fore-aft tower-top displacement (meters)
  0.0    TTDspSS   - Initial side-to-side tower-top displacement (meters)
---------------------- TURBINE CONFIGURATION ------------------------------
 35.0    TipRad    - The distance from the rotor apex to the blade tip (meters)
  1.75   HubRad    - The distance from the rotor apex to the blade root (meters)
  1      PSpnEIN   - Number of the innermost blade element which is still part of the pitchable portion of the blade for partial-span pitch
control [1 to BldNodes] [CURRENTLY IGNORED] (-)
  0.0    UndSling  - Undersling length [distance from teeter pin to the rotor apex] (meters) [unused for 3 blades]
  0.0    HubCM     - Distance from rotor apex to hub mass [positive downwind] (meters)
 -3.3    OverHang  - Distance from yaw axis to rotor apex [3 blades] or teeter pin [2 blades] (meters)
-0.1251  ParaDNM   - Distance parallel to shaft from yaw axis to nacelle CM (meters)
-0.2328  PerpDNM   - Perpendicular distance from shaft to nacelle CM (meters)
 82.39   TowerHt   - Height of tower above ground level (meters)
  1.61   Twr2Shft  - Vertical distance from the tower top to the yaw/shaft intersection (meters)
  0.0    TwrRBHt   - Tower rigid base height (meters)
  0.0    Delta3    - Delta-3 angle for teetering rotors (degrees) [unused for 3 blades]
  0.0    PreCone(1) - Blade 1 cone angle (degrees)
  0.0    PreCone(2) - Blade 2 cone angle (degrees)
  0.0    PreCone(3) - Blade 3 cone angle (degrees) [unused for 2 blades]
  0.0    AzimB1Up  - Azimuth value to use for I/O when blade 1 points up (degrees)
---------------------- MASS AND INERTIA ----------------------------------
 51.170E3 NacMass  - Nacelle mass (kg)
 15.148E3 HubMass  - Hub mass (kg)
  0.0    TipMass(1) - Tip-brake mass, blade 1 (kg)
  0.0    TipMass(2) - Tip-brake mass, blade 2 (kg)
  0.0    TipMass(3) - Tip-brake mass, blade 3 (kg) [unused for 2 blades]
 49.130E3 NacYIner - Nacelle inertia about yaw axis (kg m^2)
 58.720E3 NacTIner - Nacelle inertia about tilt axis (kg m^2)
 53.036  GenIner   - Generator inertia about HSS (kg m^2)
 34.600E3 HubIner  - Hub inertia about teeter axis (kg m^2) [unused for 3 blades]
---------------------- DRIVETRAIN -----------------------------------
100.0    GBoxEff   - Gearbox efficiency (%)
 95.0    GenEff    - Generator efficiency [ignored by the Thevenin and user-defined generator models] (%)
 87.965  GBRatio   - Gearbox ratio (-)
False    GBRevers  - Gearbox reversal {T: if rotor and generator rotate in opposite directions} (switch)
9999.9   HSSBrTqF  - Fully deployed HSS-brake torque (N-m)
9999.9   HSSBrDT   - Time for HSS-brake to reach full deployment once initiated (sec)
         DynBrkFi  - File containing a mech-gen-torque vs HSS-speed curve for a dynamic brake [CURRENTLY IGNORED] (quoted
string)
  5.6E9  DTTorSpr  - Drivetrain torsional spring (N-m/rad)
  1.0E7  DTTorDmp  - Drivetrain torsional damper (N-m/s)
---------------------- SIMPLE INDUCTION GENERATOR ----------------------------
9999.9   SIG_SlPc  - Rated generator slip percentage [>0] (%)        Now HSS side!
9999.9   SIG_SySp  - Synchronous (zero-torque) generator speed [>0] (rpm)  Now HSS side!
9999.9   SIG_RtTq  - Rated torque [>0] (N-m)                 Now HSS side!
9999.9   SIG_PORt  - Pull-out ratio (Tpullout/Trated) [>1] (-)
---------------------- THEVENIN-EQUIVALENT INDUCTION GENERATOR -----------------
9999.9   TEC_Freq  - Line frequency [50 or 60] (Hz)
9998     TEC_NPol  - Number of poles [even integer > 0] (-)
9999.9   TEC_SRes  - Stator resistance [>0] (ohms)
9999.9   TEC_RRes  - Rotor resistance [>0] (ohms)
9999.9   TEC_VLL   - Line-to-line RMS voltage (volts)
9999.9   TEC_SLR   - Stator leakage reactance (ohms)
9999.9   TEC_RLR   - Rotor leakage reactance (ohms)
9999.9   TEC_MR    - Magnetizing reactance (ohms)
---------------------- TOWER ------------------------------------
 10      TwrNodes  - Number of tower nodes used for analysis (-)
"Baseline_Tower.dat" TwrFile - Name of file containing tower properties (quoted string)
---------------------- NACELLE-YAW ------------------------------
  0.0    YawSpr    - Nacelle-yaw spring constant (N-m/rad)
  0.0    YawDamp   - Nacelle-yaw constant (N-m/rad/s)
  0.0    YawNeut   - Neutral yaw position--yaw spring force is zero at this yaw (degrees)
```

```
---------------------- NACELLE-TILT ------------------------------------------
  0.0    TiltSpr    - Nacelle-tilt linear-spring constant (N-m/rad)
  0.0    TiltDamp   - Nacelle-tilt damping constant (N-m/rad/s)
  0.0    TiltSStP   - Nacelle-tilt soft-stop position (degrees)
  0.0    TiltHStP   - Nacelle-tilt hard-stop position (degrees)
  0.0    TiltSSSp   - Nacelle-tilt soft-stop linear-spring constant (N-m/rad)
  0.0    TiltHSSp   - Nacelle-tilt hard-stop linear-spring constant (N-m/rad)
---------------------- ROTOR-TEETER ------------------------------------------
  0      TeetMod    - Rotor-teeter spring/damper model (0: none, 1: standard, 2: user-defined) (switch) [unused for 3 blades]
  0.0    TeetDmpP   - Rotor-teeter damper position (degrees) [unused for 3 blades]
  0.0    TeetDmp    - Rotor-teeter damping constant (N-m/rad/s) [unused for 3 blades]
  0.0    TeetCDmp   - Rotor-teeter rate-independent Coulomb-damping moment (N-m) [unused for 3 blades]
  0.0    TeetSStP   - Rotor-teeter soft-stop position (degrees) [unused for 3 blades]
  0.0    TeetHStP   - Rotor-teeter hard-stop position (degrees) [unused for 3 blades]
  0.0    TeetSSSp   - Rotor-teeter soft-stop linear-spring constant (N-m/rad) [unused for 3 blades]
  0.0    TeetHSSp   - Rotor-teeter hard-stop linear-spring constant (N-m/rad) [unused for 3 blades]
---------------------- TIP-BRAKE ---------------------------------------------
  0.0    TBDrConN   - Tip-brake drag constant during normal operation, Cd*Area (m^2)
  0.0    TBDrConD   - Tip-brake drag constant during fully-deployed operation, Cd*Area (m^2)
  0.0    TpBrDT     - Time for tip-brake to reach full deployment once released (sec)
---------------------- BLADE -------------------------------------------------
"Baseline_Blade.dat"   BldFile(1) - Name of file containing properties for blade 1 (quoted string)
"Baseline_Blade.dat"   BldFile(2) - Name of file containing properties for blade 2 (quoted string)
"Baseline_Blade.dat"   BldFile(3) - Name of file containing properties for blade 3 (quoted string) [unused for 2 blades]
---------------------- AERODYN -----------------------------------------------
"Test13_AD.ipt"        ADFile   - Name of file containing AeroDyn input parameters (quoted string)
---------------------- NOISE -------------------------------------------------
"Noise.dat" NoiseFile  - Name of file containing aerodynamic noise input parameters (quoted string)
---------------------- ADAMS -------------------------------------------------
"Baseline_ADAMS.dat"   ADAMSFile - Name of file containing ADAMS-specific input parameters (quoted string)
---------------------- LINEARIZATION CONTROL ---------------------------------
"Baseline_Linear.dat"  LinFile  - Name of file containing FAST linearazation parameters (quoted string)
---------------------- OUTPUT ------------------------------------------------
True     SumPrint   - Print summary data to "<RootName>.fsm" (switch)
True     TabDelim   - Generate a tab-delimited tabular output file. (switch)
"ES10.3E2" OutFmt    - Format used for tabular output except time.  Resulting field should be 10 characters. (quoted string) [not checked
for validity!]
  10.0   TStart     - Time to begin tabular output (s)
  10     DecFact    - Decimation factor for tabular output [1: output every time step] (-)
  1.0    SttsTime   - Amount of time between screen status messages (sec)
  0.99   ShftGagL   - Distance from rotor apex [3 blades] or teeter pin [2 blades] to shaft strain gages [positive for upwind rotors] (meters)
  0      NBlGages   - Number of blade nodes that have strain gages for output [0 to 5] (-)
  0      BldGagNd   - List of blade nodes that have strain gages [1 to BldNodes] (-)
         OutList    - The next line(s) contains a list of output parameters. See OutList.txt for a listing of available output channels. (-)
"WindVxt,WindVyt,WindVzt"        - Wind-speed components
"HorWndDir,VerWndDir"            - Wind directions
"BldPitch2"            - Blade 2 pitch angle
"GenPwr,LSShftFxa"            - Generator Power, Rotor Thrust
"IPDefl1, IPDefl2"         - IP blade 1,2 tip deflections
"TipAyc1,TipAyc2"            - Blade IP tip acceleration
"RootMxb2, RootMyb2, RootMzb2"    - Blade 2 root moments
"LSShftFys, LSShftFzs"         - Non-rotating LSS shear forces
"LSSTipMys, LSSTipMzs"          - Non-rotating LSS bending moments at the shaft tip
"YawBrTDxp, YawBrTDyp"          - FA and SS tower-top deflections wrt tilted tower
"YawBrMxn, YawBrMyn, YawBrMzn"    - Tower-top / yaw bearing roll, pitch, and yaw moments
```

References

[1]   *ADAMS User's Guide*, Ann Arbor, MI: Mechanical Dynamics, Inc., 2002.

[2]   Bertacchi, P., Di Monaco, A., Gerloni, M., Ferranti, G., "Eolomar - a moored platform for wind turbines"; *Wind Engineering* Vol. 18, No. 4, p189 (1994).

[3]   Buhl, M., *Crunch User's Guide*, Golden, CO: National Renewable Energy Laboratory, 2003.

[4]   Buhl, M., Jonkman, J., Wright, A., *FAST User's Guide*, Golden, CO: National Renewable Energy Laboratory, 2003.

[5]   Buhl, M., Madsen, P., Pierce, K., "Predicting Ultimate Loads for Wind Turbine Design," American Institute of Aeronautics and Astronautics, AAIA-99-0069.

[6]   Bulder, B., Henderson, A., Huijsmans, R., Peeringa, J., Pierik, J., Snijders, E., van Hees, M., Wijnants, G., Wolf, M., "Floating Wind farms for Shallow Offshore Sites", Offshore Wind Energy in the Mediterranean and other European Seas (OWEMES) Conference, Naples, Italy, 2003.

[7]   Burton, T., Sharpe, D., Jenkins, N., Bossanyi, E., *Wind Energy Handbook*, New York, NY: John Wiley & Sons, 2001.

[8]   Chopra, Anil, *Dynamics of Structures: Theories and Applications to Earthquake Engineering*, Englewood Cliffs, NJ: Prentice Hall, 1995.

[9]   DSM Dyneema ropes website, www.dsm.com/en_US/html/hpf/ropes.htm

[10]   Edwards, C. H., Penney, D. E., *Elementary Differential Equations with Boundary Value Problems*, Fourth Edition, Upper Saddle River, NJ: Prentice Hall, 2000.

[11]   Eslam Energy, Horns Rev Offshore Wind Farm homepage, www.hornsrev.dk: March 2003.

[12]   European Wind Energy Association, "86 Million Europeans to get power from the wind by 2010"; News release: October 7, 2003.

[13]   Faltinsen, O. M., *Sea Loads on Ships and Offshore Structures, Ocean Technology Series*, Cambridge, UK: Cambridge University Press, 1990.

[14]   Germanischer Lloyd, Rules and Regulations "Regulation for the Certification of Offshore Wind Energy Conversion Systems", Hamburg, 1994.Harrison, R., Hau, E., Snel, H., *Large Wind Turbines Design and Economics*, New York, NY: John Wiley & Sons, 2000.

[15]   Haslum, H., *Simplified Methods Applied to Nonlinear Motion of Spar Platforms*, Trondheim, Norway: Norwegian University of Science and Technology, 2000.

[16]   Henderson, A. R., "Analysis Tools for Large Floating Offshore Wind Farms", PhD Thesis, University College London, London, England, 2000.

[17]   Halliday, J., Henderson, A., Patel, M. Watson, G., "Floating Offshore Wind farms – An Option?", Offshore Wind Energy in the Mediterranean and other European Seas (OWEMES) Conference, Naples, Italy, 2003.

[18] Hughes, Owen F., *Ship Structural Design,* Jersey City, NJ: The Society of Naval Architects and Marine Engineers, 1988.

[19] IEC 61400-1, *Wind Turbine Generator Systems - Part 1 Design Requirements*, 3nd Edition (Draft), International Electrotechnical Commission, May 2003.

[20] IEC 61400-3, *Wind Turbine Generator Systems - Part 3: Safety Requirements for Offshore Wind Turbines* (Draft), International Electrotechnical Commission, October 2003.

[21] Kim, S. and Sclavounos, P., "Fully Coupled Response Simulations of Theme Offshore Structures in Water Depths of Up to 10,000 Feet". 11th ISOPE Conference, Stavanger, Norway, 2001.

[22] Liano, D. and Hansen, C., *AeroDyn User's Guide,* Salt Lake City, UT: Windward Engineering, 2002.

[23] Madsen, P., Pierce, K., Buhl, M., "Predicting Ultimate Loads for Wind Turbine Design", American Institute of Aeronautics and Astronautics, AIAA-99-0069.

[24] Manwell, J. F., McGowan, J. G., Rogers, A. L., *Wind Energy Explained*, New York, NY: John Wiley & Sons, 2002.

[25] Meirovitch, L., *Analytical Methods in Vibrations*, New York, NY: Macmillan Company, 1967.

[26] Molin, B., "Second-Order Hydrodynamics Applied to Moored Structures", 19th WEGEMT School, Nantes, 1993.

[27] Milne-Thomson, L.M., *Theoretical Aerodynamics*, New York, NY: Dover Publications, Inc., 1958.

[28] Newman, J. N., *Marine Hydrodynamics*, Cambridge, MA: Massachusetts Institute of Technology, 1977.

[29] NWTC Certification Committee, *Guideline DG01: Wind Turbine Design Load Analysis*, Golden, CO: National Renewable Energy Laboratory, 2003.

[30] NWTC Certification Committee, *Guideline DG02:Wind Turbine Design Strength Analysis*, Golden, CO: National Renewable Energy Laboratory, 1999.

[31] Sclavounos, P., *13.022 Surface Waves and Their Interaction with Floating Bodies, Lecture Notes*, Cambridge, MA: Massachusetts Institute of Technology, 2002.

[32] Shackelford, James F., *Introduction to Material Science for Engineers*, Third Edition, New York, NY: Macmillian Publishing Company, 1992.

[33] Shames, Irving H., Pitarresi, James M., *Introduction to Solid Mechanics*, Third Edition, Upper Saddle River, NJ: Prentice Hall, 2000.

[34] Triantafyllou, M., Chryssostomidis, C., *Environment Description, Force, Prediction and Statistics for Design Applications in Ocean Engineering*, Cambridge, MA: Massachusetts Institute of Technology, 1980.

[35] Tong, K., "Technical and economic aspects of floating offshore wind farm", Proceedings of the Offshore Wind Energy in the Mediterranean and other European Seas (OWEMES) Seminar, Rome, Italy, 1994.